2015

Statistical Analysis of High Sample Rate Time-series Data for Power System Stability Assessment

Goodarz Ghanavati
University of Vermont, goodarz.ghanavati@gmail.com

STATISTICAL ANALYSIS OF HIGH SAMPLE RATE TIME-SERIES DATA FOR POWER SYSTEM STABILITY ASSESSMENT

A Dissertation Presented

by

Goodarz Ghanavati

to

The Faculty of the Graduate College

of

The University of Vermont

In Partial Fullfillment of the Requirements
for the Degree of Doctor of Philosophy
Specializing in Electrical Engineering

May, 2015

Defense date: Nov 20, 2014
Dissertation Examination Committee:

Paul D. H. Hines, Ph.D., Co-Advisor
Taras I. Lakoba, Ph.D., Co-Advisor
Peter S. Dodds, Ph.D., Chairperson
Kurt E. Oughstun, Ph.D.
Mads Almassalkhi, Ph.D.
Cynthia J. Forehand, Ph.D., Dean of the Graduate College

ABSTRACT

The motivation for this research is to leverage the increasing deployment of the phasor measurement unit (PMU) technology by electric utilities in order to improve situational awareness in power systems. PMUs provide unprecedentedly fast and synchronized voltage and current measurements across the system. Analyzing the big data provided by PMUs may prove helpful in reducing the risk of blackouts, such as the Northeast blackout in August 2003, which have resulted in huge costs in past decades.

In order to provide deeper insight into early warning signs (EWS) of catastrophic events in power systems, this dissertation studies changes in statistical properties of high-resolution measurements as a power system approaches a critical transition. The EWS under study are increases in variance and autocorrelation of state variables, which are generic signs of a phenomenon known as critical slowing down (CSD).

Critical slowing down is the result of slower recovery of a dynamical system from perturbations when the system approaches a critical transition. CSD has been observed in many stochastic nonlinear dynamical systems such as ecosystem, human body and power system. Although CSD signs can be useful as indicators of proximity to critical transitions, their characteristics vary for different systems and different variables within a system.

The dissertation provides evidence for the occurrence of CSD in power systems using a comprehensive analytical and numerical study of this phenomenon in several power system test cases. Together, the results show that it is possible extract information regarding not only the proximity of a power system to critical transitions but also the location of the stress in the system from autocorrelation and variance of measurements. Also, a semi-analytical method for fast computation of expected variance and autocorrelation of state variables in large power systems is presented, which allows one to quickly identify locations and variables that are reliable indicators of proximity to instability.

CITATIONS

Material from this dissertation has been published in the following form:

Ghanavati, G., Hines, P. D. H., Lakoba, T. I. and Cotilla-Sanchez, E.. (2014) Understanding early indicators of critical transitions in power systems from autocorrelation functions. IEEE Trans. Circuits Syst. I, vol. 61, no. 9, 2747–2760.

AND

Material from this dissertation has been published in the following form:

Ghanavati, G., Hines, P. D. H. and Lakoba, T. I.. (2014) Investigating early warning signs of oscillatory instability in simulated phasor measurements. Proc. IEEE Power and Energy Soc. General Meeting, 1–5.

AND

Material from this dissertation has been submitted for publication in *IEEE Trans. Power System* on 10/04/2014 in the following form:

Ghanavati, G., Hines, P. D. H. and Lakoba, T. I.. (2014) Identifying useful statistical indicators of proximity to instability in stochastic power systems. IEEE Trans. Power System.

Dedicated to my parents, Mohammadali and Mahvash and my sister, Gilda for their love and support.

ACKNOWLEDGEMENTS

I would like to thank my advisor Dr. Paul D. H. Hines for his excellent mentoring and support. During the whole time that we have been working together, he has been tremendously resourceful, supportive and encouraging. Also, I am grateful for Dr. Taras I. Lakoba's help. His help contributed immensely to the successful completion of this work. Working with Paul and Taras has been a very valuable, fulfilling and enjoyable experience for me. They are both great researchers and also very nice and kind. I also would like to express my gratitude to the other members of my thesis committee Dr. Kurt E. Oughstun, Dr. Peter S. Dodds and Dr. Mads Almassalkhi for their helpful feedback. I also wish to thank Dr. Eduardo Cotilla-Sanchez and Dr. Christopher Danforth for helpful contributions to this research. Thank you also to my friends Pooya Rezaei and Dr. Mert Korkali for valuable discussions and their assistance. Finally, I wish to thank my family and friends who supported me during my Ph. D. studies.

TABLE OF CONTENTS

LIST OF TABLES

Table Page

LIST OF FIGURES

Figure Page

ABBREVIATIONS

A/D	Analog to digital
ANN	Artificial neural network
ARMA	Autoregressive moving average
CSD	Critical slowing down
CTMC	Continuous-time Markov chain
DAE	Differential algebraic equation
emf	Electromotive force
EWS	Early warning sign
GPS	Global positioning system
PDF	Probability density function
PMU	Phasor measurement unit
PSAT	Power system analysis toolbox
PSD	Power spectral density
PSS	Power system stabilizer
SCADA	Supervisory control and data acquisition
SDAE	Stochastic differential algebraic equations
SDE	Stochastic differential equation
SMIB	Single machine infinite bus
SMSL	Single machine single load
TCSC	Thyristor-controlled series capacitor
ULTC	Under-load tap changer

CHAPTER 1: INTRODUCTION

1.1 Abstract

This dissertation presents the study of two early warning signs (EWS) of critical bifurcations in power system. These EWS are variance and autocorrelation of state variables, which are signs of a phenomenon known as critical slowing down. The thesis presents an analytical and numerical study of changes in autocorrelation and variance of the variables in the proximity of Saddle-node and Hopf bifurcations. These two bifurcations are associated with two types of catastrophic events in power grids known as voltage and oscillatory instability. The contributions of this dissertation can be useful in developing novel power system stability monitoring methods, which subsequently can help towards a more reliable electric grid.

1.2 Motivation

The primary motivation of this research is to help reduce the likelihood of blackouts in power grids by improving the understanding about early warning signs of such events. EWS can be obtained from high-sample rate measurements, which are becoming more and more available via the deployment of the phasor measurement unit (PMU) technology by utilities. PMUs provide many more measurements (30 or 60 Hz) relative to traditional supervisory control and data acquisition (SCADA) systems (with maximum sampling rates between 0.1 Hz to 0.5 Hz), which are widely used by utilities at present. Also, PMU measurements are time synchronized using the GPS technology, which allows one to reconstruct blackout and near-blackout events with precision. Older SCADA systems frequently had clocks that would drift, making it difficult to reconstruct the order of events after complicated disturbances.

1.2.1 Blackout Mitigation

Blackouts have caused significant economic and social costs worldwide in the past three to four decades. For example, estimates of total costs of the August 14, 2003 blackout in the United States range between $4 billion and $10 billion and in Canada, gross domestic product was down 0.7% in August 2003 (Abraham and Efford 2004). The July 30, 2012 blackout in India affected more than 600 million people (Romero 2012).

A variety of factors are common among major blackouts, e.g., contact of conductors with trees, insufficient reactive power generation, inadequate system visibility tools, system operation beyond safe limits, etc. (Abraham and Efford 2004). Also, large blackouts are usually caused by a combination of events such as voltage problems, transmission line tripping and undamped electromechanical oscillations.

Investigation of some widespread blackouts has shown that signs of stress were present minutes to hours before large-scale cascading began. For example, the report of the August 14, 2003 blackout states that (Abraham and Efford 2004):

> During the days before August 14 and throughout the morning and mid-day on August 14, voltages were depressed across parts of northern Ohio because of high air conditioning demand and other loads, and power transfers into and to a lesser extent across the region.

Clearly, advanced monitoring algorithms and tools could help operators to avert widespread outages in situations like the above by giving them warning of the increased system stress with sufficient early warning to take timely action. One of the practices deemed to be very effective for blackout mitigation is to turn high-resolution, synchronized measurements provided by PMUs into useful information to improve situational awareness of system operators (FERC and NERC 2012).

1.2.2 Synchronized Phasor Measurement Systems

Phasor measurement units provide high-resolution synchronized measurements of currents and voltages (magnitude and phase) across power grid. PMUs are equipped with analog to digital (A/D) converters, which transform current and voltage measurements into digital signals. The synchronization is achieved by using a sampling clock that receives the signal provided by a GPS receiver (De La Ree et al. 2010).

After the invention of the PMU in the late 80's (Phadke 1993), utilities have been gradually deploying them to create wide area measurement systems. In power systems, phasor data concentrators collect data from a number of PMUs and use time-stamps to correlate them by time in order to create a system-wide measurement set (Gómez-Expósito et al. 2011).

Prior studies have proposed various applications for PMU data (Centeno et al. 1993), (Gou and Abur 2001), (Zhong et al. 2005). (De La Ree et al. 2010) describe several applications of PMU in power system monitoring, protection and control. This dissertation examines the transformation of data from PMU systems into information about grid stress, making use of the theory of "critical slowing down".

1.3 Critical Slowing Down

Prior research suggests that signs of a phenomenon known as critical slowing down (CSD) can provide early warning of critical bifurcations (Boettiger et al. 2013). CSD is the slower recovery of a dynamical system from perturbations as it approaches a critical bifurcation. CSD has been observed in various dynamical systems such as ecosystems (Scheffer et al. 2001) and climate (Lenton et al. 2012).

Critical slowing down has several indicators. The two most generic ones are increases in variance and autocorrelation of state variables. As the system slows down, the impact of shocks decay slower, which results in increased variance for state variables (Scheffer et al. 2009). Also, the intrinsic rates of change in the system decrease due to CSD and the state of the system becomes more and more like its past state, which leads to

increased autocorrelation (Scheffer et al. 2009). Other indicators such as flickering, spatial patterns and increases in skewness have also been suggested as CSD signs (Scheffer et al. 2009). However, they are not as generic as the increase in variance and autocorrelation.

Recent research has shown that not all systems that undergo regime shifts exhibit CSD (Boettiger et al. 2013), (Boerlijst et al. 2013). (Boerlijst et al. 2013) show that even in cases where a system exhibits CSD, its signs may not be observable in all of the system variables. These findings show that CSD is not a strictly universal phenomenon and it is necessary to analyze a particular system in order to understand the conductions under which CSD does occur for that system. Earlier research has shown that CSD does occur in power system (Cotilla-Sanchez et al. 2012). (Chertkov et al. 2011) study a radial power system (see Fig. 1.1) and shows that voltage variations at the end of a distribution line increase as the system approaches voltage instability (saddle-node bifurcation). (Podolsky and Turitsyn 2013b) derive an approximate analytical autocorrelation function (from which autocorrelation and variance can be found) for state variables in a power system model in proximity of the saddle-node bifurcation and shows that CSD occurs in the system near this type of bifurcation.

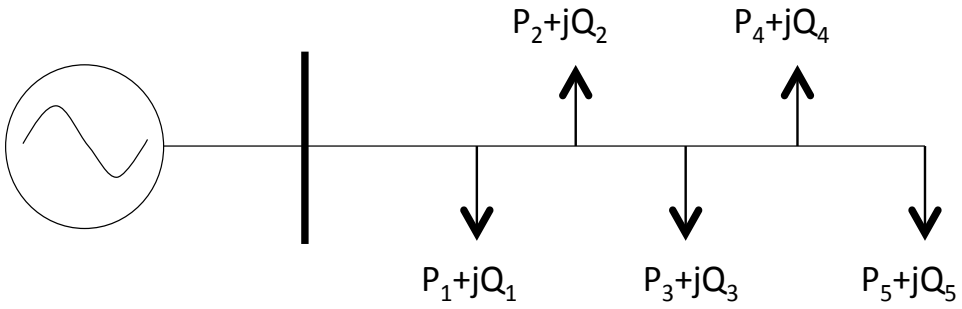

Figure 1.1: A radial power system. A distribution line connects a generator and several loads.

In order to study CSD mathematically, the use of stochastic models is necessary. The next section discusses the stochastic modeling and dynamics of power systems.

1.4 Stochastic Dynamics of Power Systems

A power system is a stochastic dynamical system in nature. Random sources such as load switching, and changes in renewable energy sources such as wind and solar excite the

system constantly. The majority of existing studies on power grid dynamics have focused on the dynamics of deterministic models. However, increasing integration of renewable energy sources has directed attention to the analysis of stochastic power system dynamics (Odun-Ayo and Crow 2012).

Power system dynamics are typically modeled with differential-algebraic equations. The differential equations model the dynamics of equipment such as generator, exciter[1] and turbine-governor[2]. The algebraic equations model the flow of power through the transmission system. The dynamics within the transmission system are much faster than the equipment dynamics. That is why power flows in the system are assumed to be instantaneous and described using algebraic equations (Dobson et al. 2002).

Considering random changes in power system such as load perturbations requires the use of stochastic differential algebraic equations (SDAE) for modeling the system dynamics. In (Milano and Zarate–Minano 2013), a general approach to model power systems as continuous SDAEs is proposed. The paper presents a systematic approach to include stochastic terms in power system models. It also presents a tool for evaluating the weight of stochastic perturbations on the power system transient behavior.

A number of researchers have used stochastic methods to study the impact of load and generation perturbations on power system dynamic stability. (Wang and Crow 2013) study the stability of the stochastic single machine infinite bus system[3] by analyzing the probability density function of state variables. The results show that addition of noise (load perturbations) may improve dynamic stability under some conditions. In (Dhople et al. 2013), a framework is proposed to study the impact of stochastic active/reactive power injections (power generation sources and loads) on power system dynamics with a focus on time scales involving electromechanical phenomena. In their framework, active/reactive power injections evolve according to a continuous-time Markov chain (CTMC), while the standard differential algebraic equation (DAE) model describes the power system dynam-

[1] Exciter controls the output voltage of a generator.

[2] Turbine-governor controls the output power of a generator.

[3] A system that consists of a generator that is connected to a large power grid such that the generator can not impact the grid's dynamics.

ics. The paper presents the application of the framework to calculation of long-term power system state statistics, and to short-term probabilistic dynamic performance/reliability assessment.

(Dong et al. 2012) propose a framework for assessment of power system transient stability (stability after a large disturbance). The framework models load level as well as discrete random events such as system faults (or any event that results in network reconfiguration) using stochastic processes. (Odun-Ayo and Crow 2012) propose a new method for analyzing stochastic transient stability using the transient energy function. It presents a method to integrate the transient energy function and recloser[4] probability distribution function to provide a quantitative measure of probability of stability.

(Perninge et al. 2010) present a method for calculation of the probability distribution of the time to voltage instability (See Sec. 1.5.) with uncertain future loading scenarios, which are modeled with the Brownian motion random process. (De Marco and Bergen 1987) propose a security measure indicating the vulnerability to voltage instability driven by small disturbances in load. The measure is based on the expected exit time from the region of attraction for the stable equilibrium point of the underlying deterministic system.

This dissertation uses a stochastic approach in order to study the CSD phenomenon for two common types of critical bifurcations in power system, which will be discussed in the next section.

1.5 Critical Bifurcations in Power System

In this dissertation, a critical bifurcation is defined to be a bifurcation where a slowly-varying parameter moves the system towards a catastrophic regime change. Voltage instability and oscillatory instability are two types of critical bifurcations that are known to occur in power system models and have contributed to large blackouts in recent years.

[4] A circuit breaker that is equipped with an automatic closing mechanism after disconnection of a transmission line.

1.5.1 Voltage Stability

Voltage stability refers to the ability of a power system to maintain steady voltages at all buses (system nodes) in the system after being subjected to a disturbance from a given initial operating condition. Instability that may result occurs in the form of a progressive fall or rise of voltages of some buses. A possible outcome of voltage instability is loss of load in an area, or tripping of transmission lines and other elements by their protective systems leading to cascading outages (Kundur et al. 2004). Voltage instability has caused or contributed to many large blackouts, e.g., August 2003 blackout in the US & Canada (Abraham and Efford 2004).

Loads and reactive power sources play important roles in voltage stability of power grid. Increase in load puts stress on the transmission network and limits its capability to transfer power and support voltage (Kundur et al. 2004). Insufficient reactive power generation also reduces the ability of the system to provide voltage support. Voltage stability is threatened when a disturbance increases the reactive power demand beyond the sustainable capacity of the available reactive power resources (Kundur et al. 2004).

Voltage stability is associated with the saddle-node bifurcation, i.e., two equilibria of a power system model collide and annihilate each other. Figs. 1.2 and 1.3 illustrate how voltage stability is related to saddle-node bifurcation. Fig. 1.2 shows a simple power system model consisting of a generator, a transmission line and a constant power load $(P_d + jQ_d)$. The generator is modeled with a voltage source E'_a and a reactance X'_d and the transmission line is modeled with a resistance r_l and a reactance X_l. δ is angle of the generator's rotor relative to a synchronously rotating reference frame. $V_g,\ V_d,\ \theta_g,\ \theta_d$ represent the voltage magnitudes and angles of generator and load nodes. Fig. 1.3 shows that as the load power increases, its voltage decreases. When the equivalent impedance of the load matches the value of the line impedance, then the system reaches its critical loading. Before this point, for each load power value, there are two equilibria. The equilibrium located in the upper branch of the curve is stable while the other one is unstable. As the load power increases,

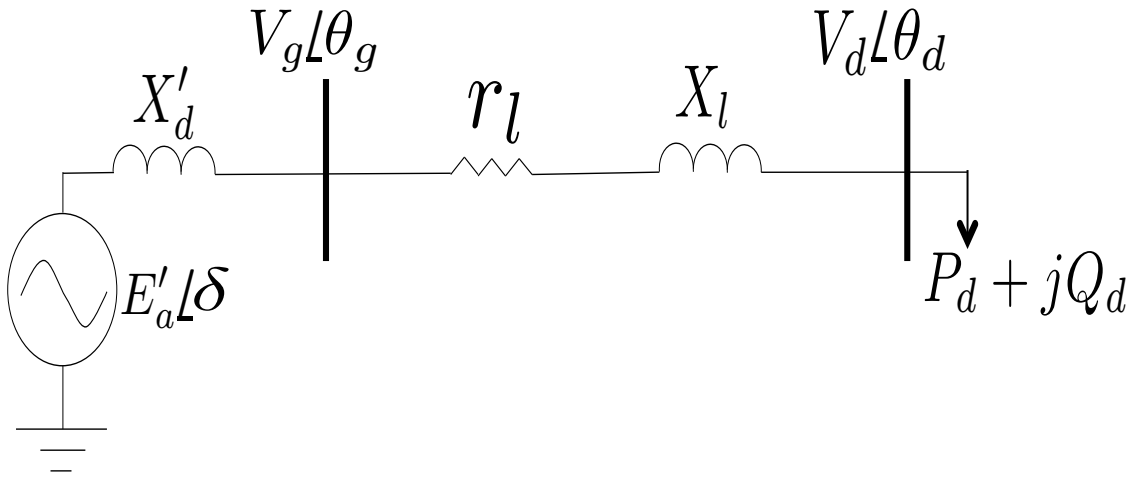

Figure 1.2: A single machine single load system. The system model consists of a generator, a transmission line and a constant power load.

these two equilibria approach each other and coalesce at the critical loading. Therefore, a saddle-node bifurcation occurs at the critical loading.

Several control actions can be used for mitigating voltage instability. A common method is switching on capacitor banks near load centers to meet the reactive power demand. This action helps with the voltage stability of the system either by relieving stress on transmission lines (since less reactive power will flow through the lines) or compensating for the lack of sufficient reactive power generation. Other methods such as load shedding and generation rescheduling can also be used to improve the voltage stability of the system.

Voltage stability time scales

Voltage stability may be either a short-term or a long-term phenomenon. The time frame of interest for voltage stability problems ranges from a few seconds to tens of minutes (Kundur et al. 2004). Short term voltage stability is associated with electromechanical transients on transmission lines and synchronous generators and voltage collapse may occur in the time range of seconds (Dobson et al. 2002). Long term voltage stability involves slower acting equipment such as tap-changing transformers and generator current limiters. The disturbance could also be in the form of sustained load buildup (Kundur et al. 2004). The time-scale of long term voltage collapse ranges from tens of seconds to several minutes.

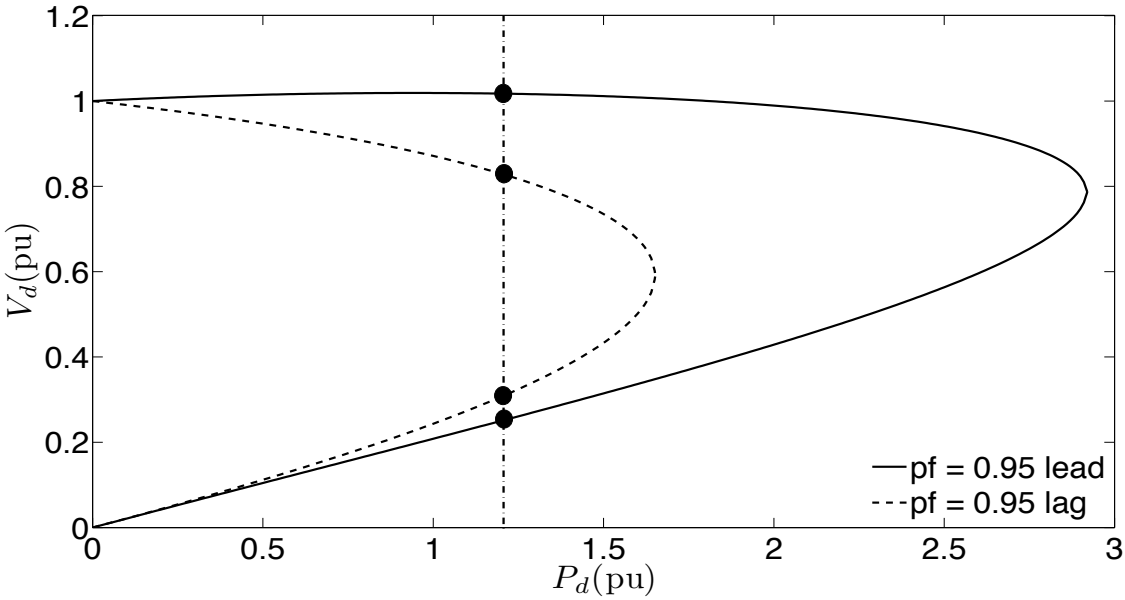

Figure 1.3: Load voltage versus its power. The vertical line represents the load power for a normal operating condition. The circles show the system equilibria.

This dissertation focuses on using CSD for monitoring long term voltage stability of a power system.

Voltage stability monitoring

The first step in the prevention of voltage instability is monitoring. Fig. 1.3 illustrates the necessity of voltage stability monitoring. In this figure, the system becomes unstable at very distinctly different points for two load power factor[5] values. Therefore, for a given load power, distance of the system from the bifurcation is very different for two cases. This example shows that changes in system parameters can have a significant impact on voltage stability of the system. Since many other parameters, e.g., voltage dependence of loads, reactive power generation capacity, etc., can also impact the voltage stability of a large power system, it is necessary to develop methods for estimating the distance to the saddle-node bifurcation.

Numerous studies have focused on the voltage stability monitoring problem. Various methods such as the methods based on the maximum power transfer theorem (or the

[5]Load power factor is: $pf = {}^{P_d}/\sqrt{P_d^2+Q_d^2}$

Thevenin circuit) (Milosevic and Begovic 2003), monitoring reactive power reserves (Bao et al. 2003) and artificial neural networks (ANN) (Zhou et al. 2010) are suggested for monitoring of voltage stability.

In the maximum power transfer method, a circuit consisting of a Thevenin equivalent voltage source and impedance, model the network as seen from a node (except the load connected to that node). Based on the maximum power transfer theorem, the maximum power is transferred when the load impedance equals the complex conjugate of the Thevenin equivalent impedance. This fact is the basis of the maximum power transfer method for voltage stability monitoring. The voltage stability indices calculated based on this method give an estimate of the local voltage stability. (Milosevic and Begovic 2003) present a local voltage stability indicator based on local voltage and current phasor measurements and load characteristics. In reference (Smon et al. 2006), a method for calculation of Thevenin parameters from two consecutive phasor measurements is presented using the Tellegen's theorem.

Another class of voltage stability monitoring methods is based on monitoring generator reactive power reserves. The correlation between the generator reactive power reserves and the system voltage stability margin has been observed by system operators for many years (Bao et al. 2003). Using this relationship, (Bao et al. 2003) develops a method for online voltage stability monitoring. (Milosevic and Begovic 2003) use information on reactive power reserves of the system along with the maximum power transfer theorem to develop an online voltage stability monitoring indicator.

Voltage stability monitoring methods based on ANN use analytical (i.e. model-based) studies to train their networks. The network inputs are some of the system measurements such as voltage magnitudes and angles of system buses and the output is the calculated voltage stability index (Zhou et al. 2010), (Popović et al. 1998).

1.5.2 Oscillatory Stability

Another type of critical bifurcation that occurs in power systems is the oscillatory instability (Kosterev et al. 1997), which is typically associated with the Hopf bifurcation. In other words, a pair of complex conjugate eigenvalues of the state matrix cross the imaginary axis of the complex plane after the system undergoes a contingency (Kundur et al. 1994).

There are two types of oscillatory stability problems: local plant mode and inter-area oscillations. The local plant mode occurs when a generator's rotor angle oscillates against the rest of the system. In Inter-area oscillations, generators in one area of the system swing against generators in another area (Kundur et al. 2004). Oscillatory modes in both cases have relatively low frequencies. Local modes and inter-area modes typically have frequencies in the range of 0.7 Hz to 2 Hz and 0.1 Hz to 0.8 Hz (Kundur et al. 2004). Inter-area oscillations can have widespread impacts such as the August 10, 1996 blackout in Western North America (Kosterev et al. 1997). The time frame of interest in small-disturbance oscillatory stability studies is on the order of 10 to 20 seconds following a disturbance (Kundur et al. 2004).

Substantial research has focused on the fundamentals of inter-area oscillations. It is well-known that weak tie-lines, i.e., long and high impedance transmission lines, between two areas of a power system can lead to low frequency, weakly damped inter-area oscillatory modes (Klein et al. 1991). Also, increased power transfer between weakly connected areas can reduce the damping of the modes, which may lead to instability. (Klein et al. 1991) analyze the effects of excitation systems, loads and DC links on inter-area oscillations. The results show that change of load types and fast or slow action of exciters affect the damping and the frequency of inter-area modes in a mixed way.

Various methods have been suggested for the stabilization of inter-area modes. Power system stabilizers (PSS), which is a generator control device, can improve the damping of these modes. PSS, a type of generator control device, was introduced in mid-1960s and has been used by utilities extensively (Kundur et al. 2003). However, PSSs require

regular retuning in order to perform suitably. Another device for damping inter-area oscillations is thyristor controlled series capacitor (TCSC) (Yang et al. 1998). Impedance of the tie-line between two areas of a system has significant impact on the damping of inter-area modes. TCSC can modulate the line impedance rapidly (Yang et al. 1998). As a result, it can be used to increase the damping of inter-area modes. (Huang et al. 2011) take a different approach to damping inter-area modes. Their approach adjusts the system operating conditions (like generators dispatch) to increase the system damping.

Oscillatory stability monitoring

Several methods have been proposed for monitoring inter-area oscillations (Cai et al. 2013), (Peng and Nair 2012) and (Browne et al. 2008). The typical method for monitoring oscillatory stability is to use modal identification methods to estimate the system's dominant modes from measurements.

There are two approaches to the estimation of dominant modes from measurement data: 1) ringdown, 2) ambient (Zhou et al. 2012). The ambient detection refers to monitoring the network under an equilibrium condition with small-amplitude random load variations. On the other hand, ringdown detection methods track the oscillatory behavior after the system has experienced some major disturbances (Peng and Nair 2012). Ambient data, which are the measured response of the system to small perturbations, is a random process. Stochastic models such as auto-regressive model, auto-regressive moving-average (ARMA) model, and stochastic state-space model have been used in this case (Ghasemi and Cañizares 2008). The Prony method, which uses a deterministic model, has been widely used to analyze ring-down data in power systems (Ghasemi and Cañizares 2008).

From another perspective, the algorithms for identification of dominant oscillatory modes can be classified into two categories: block processing and recursive processing (Cai et al. 2013). Block processing algorithms process a set of data belonging to a single sliding data window simultaneously. On the contrary, recursive algorithms update the mode estimates based upon a new time sample and the previous estimate (Cai et al. 2013).

Prony analysis, Hilbert transform and ARMA are examples of block processing algorithms suggested in literature (Cai et al. 2013), (Browne et al. 2008). Kalman filter is the most widely used recursive processing algorithm (Peng and Nair 2012).

The block processing algorithms for modal identification have limitations with regard to measurement noise, accuracy and discriminating between similar modes (Cai et al. 2013), (Browne et al. 2008). The challenge with recursive processing algorithms is that prior knowledge of the system is essential for these methods. Also, inadequate selection of initial conditions may cause the latter algorithms to produce biased results or lead to convergence errors (Peng and Nair 2012).

1.6 Dissertation outline

This research takes a different approach to monitoring power system stability by using the statistics of phasor measurements. Until recent years, it was not possible to use statistics of measured quantities for monitoring some phenomena in power system since the resolution of measurements in the timescale associated with those events was so low that data statistics could not represent the true statistics of variables.

One motivation for the present approach is to use measurements' statistics for signaling an impending critical transition. Merely measuring the mean values of measured quantities, which is widely used in stability monitoring algorithms, does not provide such information sometimes. Another reason for pursuing this method is to form the basis of algorithms that are less dependent on system models and more on data characteristics. The reason for this is that any model has some inherent error. Also, detailed dynamic parameters for power system models are frequently imprecise, or unavailable.

The remainder of the dissertation is organized as follows. Chapter 2 presents an analytical study of CSD for various power system test cases. It presents analytical autocorrelation functions of state variables for three small power systems. Using the functions, it examines changes in variance and autocorrelation of state variables as the systems approach a saddle-node bifurcation. The chapter also includes a numerical study of CSD for a larger multimachine power system test case.

Chapter 3 presents a numerical study of CSD in proximity of a Hopf bifurcation in a small power system model. Also, the chapter examines the reason that CSD signs are better observable in some variables compared to others.

Chapter 4 presents a semi-analytical method for fast calculation of variance and autocorrelation of state variables in large power systems to quickly identify variables and locations that are better indicators of system stability. It also analyzes the impact of measurement noise on observability of CSD signs. Lastly, the chapter presents a method for detection of stressed areas in a power system using variance and autocorrelation of phasor measurements.

Chapter 5 summarizes the conclusions and the contributions of the dissertation. It also presents the future directions for this research.

Appendix A presents some MATLAB scripts for simulating a dynamic power system model with stochastic changes in load using power system analysis toolbox (PSAT) (Milano 2005).

CHAPTER 2: UNDERSTANDING EARLY INDICATORS OF CRITICAL TRANSITIONS IN POWER SYSTEMS FROM AUTOCORRELATION FUNCTIONS

2.1 Abstract

In order to better understand the extent to which critical slowing down (CSD) can be used as an indicator of proximity to bifurcation in power systems, this chapter derives autocorrelation functions for three small power system models, using the stochastic differential algebraic equations (SDAE) associated with each. The analytical results, along with numerical results from a larger system, show that, although CSD does occur in power systems, its signs sometimes appear only when the system is very close to transition. On the other hand, the variance in voltage magnitudes consistently shows up as a good early warning of voltage collapse.

2.2 Introduction

There is increasing evidence that time-series data taken from stochastically forced dynamical systems show statistical patterns that can be useful in predicting the proximity of a system to critical transitions (Scheffer et al. 2009), (Lenton et al. 2012). Collectively this phenomenon is known as Critical Slowing Down, and is most easily observed by testing for autocorrelation and variance in time-series data. Increases in autocorrelation and variance have been shown to give early warning of critical transitions in climate models (Dakos et al. 2008), ecosystems (Dakos et al. 2011), the human brain (Litt et al. 2001) and electric power systems (Cotilla-Sanchez et al. 2012, Podolsky and Turitsyn 2013b, Podolsky and Turitsyn 2013a).

Scheffer et al. (Scheffer et al. 2009) provide some explanation as to why increasing variance and autocorrelation can indicate proximity to a critical transition. They illustrate that increasing autocorrelation results from the system returning to equilibrium more slowly after perturbations, and that increased variance results from state variables spending more

time further away from equilibrium. Reference (Kuehn 2011) uses the mathematical theory of the stochastic fast-slow dynamical systems and the Fokker–Planck equation to explain the use of autocorrelation and variance as indicators of CSD.

While CSD is a general property of critical transitions (Boerlijst et al. 2013), its signs do not always appear early enough to be useful as an early warning, and do not universally appear in all variables (Boerlijst et al. 2013, Hastings and Wysham 2010). References (Boerlijst et al. 2013) and (Hastings and Wysham 2010) both show, using ecological models, that the signs of CSD appear only in a few of the variables, or even not at all.

Several types of critical transitions in deterministic power system models have been explained using bifurcation theory. Reference (Dobson 1992) explains voltage collapse as a saddle-node bifurcation. Reference (Dobson et al. 2002) describes voltage instability caused by the violation of equipment limits using limit-induced bifurcation theory. Some types of oscillatory instability can be explained as a Hopf bifurcation (Ajjarapu and Lee 1992),(Cañizares et al. 2004). Reference (Avalos et al. 2009) describes an optimization method that can find saddle-node or limit-induced bifurcation points. Reference (Revel et al. 2010) shows that both Hopf and saddle-node bifurcations can be identified in a multi-machine power system, and that their locations can be affected by a power system stabilizer.

Substantial research has focused on estimating the proximity of a power system to a particular critical transition. References (Dobson et al. 2002), (Chiang et al. 1990), (Begovic and Phadke 1992) and (Glavic and Van Cutsem 2009) describe methods to measure the distance between an operating state and voltage collapse with respect to slow-moving state variables, such as load. Although these methods provide valuable information about system stability, they are based on the assumption that the current network model is accurate. However, all power system models include error, both in state variable estimates and network parameters, particularly for areas of the network that are outside of an operator's immediate control.

An alternate approach to estimating proximity to bifurcation is to study the response of a system to stochastic forcing, such as fluctuations in load, or variable production from renewable energy sources. To this end, a growing number of papers study power system stability using stochastic models (De Marco and Bergen 1987), (Nwankpa et al. 1992), (Anghel et al. 2007), (Dong et al. 2012), (Wang and Crow 2013) and (Dhople et al. 2013). Reference (De Marco and Bergen 1987) models power systems using Stochastic Differential Equations (SDEs) in order to develop a measure of voltage security. In (Dong et al. 2012), numerical methods are used to assess transient stability in power systems, given fluctuating loads and random faults. Reference (Wang and Crow 2013) uses the Fokker–Planck equation to calculate the probability density function (PDF) for state variables in a single machine infinite bus system (SMIB), and uses the time evolution of this PDF to show how random load fluctuations affect system stability. In (Dhople et al. 2013), an analytical method to compute bounds on the distribution of system states or bounds on probabilities of different events of interest in stochastic power systems is presented. Reference (Milano and Zarate–Minano 2013) proposes a systematic approach to model power systems as continuous stochastic differential-algebraic equations.

The results above clearly show that power system stability is affected by stochastic forcing. However, they provide little information about the extent to which CSD can be used as an early warning of critical transitions given fluctuating measurement data. Given the increasing availability of high-sample-rate synchronized phasor measurement unit (PMU) data, and the fact that insufficient situational awareness has been identified as a critical contributor to recent large power system failures (e.g., (Abraham and Efford 2004), (FERC and NERC 2012)) there is a need to better understand how statistical phenomena, such as CSD, might be used to design good indicators of stress in power systems.

Results from the literature on CSD suggest that autocorrelation and variance in time-series data increase before critical transitions. Empirical evidence for increasing autocorrelation and variance is provided for an SMIB and a 9-bus test case in (Cotilla-Sanchez et al. 2012). Reference (Chertkov et al. 2011) shows that voltage variance at the end of

a distribution feeder increases as it approaches voltage collapse. However, the results do not provide insight into autocorrelation. To our knowledge, only (Podolsky and Turitsyn 2013a), (Podolsky and Turitsyn 2013b) derive approximate analytical autocorrelation functions (from which either autocorrelation or variance can be found) for state variables in a power system model, which is applied to the New England 39 bus test case. However, the autocorrelation function in (Podolsky and Turitsyn 2013a), (Podolsky and Turitsyn 2013b) is limited to the operating regime very close to the threshold of system instability. Furthermore, there is, to our knowledge, no existing research regarding which variables show the signs of CSD most clearly in power system, and thus which variables are better indicators of proximity to critical transitions. In (Ghanavati et al. 2013), the authors derived the general autocorrelation function for the stochastic SMIB system. This chapter extends the SMIB results in (Ghanavati et al. 2013), and studies two additional power system models using the same analytical approach. Also, this chapter includes new numerical simulation results for two multi-machine systems, which illustrate insights gained from the analytical work.

Motivated by the need to better understand CSD in power systems, the goal of this chapter is to describe and explain changes in the autocorrelation and variance of state variables in several power system models, as they approach bifurcation. To this end, we derive autocorrelation functions of state variables for three small models. We use the results to show that CSD does occur in power systems, explain why it occurs, and describe conditions under which autocorrelation and variance signal proximity to critical transitions. The remainder of this chapter is organized as follows. Section 2.3 describes the general mathematical model and the method used to derive autocorrelation functions in this chapter. Analytical solutions and illustrative numerical results for three small power systems are presented in Secs. 2.4, 2.5 and 2.6. In Sec. 2.7, the results of numerical simulations on two multi-machine power system models including the New England 39 bus test case are presented. Finally, Sec. 3.5 summarizes the results and contributions of this chapter.

2.3 Solution Method for Autocorrelation Functions

In this section, we present the general form of the Stochastic Differential Algebraic Equations (SDAEs) used to model the three systems studied in this chapter. Then, the solution of the SDAEs and the expressions for autocorrelations and variances of both algebraic and differential variables of the systems are presented. Finally, the method used for simulating the SDAEs numerically is described.

2.3.1 The Model

All three models studied analytically in this chapter include a single second-order synchronous generator. These systems can be described by the following SDAEs:

$$\ddot{\delta} + 2\gamma\dot{\delta} + F_1\left(\delta, \underline{y}, \eta\right) = 0 \tag{2.1}$$

$$\underline{F_2}\left(\delta, \underline{y}, \eta\right) = 0 \tag{2.2}$$

where δ is angle of the synchronous generator's rotor relative to a synchronously rotating reference axis, $\underline{y}$ is the vector of algebraic variables, γ is the damping coefficient, $F_1, \underline{F_2}$ form a set of nonlinear algebraic equations of the systems, and η is a Gaussian random variable. η has the following properties:

$$\mathrm{E}\left[\eta\left(t\right)\right] = 0 \tag{2.3}$$

$$\mathrm{E}\left[\eta\left(t\right)\eta\left(s\right)\right] = \sigma_\eta^2 \cdot \delta_I\left(t - s\right) \tag{2.4}$$

where t, s are two arbitrary times, σ_η^2 is the intensity of noise, and δ_I represents the unit impulse (delta) function (which should not be confused with the rotor angle δ).

Equation (2.4) implies that we model the noise as having zero correlation time. In practical power systems, such noise originates from stochastic changes from loads and generators, as well as electromagnetic interferences, which occur over many time scales. To our knowledge, no empirical studies have quantified the spectral density, or correlation time, of fluctuations in power systems. In this chapter, we assume that the spectral density

of noise sources is flat over a certain frequency range, while acknowledging that this model is likely to have limitations. The higher end of the frequency range of interest is set by the sampling rate of the PMU, which is commonly 30 Hz. (Note that this is higher than the highest frequency of the system oscillations, which in our examples is in the range 1–10 Hz.) The lower end of the frequency range is set by the length of our simulated time window, which is 2 minutes, corresponding to a frequency of about 0.01 Hz. If one were to measure for CSD in a practical power system one would want to look at the statistical properties of data with a similar window length. Following the methods in (Dakos et al. 2008), the window of data would be initially low-pass filtered to remove slow trends. This would ensure that the resulting data stream has zero mean, as does η in (2.3). The detrended dataset would retain the important oscillations that might indicate instability (typically well above 0.01 Hz), but discard slower trends. Thus, the noise model described by (2.3) and (2.4) is based on the assumption that the spectral density of noise sources is nearly constant over the frequency range of 0.01 Hz to 30 Hz. For this model to be accurate, the correlation time of the noise needs to be somewhat smaller than 1/30s. Our numerical simulations, which use a time step size of 0.01s, inject noise at each time step, thus implicitly assuming that the correlation time of the noise is 0.01s (see the discussion after (2.20) and Sec. 2.3.4). It should be noted that other studies (Milano and Zarate–Minano 2013), (Hauer et al. 2007) have used noise models in which the noise spectral density falls off at frequencies above approximately 1 Hz, rather than our value of 30 Hz. It is likely that, as assumed in (Milano and Zarate–Minano 2013) and (Hauer et al. 2007), there is some frequency dependence in the spectral density of empirical measurements from power systems. However, the exact structure of the noise is yet to be verified empirically. Future work is needed to determine the impact of frequency dependence (or, equivalently, the noise's finite correlation time) on the results presented in this chapter.

In order to solve (2.1) and (2.2) analytically, we linearized F_1 and $\underline{F_2}$ around the stable equilibrium point. Then (2.1) and (2.2) were combined into a single damped harmonic oscillator equation with stochastic forcing:

$$\Delta\ddot{\delta} + 2\gamma\Delta\dot{\delta} + \omega_0^2\Delta\delta = -f\eta \tag{2.5}$$

where ω_0 is the undamped angular frequency of the oscillator, f is a constant, and $\Delta\delta = \delta - \delta_0$ is the deviation of the rotor angle from its equilibrium value. Both ω_0 and f change with the system's equilibrium operating state. Equation (2.5) can be written as a multivariate Ornstein–Uhlenbeck process (Gardiner 2010):

$$\dot{\underline{z}}\,(t) = A\underline{z}\,(t) + B \begin{bmatrix} 0 \\ \eta\,(t) \end{bmatrix} \tag{2.6}$$

where $\underline{z} = \begin{bmatrix} \Delta\delta & \Delta\dot{\delta} \end{bmatrix}^T$ is the vector of differential variables, $\Delta\dot{\delta}$ is the deviation of the generator speed from its equilibrium value, and A and B are constant matrices:

$$A = \begin{bmatrix} 0 & 1 \\ -\omega_0^2 & -2\gamma \end{bmatrix} \tag{2.7}$$

$$B = \begin{bmatrix} 0 & 0 \\ 0 & -f \end{bmatrix} \tag{2.8}$$

Given (2.7), the eigenvalues of A are $-\gamma \pm \sqrt{\gamma^2 - \omega_0^2}$. At $\omega_0 = 0$, one of the eigenvalues of matrix A becomes zero, and the system experiences a saddle-node bifurcation.

Equation (2.5) can be interpreted in two different ways: using either Itô SDE and Stratonovich SDEs. Here, we use the Stratonovich interpretation (Stratonovich 1963), where noise has finite, albeit very small, correlation time (Gardiner 2010). The reason why we chose the Stratonovich interpretation is that it allows the use of ordinary calculus, which is not possible with the Itô interpretation.

If $\gamma < \omega_0$ (which holds until very close to the bifurcation in two of our systems), the solution of (2.6) is (Blanchard et al. 2006):

$$\Delta\delta(t) = f \cdot \int_{-\infty}^{t} \exp\left(\gamma\left(t'-t\right)\right)\eta\left(t'\right) \cdot \frac{\sin\left(\omega'(t'-t)\right)}{\omega'} dt' \tag{2.9}$$

$$\Delta\dot{\delta}\left(t\right) = -f \cdot \int_{-\infty}^{t} \exp\left(\gamma\left(t'-t\right)\right)\eta\left(t'\right) \cdot \frac{\sin\left(\omega'(t'-t)+\phi\right)\omega_0}{\omega'} dt' \tag{2.10}$$

where $\omega' = \sqrt{\omega_0^2 - \gamma^2}$ and $\phi = \arctan(\omega'/\gamma)$.

In the system in Sec. 2.5, $\omega_0 = 0$ for all system parameters, so the condition $\gamma < \omega_0$ does not hold. Therefore, the solution of (2.5) in that system is different from (2.9), (2.10):

$$\Delta\dot{\delta} = -f \int_{-\infty}^{t} \exp\left(-2\gamma\left(t-t'\right)\right)\eta\left(t'\right) dt' \tag{2.11}$$

2.3.2 Autocorrelation and Variance of Differential Variables

Given that the eigenvalues of A have negative real part (because $\gamma > 0$), one can calculate the stationary variances and autocorrelations of $\Delta\delta$ and $\Delta\dot{\delta}$ using (2.3), (2.4), (2.9) and (2.10). The variances of the differential variables are as follows:

$$\sigma_{\Delta\delta}^2 = \frac{f^2\sigma_\eta^2}{4\gamma\omega_0^2} \tag{2.12}$$

$$\sigma_{\Delta\dot{\delta}}^2 = \frac{f^2\sigma_\eta^2}{4\gamma} \tag{2.13}$$

If $\gamma < \omega_0$, their normalized autocorrelation functions are:

$$\frac{\mathrm{E}\left[\Delta\delta\left(t\right)\Delta\delta\left(s\right)\right]}{\sigma_{\Delta\delta}^2} = \exp\left(-\gamma\Delta t\right)\frac{\omega_0}{\omega'} \cdot \sin\left(\omega'\Delta t + \phi\right) \tag{2.14}$$

$$\frac{\mathrm{E}\left[\Delta\dot{\delta}\left(t\right)\Delta\dot{\delta}\left(s\right)\right]}{\sigma_{\Delta\dot{\delta}}^2} = \exp\left(-\gamma\Delta t\right)\frac{-\omega_0}{\omega'} \cdot \sin\left(\omega'\Delta t - \phi\right) \tag{2.15}$$

where $\Delta t = t - s$ and $\omega' = \sqrt{\omega_0^2 - \gamma^2}$ as above.

If $\omega_0 = 0$, the variance of $\Delta\dot{\delta}$ can be calculated from (2.13) and the autocorrelation of $\Delta\dot{\delta}$ is as follows:

$$\frac{\mathrm{E}\left[\Delta\dot{\delta}\left(t\right)\Delta\dot{\delta}\left(s\right)\right]}{\sigma^2_{\Delta\dot{\delta}}} = \exp\left(-2\gamma\Delta t\right) \tag{2.16}$$

2.3.3 Autocorrelation and Variance of Algebraic Variables

In order to compute the autocorrelation functions of the algebraic variables, we calculated the algebraic variables as linear functions of the differential variable $\Delta\delta$ and the noise η, by linearizing $\underline{F_2}$ in (2.2):

$$\Delta y_i\left(t\right) = C_{i,1}\Delta\delta\left(t\right) + C_{i,2}\eta \tag{2.17}$$

where y_i is an algebraic variable, and $C_{i,1}, C_{i,2}$ are constants. Then, the autocorrelation of Δy_i for $t \geq s$ is:

$$\begin{aligned}\mathrm{E}\left[\Delta y_i\left(t\right)\Delta y_i\left(s\right)\right] &= C^2_{i,1}\cdot\mathrm{E}\left[\Delta\delta\left(t\right)\Delta\delta\left(s\right)\right] + \\ &\quad C_{i,1}C_{i,2}\cdot\mathrm{E}\left[\Delta\delta\left(t\right)\eta\left(s\right)\right] + \\ &\quad C^2_{i,2}\cdot\mathrm{E}\left[\eta\left(t\right)\eta\left(s\right)\right]\end{aligned} \tag{2.18}$$

In deriving (2.18), we used the fact that $\mathrm{E}\left[\Delta\delta\left(s\right)\eta\left(t\right)\right] = 0$ since the system is causal. Equation (2.18) shows that, in order to calculate the autocorrelation of $\Delta y_i\left(t\right)$, it is necessary to calculate $\mathrm{E}\left[\Delta\delta\left(t\right)\eta\left(s\right)\right]$, which can be found from (2.9):

$$\begin{aligned}\mathrm{E}\left[\Delta\delta\left(t\right)\eta\left(s\right)\right] &= -\exp\left(-\gamma\Delta t\right)\cdot\frac{f}{\omega'}\cdot \\ &\quad \sin\left(\omega'\Delta t\right)\sigma^2_\eta\end{aligned} \tag{2.19}$$

This shows that $\mathrm{cov}\left(\Delta\delta, \eta\right) = 0$.

In order to use (2.18) to compute the variance of Δy_i, we need to carefully consider our model of noise in numerical computations. According to (2.4), the variance of η is

infinite, because the delta function is infinite at $t = s$, which would mean that the variance of Δy_i could be infinite. However, the noise in numerical simulations must have a finite variance. To determine it, we rewrite (2.6) as follows:

$$d\underline{z}\left(t\right) = A\underline{z}\left(t\right)dt + Bd\underline{W}\left(t\right) \tag{2.20}$$

where $d\underline{W}\left(t\right) = \eta dt$ is the Wiener process. It is well-known that the variance of $dW\left(t\right)$ is $\sigma_\eta^2 dt$ (Gardiner 2010). In numerical simulations, $dt = \tau_{\text{int}}$, where τ_{int} is the integration time step. Thus, $E\left[dW_{\text{num}}^2\right] = \mathrm{E}\left[\left(\eta_{\text{num}}\tau_{int}\right)^2\right] = \sigma_\eta^2\tau_{\text{int}}$. Hence, $E\left[\eta_{\text{num}}^2\right] = \sigma_\eta^2/\tau_{\text{int}}$. Then from (2.17),

$$\sigma_{\Delta y_i}^2 = C_{i,1}^2\sigma_{\Delta\delta}^2 + C_{i,2}^2\frac{\sigma_\eta^2}{\tau_{\text{int}}} \tag{2.21}$$

Combining (2.12) and (2.21) results in the following:

$$\sigma_{\Delta y_i}^2 = \left(\frac{C_{i,1}^2 f^2}{4\gamma\omega_0^2} + \frac{C_{i,2}^2}{\tau_{\text{int}}}\right)\sigma_\eta^2 \tag{2.22}$$

Combining (2.12), (2.14), (2.18) , (2.19) and (2.22), we calculated the normalized autocorrelation function of Δy_i:

$$\begin{aligned}\frac{\mathrm{E}\left[\Delta y_i\left(t\right)\Delta y_i\left(s\right)\right]}{\sigma_{\Delta y_i}^2} &= \exp\left(-\gamma\Delta t\right)\sin\left(\omega'\Delta t + \phi_{\Delta y_i}\right)\cdot \\ &\quad \frac{C_{i,1}f\omega_0\sqrt{\lambda}}{\omega'\left(C_{i,1}^2 f^2 + 4C_{i,2}^2\gamma\omega_0^2\right)}\end{aligned} \tag{2.23}$$

where $\lambda = \sqrt{C_{i,1}f\left(C_{i,1}f - 8C_{i,2}\gamma^2\right) + \left(4C_{i,2}\omega_0\gamma\right)^2}$, $\phi_{\Delta y_i} = \arctan\left(\frac{C_{i,1}f\omega'}{\left(C_{i,1}f\gamma - 4C_{i,2}\gamma\omega_0^2\right)}\right)$.

2.3.4 Numerical Simulation

We numerically solved (2.1) and (2.2) using a trapezoidal ordinary differential equation solver, as follows. First, (2.1) was written as:

$$\dot{\underline{z}} = \underline{\mathcal{F}_1} \equiv \begin{bmatrix} z_2 \\ -2\gamma z_2 - F_1 \end{bmatrix} \tag{2.24}$$

where $\underline{z} = (z_1, z_2)^T$was defined after (2.6). Then, (2.1) and (2.2) were discretized:

$$\underline{z}^{(n+1)} - \underline{z}^{(n)} = \frac{\tau_{int}}{2}\left(\underline{\mathcal{F}_1}^{(n)} + \underline{\mathcal{F}_1}^{(n+1)}\right) \tag{2.25}$$

$$0 = \underline{\mathcal{F}_2}^{(n+1)} \tag{2.26}$$

where τ_{int} is a fixed integration time step, $\underline{z}^{(n)}, \underline{z}^{(n+1)}$ are the solutions at times $t^{(n)} = n\tau_{int}$ and $t^{(n+1)} = (n+1)\,\tau_{int}$, $\underline{F_2^{(n+1)}} \equiv \underline{F_2}\left(\underline{z}^{(n+1)}, \underline{y}^{(n+1)}, \eta^{(n+1)}\right)$, and similarly for $\underline{\mathcal{F}_1}^{(n)}, \underline{\mathcal{F}_1}^{(n+1)}$. The nonlinear algebraic system (2.25), (2.26) was solved by Newton's method for $\underline{z}^{(n+1)}$ and $\underline{y}^{(n+1)}$, with values $\underline{z}^{(n)}$ and $\underline{y}^{(n)}$ being known from the previous step and $\eta^{(n+1)}$ being a random variable generated at $t^{(n+1)}$. Note that $\eta^{(n)}$ and $\eta^{(n+1)}$ are uncorrelated, and, according to the discussion after (2.20), the variance of $\eta^{(n)}$ was $\sigma_\eta^2/\tau_{\text{int}}$. The integration time step τ_{int} was chosen to be 0.01s, which is about ten times smaller than Δt, where Δt is the time lag for calculation of the autocorrelation.

In order to determine numerical mean values in this chapter, each set of SDEs was simulated 100 times. In each case the resulting averages were compared with analytical means.

2.4 Single Machine Infinite Bus System

Analysis of small power system models can be helpful for understanding the concepts of power system stability. The single machine infinite bus system has long been used to understand the behavior of a generator connected to a larger system through a long transmission line. It has also been used to explore the small signal stability of synchronous

machines (Demello and Concordia 1969) and to evaluate control techniques to improve transient stability and voltage regulation (Wang et al. 1993). Recently, there has been increased interest in stochastic behavior of power systems, in part due to the integration of renewable energy sources. A few of these papers use stochastic SMIB models. For example, references (Wang and Crow 2013), (Wei and Luo 2009) studied stability in a stochastic SMIB system.

2.4.1 Stochastic SMIB System Model

Fig. 2.1 shows the stochastic SMIB system. Equation (2.27), which combines the mechanical swing equation and the electrical power produced by the generator, fully describes the dynamics of this system:

$$M\ddot{\delta} + D\dot{\delta} + \frac{(1+\eta)E'_a}{X}\sin(\delta) = P_m \tag{2.27}$$

where $(\eta \sim \mathcal{N}(0, 0.01))$ is a white Gaussian random variable added to the voltage magnitude of the infinite bus to account for the noise in the system, M and D are the combined inertia constant and damping coefficient of the generator and turbine, and $E_a^{'}$ is the transient emf. The reactance X is the sum of the generator transient reactance $(X_d^{'})$ and the line reactance (X_l), and P_m is the input mechanical power. The values of parameters used in this section are given below:

$$D = 0.03\tfrac{\text{pu}}{rad/s}, H = 4\tfrac{MW.s}{MVA}, X'_d = 0.15\text{pu},$$

$$X_l = 0.2\text{pu}, \omega_s = 2\pi \cdot 60\text{rad/s}$$

Note that $M = 2H/\omega_s$, where H is the inertia constant in seconds, and ω_s is the rated speed of the machine. The generator and the system base voltage levels are 13.8kV and 115kV, and both the generator and system per unit base are set to 100MVA. The generator transient reactance $X_d^{'} = 0.15 \cdot (13.8/115)^2$ pu, on the system pu base. The third term on the left-hand side of (2.27) is the generator's electrical power (P_g).

In order to test the system at various load levels, we solved the system for different equilibria, with the generator's mechanical and electrical power equal at each equilibrium:

$$P_m = P_{g0} = \frac{E_a^{'}}{X} \sin\left(\delta_0\right) \tag{2.28}$$

where δ_0 is the equilibrium value of the generator's rotor angle.

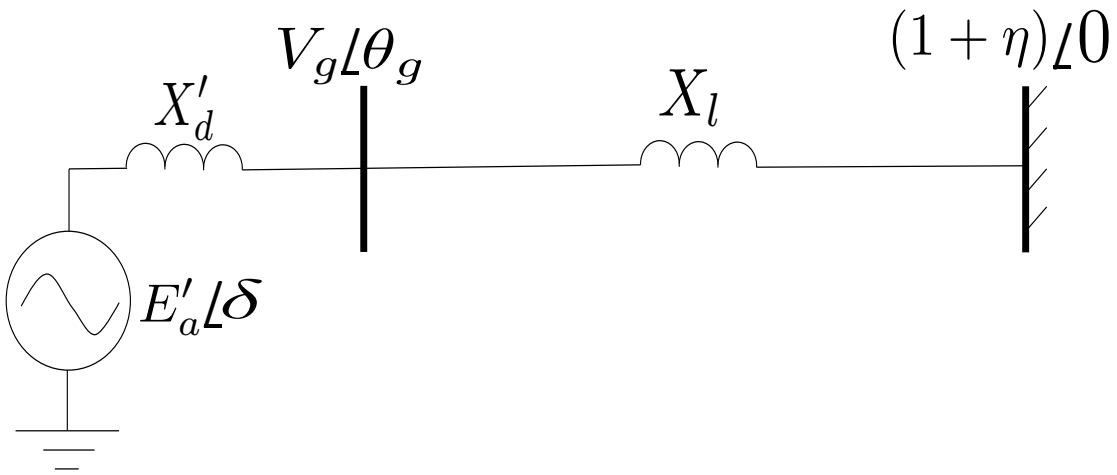

Figure 2.1: Stochastic single machine infinite bus system used in Sec. 2.4. The notation $V_g \underline{/\theta_g}$ represents $V_g \exp\left[j\theta_g\right]$.

2.4.2 Autocorrelation and Variance

In this section, we calculate the autocorrelation and variance of the algebraic and differential variables of this system using the method in Sec. 2.3. Equations (2.1) and (2.2) describe this system for which the following equalities hold:

$$\gamma = \frac{D}{2M};\ \omega_0 = \sqrt{\frac{E_a' \cos\delta_0}{MX}};\ \underline{y} = \begin{bmatrix} V_g & \theta_g \end{bmatrix}^T \tag{2.29}$$

$$f = \frac{P_{g0}}{M};\ F_1\left(z, \underline{y}, \eta\right) = \frac{\left(\frac{(1+\eta)E_a^{'}}{X} \sin\delta - P_m\right)}{M} \tag{2.30}$$

where $\Delta V_g = V_g - V_{g0}, \Delta\theta_g = \theta_g - \theta_{g0}$ are the deviations of, respectively, the generator terminal busbar's voltage magnitude and angle from their equilibrium values. Equations (2.29) and (2.30) show that f increases, while ω_0 decreases, with δ_0.

In order to calculate the algebraic equations, which form $\underline{F_2}(\delta, y, \eta)$ in (2.2), we wrote Kirchhoff's current law at the generator's terminal:

$$\frac{E'_a e^{j\delta} - V_g e^{j\theta_g}}{jX'_d} + \frac{1 + \eta - V_g e^{j\theta_g}}{jX_l} = 0 \tag{2.31}$$

Separating the real and imaginary parts in (2.31) gives:

$$V_g \sin(\theta_g) = \alpha E'_a \sin(\delta) \tag{2.32}$$

$$V_g \cos(\theta_g) = \alpha E'_a \cos(\delta) + (1 + \eta)(1 - \alpha) \tag{2.33}$$

where $\alpha = X_l/(X_l + X'_d)$. Equations (2.32) and (2.33) combine to make $\underline{F_2}(\delta, y, \eta)$ in (2.2).

Linearizing (2.32) and (2.33) yields the coefficients in (2.17), which are necessary for calculating the autocorrelation and variance of the algebraic variables ($y_1 = \Delta V_g, y_2 = \Delta\theta_g$):

$$C_{1,1} = \alpha E'_a \sin(\theta_{g0} - \delta_0) \tag{2.34}$$

$$C_{1,2} = (1 - \alpha)\cos(\theta_{g0}) \tag{2.35}$$

$$C_{2,1} = \alpha E'_a \cos(\theta_{g0} - \delta_0) \tag{2.36}$$

$$C_{2,2} = -(1 - \alpha)\sin(\theta_{g0}) \tag{2.37}$$

Fig. 2.2 shows the decrease of ω', which is the imaginary part of the eigenvalues of A in (2.7), with P_m. Note that the bifurcation occurs at $b = 5$pu. This figure illustrates how it can be difficult to accurately foresee a bifurcation by computing the eigenvalues of a system (as in, e.g., (Chiang et al. 1990)), if there is noise in the measurements feeding the

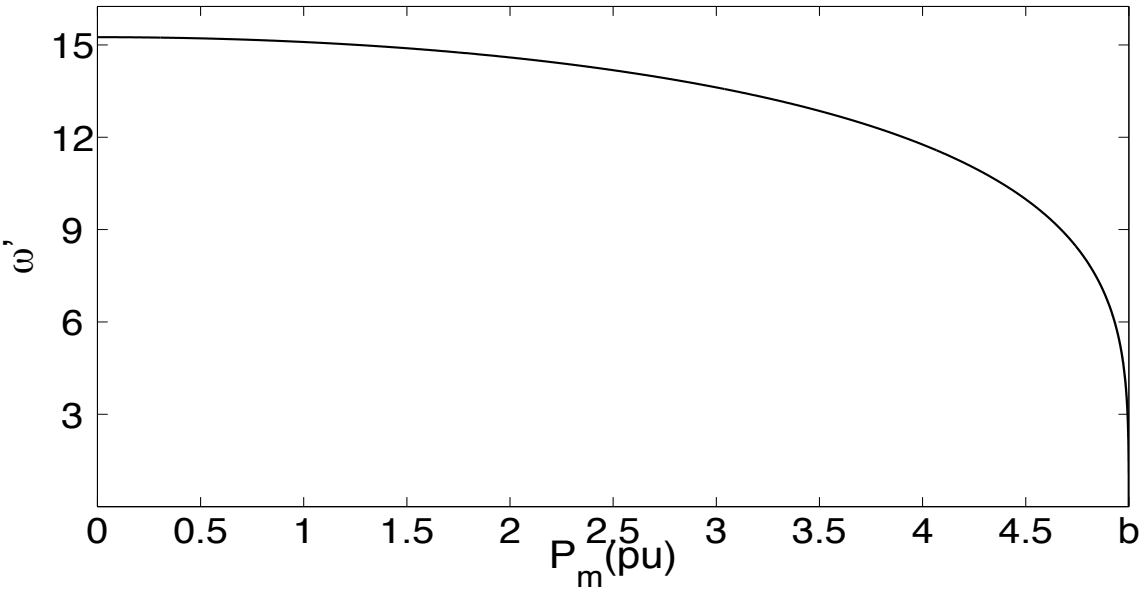

Figure 2.2: The decrease of ω' with P_m in the SMIB system. Near the bifurcation, ω' is very sensitive to changes in P_m. In this figure, and most that follow, b is the value of the bifurcation parameter (P_m in this system) at the bifurcation.

calculation. The value of $\omega' \sim (P_m - \text{b})^{1/4}$ does not decrease by a factor of two (compared to its value at $P_m = 1.0$pu) until $P_m = 4.83$pu (only $< 3.4\%$ away from the bifurcation). It decreases by another factor of two at $P_m = 4.99$pu (0.2% away from the bifurcation). Also, note that the real part of the eigenvalues equals $-\gamma$ until very close to the bifurcation (0.1% away from the bifurcation), so it does not provide a useful indication of proximity to the bifurcation either, Thus, one can confidently predict from ω' the imminent occurrence of the bifurcation only very near it, which may be too late to avert it. On the other hand, we will demonstrate below that for this system, autocorrelation functions can provide substantially more advanced warning of the bifurcation.

Using autocorrelation as an early warning sign of a bifurcation requires one to carefully select a time lag, $\Delta t = t - s$, such that changes in autocorrelation are observable. To understand the impact of different time lags, we computed the autocorrelation function of $\Delta\delta$ (see Fig. 2.3). From (2.14), the autocorrelation of $\Delta\delta$ crosses zero at $\Delta t_0 = \frac{2\pi - \phi}{\omega'}$. We note that choosing Δt close to, but below, Δt_0 allows one to observe a monotonic increase of autocorrelation as P_m increases. Indeed, for $\Delta t > \Delta t_0$, autocorrelation may not increase

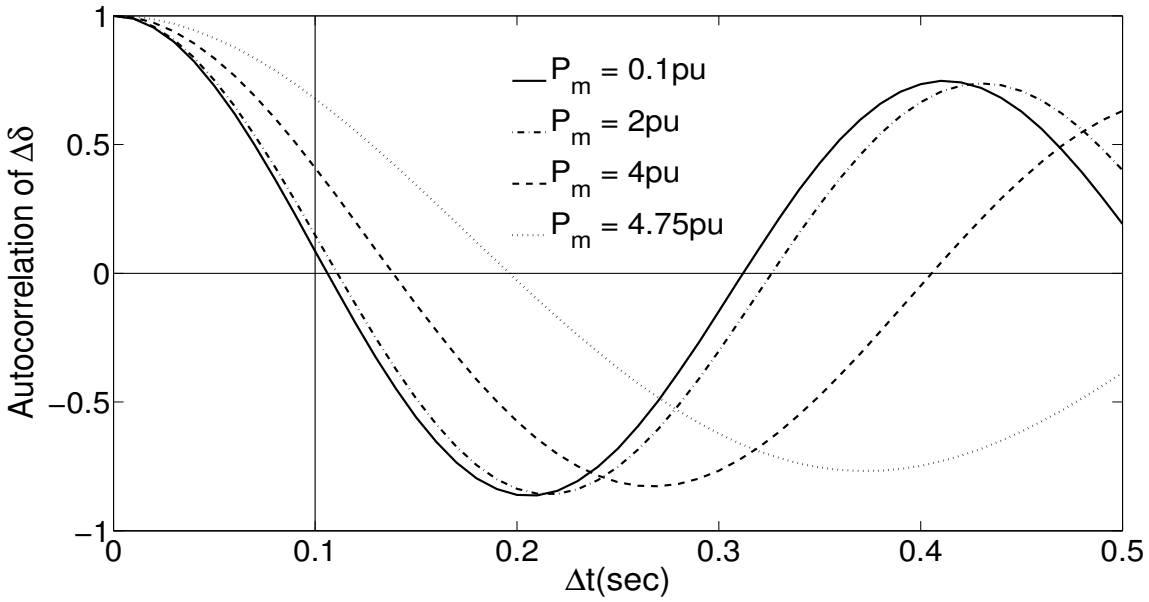

Figure 2.3: Autocorrelation function of $\Delta\delta$. $\Delta t = 0.1$s is close to 1/4 of the smallest period of the function for all values of P_m.

monotonically, or the autocorrelation for some values of P_m may be negative. For example, in Fig. 2.3 for $\Delta t = 0.3$s, the autocorrelation decreases first and then increases with P_m. On the other hand, for Δt considerably smaller than Δt_0, the increase of the autocorrelation may not be large enough to be measurable. In Fig. 2.3, the curves converge as $\Delta t \to 0$. Given that the smallest period of oscillation $(T = 2\pi/\omega')$ in this system is 0.41s, we chose $\Delta t = 0.1$s for the autocorrelation calculations in this section.

Using (2.12)–(2.15), we calculated the variance and autocorrelation of $\Delta\delta$, $\Delta\dot{\delta}$ at different operating points. In Fig. 2.4, these analytical results are compared with the numerical ones. To initialize the numerical simulations, we assumed that $V_{g0} = 1$pu and solved for E'_a in (2.32), (2.33) to obtain $V_g = V_{g0}$ (for $\eta = 0$). We chose the integration step size $\tau_{int} = 0.01$s, which is much shorter than the the smallest period of oscillation ($T = 0.41$s) and the time lag Δt. The numerical results are shown for the range of bifurcation parameter values for which the numerical solutions were stable.

In order to determine if variance and autocorrelation measurably increase as load approaches the bifurcation, we compared a base load level (the normal operating condition of the system) with a load level that is high, and closer to the bifurcation, but still some

distance from the bifurcation (far enough that an operator would have time to take precautionary control actions). Since our aim is to study early warning signs of the bifurcation, we use the differences between these two states as an indication of whether particular variables provide observable early warning. While different load values for these two points could be chosen for different systems, in this chapter we assume that the base level is 20% of the load at the bifurcation point , and the high load level is at 80%. Therefore, we computed the ratio of each statistic when load is at 80% of the bifurcation value to the value when load is at 20% of b. This ratio, $q_{\frac{80}{20}}$ in Fig. 2.4, is defined as follows:

$$q_{\frac{80}{20}} = \frac{\text{Autocorrelation of } u \text{ or } \sigma_u^2|_{P_m=0.8b}}{\text{Autocorrelation of } u \text{ or } \sigma_u^2|_{P_m=0.2b}} \tag{2.38}$$

where u is the plot's variable. In subsequent figures, $q_{\frac{80}{20}}$ is defined similarly.

Fig. 2.4 shows that the variance of both $\Delta\delta$ and $\Delta\dot{\delta}$ increases substantially with P_m, and thus appears to be a good warning sign of the bifurcation. However, the two variances grow with different rates. (This becomes clear when comparing the ratios $q_{\frac{80}{20}}$ for $\Delta\delta$ and $\Delta\dot{\delta}$.) The difference becomes even more noticeable near the bifurcation where the variance of $\Delta\delta$ increases much faster than the variance of $\Delta\dot{\delta}$. This is caused by the term ω_0^2 in the denominator of the expression for the variance of $\Delta\delta$ in (2.12). In Fig. 2.4, the autocorrelation of $\Delta\delta$ and $\Delta\dot{\delta}$ increases with P_m. Similar to the variance, the autocorrelation is a good early warning sign of the bifurcation. Comparing Fig. 2.4 with Fig. 2.2 (where an equivalent $q_{\frac{80}{20}}$ would be 1.28) shows that the autocorrelations and variances of $\Delta\delta$ and $\Delta\dot{\delta}$ provide a substantially stronger early warning sign, relative to using eigenvalues to estimate the distance to bifurcation in this system.

The results for the algebraic variables are mainly similar. Fig. 2.5 show the variance and autocorrelation of $\Delta V_g, \Delta\theta_g$ as a function of load. In Fig. 2.5, the variance of ΔV_g decreases with P_m until the system gets close to the bifurcation, while the variance of $\Delta\theta_g$ increases with P_m even if the system is far from the bifurcation. The autocorrelations of both ΔV_g and $\Delta\theta_g$ in Fig. 2.5 increase with P_m. However, the ratio $q_{\frac{80}{20}}$ in (2.38) is much

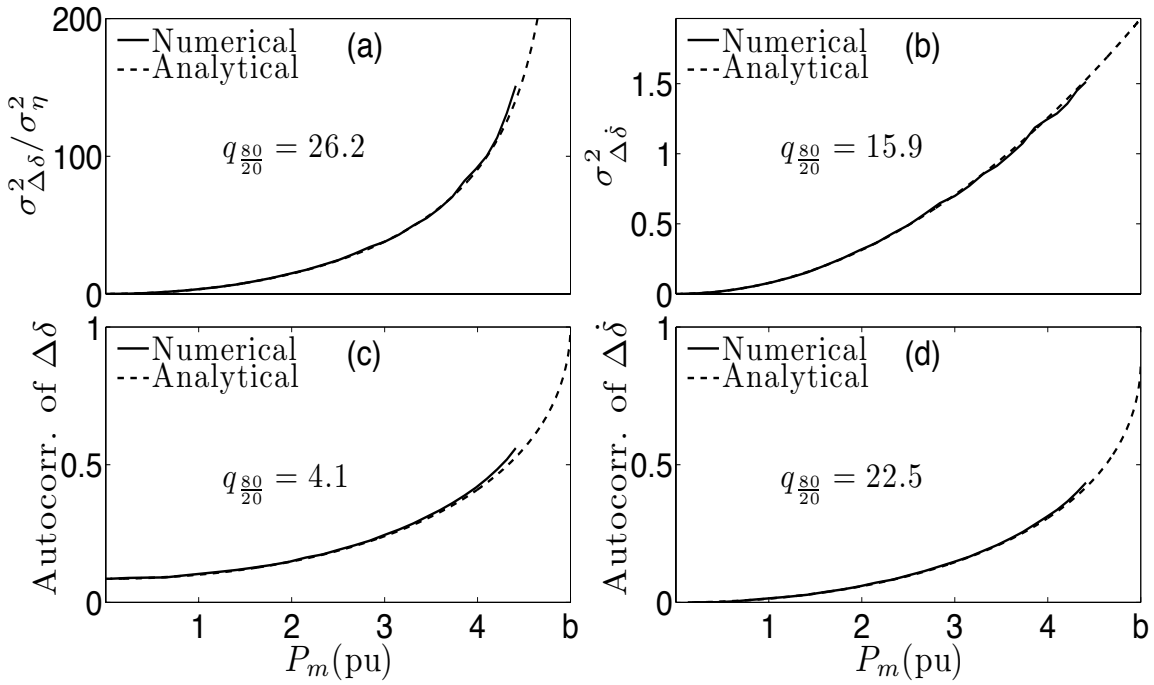

Figure 2.4: Panels a,b show the variances of $\Delta\delta, \Delta\dot{\delta}$ versus mechanical power (P_m) values. Panels c,d show the autocorrelations of $\Delta\delta, \Delta\dot{\delta}$ versus mechanical power (P_m) values. The autocorrelation values are normalized by dividing by the variances of the variables.

larger for ΔV_g than for $\Delta\theta_g$. This is caused by the autocorrelation of ΔV_g being very close to zero for small values of P_m.

2.4.3 Discussion

These results can be better understood by observing the trajectory of the eigenvalues of the SMIB system (Fig. 2.6). Near the bifurcation, the eigenvalues are very sensitive to changes in the bifurcation parameter. As a result, the system is in the overdamped regime $(\omega_0 < \gamma)$ for much less than 0.1% distance in terms of P_m to the critical transition. This implies that, at least for this system, the autocorrelation function in (Podolsky and Turitsyn 2013a) and (Podolsky and Turitsyn 2013b), is valid only when the system is within 0.1% of the saddle-node bifurcation. By considering a range of system parameters, we observed that the region where one eigenvalue determines the system dynamics is within 1.5% of the bifurcation point at most. The width of this region scales approximately with D^2, X_l and $1/H$. Because the method in (Podolsky and Turitsyn 2013a) and (Podolsky and

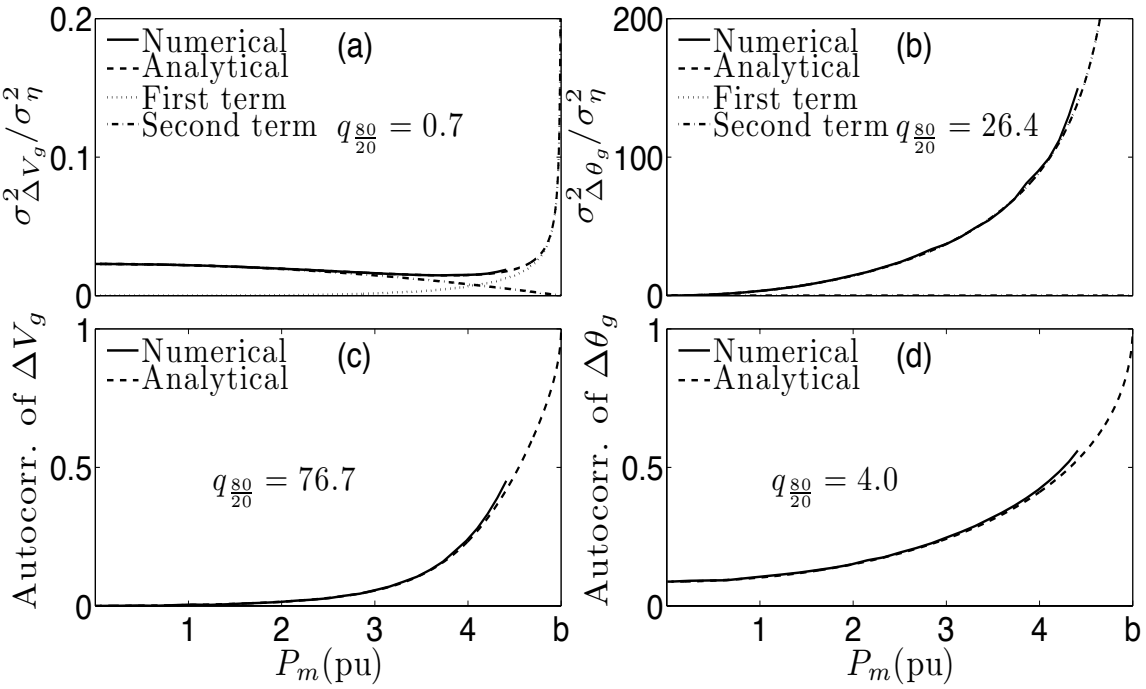

Figure 2.5: Panels a,b show the variances of ΔV_g and $\Delta\theta_g$ versus mechanical power (P_m) levels. The two terms comprising the variances in (2.21) are also shown. Panels c,d show the autocorrelations of ΔV_g and $\Delta\theta_g$ versus P_m.

Turitsyn 2013b), can provide a good estimate of the autocorrelations and variances of state variables only for a very short range of the bifurcation parameter, it may not be particularly useful as an early warning sign of bifurcation.

From Figs. 2.4,2.5, we can observe that, except for the variance of ΔV_g, the variances and autocorrelations of all state variables increase when the system is more loaded. This demonstrates that CSD occurs in this system as it approaches bifurcation, as suggested both by general results (Kuehn 2011), and prior work for power systems (Cotilla-Sanchez et al. 2012, Podolsky and Turitsyn 2013b). As an example, we calculated the variances of $\Delta\delta$ and $\Delta\dot{\delta}$ as a function of the system parameters using (2.12), (2.13) and (2.29):

$$\sigma^2_{\Delta\delta} = \frac{E'_a\sigma^2_\eta}{2X^2D}\cdot\frac{\sin^2\delta_0}{\cos\delta_0} \tag{2.39}$$

$$\sigma^2_{\Delta\dot{\delta}} = \frac{E'^2_a\sigma^2_\eta}{2MX^2D}\cdot\sin^2\delta_0 \tag{2.40}$$

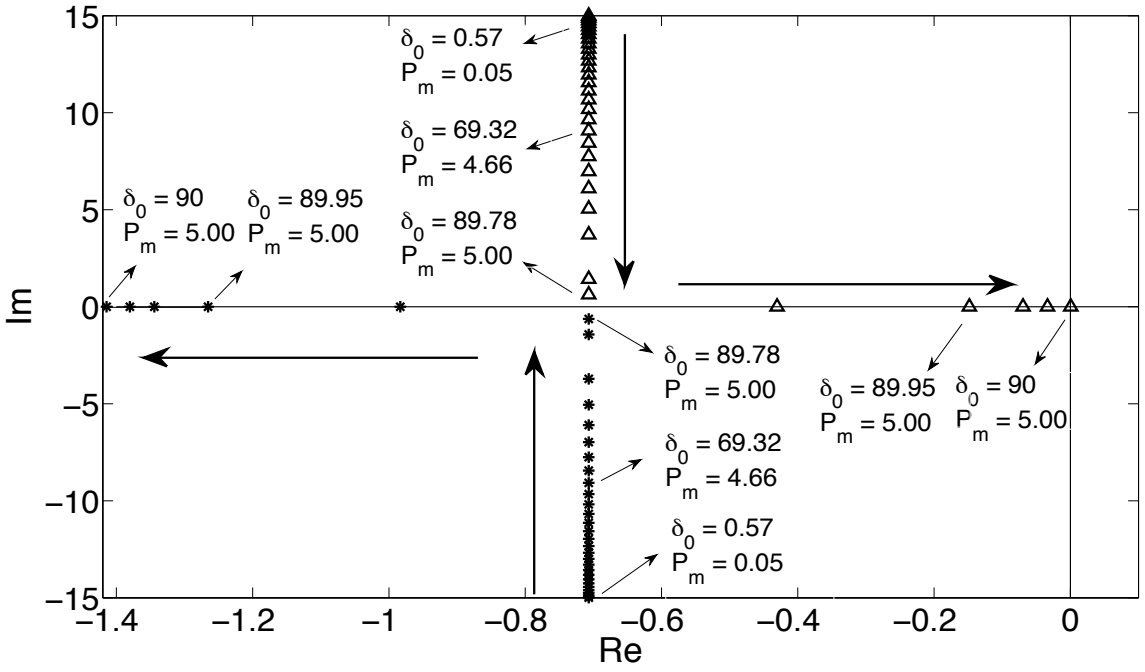

Figure 2.6: Eigenvalues of the first system as the bifurcation parameter (mechanical power) is increased. The arrows show the direction of the eigenvalues' movement in the complex plane as P_m is increased. The values of P_m and δ_0 are given for several eigenvalues.

It can be observed from these expressions that as the system approaches the bifurcation ($\delta_0 \longrightarrow 90$), the variable terms $\frac{\sin^2 \delta_0}{\cos \delta_0}, \sin^2 \delta_0$ also increase. As a result, variance of $\Delta\delta, \Delta\dot{\delta}$ both increase under all conditions.

In addition to validating these prior results, several new observations can be made. For example, the signs of CSD are more clearly observable in some variables than in others. While all of the variables show some increase in autocorrelation and variance, they are less clearly observable in ΔV_g. The variance of ΔV_g decreases with P_m slightly until the vicinity of the bifurcation. In comparison, the variance of $\Delta\theta_g$ always increases with P_m. Fig. 2.5 shows the two terms of the expressions for the variances of ΔV_g and $\Delta\theta_g$ in (2.21). The second term of the variance of $\Delta\theta_g$ is very small compared to the first term, and the first term is always dominant and growing. On the other hand, the second term of the variance of ΔV_g is more significant for small P_m. This term decreases with P_m, which can be observed from the expression for $C_{1,2}$ in (2.35). Accordingly, decrease of $C_{1,2}$ with P_m causes the the variance of ΔV_g to decrease with P_m until the vicinity of the bifurcation.

In conclusion, the variance of $\Delta\theta_g$ is a better indicator of proximity to the bifurcation. Because the variables $\Delta\delta$ and $\Delta\dot{\delta}$ are highly correlated with $\Delta\theta_g$, their variances are also good indicators of proximity to the bifurcation.

The rate at which autocorrelation increases with P_m differs significantly in Figs. 2.4 and 2.5. In Fig. 2.4, the ratio $q_{\frac{80}{20}}$ in (2.38) is 5.5 times larger for $\Delta\dot{\delta}$ than for $\Delta\delta$. The normalized autocorrelation functions of $\Delta\delta$ and $\Delta\dot{\delta}$ are as follows:

$$\begin{aligned} \mathrm{E}\left[\Delta\delta\left(t\right)\Delta\delta\left(s\right)\right]/\sigma_{\Delta\delta}^{2} &= \exp\left(-\gamma\Delta t\right)\frac{\omega_0}{\omega'} \\ &\quad\cdot\sin\left(\omega'\Delta t+\phi\right) \end{aligned} \tag{2.41}$$

$$\begin{aligned} \mathrm{E}\left[\Delta\dot{\delta}\left(t\right)\Delta\dot{\delta}\left(s\right)\right]/\sigma_{\Delta\dot{\delta}}^{2} &= \exp\left(-\gamma\Delta t\right)\frac{\omega_0}{\omega'} \\ &\quad\cdot\sin\left(\omega'\Delta t+\pi-\phi\right) \end{aligned} \tag{2.42}$$

The difference between the two functions is in the phase of the sine function which causes the values of the two autocorrelations to be different. $q_{\frac{80}{20}}$ is so much larger for $\Delta\dot{\delta}$ than for $\Delta\delta$ because of the time lag (Δt) used to compute autocorrelation. $\Delta t = 0.1$s is close to the zero crossing of the autocorrelation function of $\Delta\dot{\delta}$, causing the large $q_{\frac{80}{20}}$. This difference illustrates the importance of choosing an appropriate time lag.

It is important to note that although the growth ratio of the autocorrelation for $\Delta\delta$ is not large compared to $\Delta\dot{\delta}$, it can be increased by subtracting a bias value from the autocorrelation values for $P_m = 0.2b$(pu) and $P_m = 0.8b$(pu). For example, if the value of 0.075 is subtracted from the autocorrelation values, the ratio $q_{\frac{80}{20}}$ increases from 4.1 to 13.0.

The results also show the nonlinearity of F_1 in (2.30), causes the changes in autocorrelation and variance of the system variables. In (Gardiner 2010), it is shown that the stationary time correlation matrix of (2.6) can be calculated using the following equation:

$$\mathrm{E}\left[\underline{Z}\left(t\right)\underline{Z}^{T}\left(s\right)\right] = \exp\left[-A\Delta t\right]\sigma \tag{2.43}$$

where σ is the covariance matrix of the state variables. Thus, the normalized autocorrelation matrix depends only on A and the time lag. One of the elements of the state

matrix $(-\omega_0^2)$ in (2.7) changes with P_m because of the nonlinear relationship between the electrical power (P_g) and the rotor angle in F_1. Thus, in this system, CSD is caused by the nonlinearity of F_1.

2.5 Single Machine Single Load System

The single machine infinite bus system illustrates how CSD can occur in a generator connected to a large power grid, through a long line. In this section we use a generator to represent the bulk grid, and look for signs of CSD caused by a stochastically varying load. Some form of the single machine single load (SMSL) model used in this section has been used extensively to study voltage collapse (e.g., (Dobson et al. 2002, Kundur et al. 1994)).

2.5.1 Stochastic SMSL System Model

The second system (shown in Fig. 2.7) consists of one generator, one load and a transmission line between them. The random variable η defined in (2.3) and (2.4), is added to the load to model its fluctuations. The load consists of both active and reactive components. In order to stress the system, the baseline load S_d is increased, while keeping the noise intensity (S_{d0}) and the load's power factor constant. The reason for keeping the noise intensity constant was to ensure that the increase of variables' variances is not due to the increase of the noise level.

A set of differential-algebraic equations comprising the swing equation and power flow equations describe this system. The swing equation and the generator's electrical power equation are given below:

$$M\ddot{\delta} + D\dot{\delta} = P_m - P_g \tag{2.44}$$

$$\begin{aligned} P_g &= E_a^{'} V_l G_{gl} \cos(\delta - \theta_l) \\ &\quad + E_a^{'} V_l B_{gl} \sin(\delta - \theta_l) + E_a^{'2} G_{gg} \end{aligned} \tag{2.45}$$

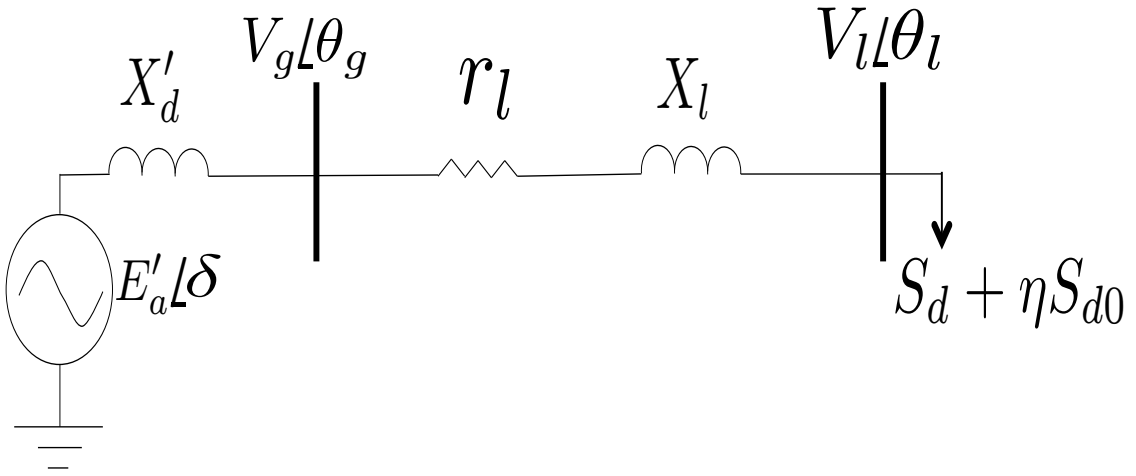

Figure 2.7: Single machine single load system.

where V_l, θ_l are voltage magnitude and angle of the load busbar, G_{gl}, G_{gg} and B_{gl} are as follows:

$$G_{gg} = -G_{gl} = \mathsf{Re}\left(\frac{1}{r_l + jX_l}\right) \tag{2.46}$$

$$B_{gl} = -\mathsf{Im}\left(\frac{1}{r_l + jX_l}\right) \tag{2.47}$$

The power flow equations at the load bus are as follows:

$$\begin{aligned} -P_d - P_{d0}\eta &= E_a^{'} V_l G_{gl} \cos(\theta_l - \delta) \\ &\quad + E_a^{'} V_l B_{gl} \sin(\theta_l - \delta) + V_l^2 G_{ll} \end{aligned} \tag{2.48}$$

$$\begin{aligned} -Q_d - Q_{d0}\eta &= E_a^{'} V_l G_{gl} \sin(\theta_l - \delta) \\ &\quad - E_a^{'} V_l B_{gl} \cos(\theta_l - \delta) - V_l^2 B_{ll} \end{aligned} \tag{2.49}$$

where $G_{ll} = G_{gg}$, $B_{ll} = -B_{gl}$, and P_{d0}, Q_{d0} are constant values. The parameters of this system are similar to the SMIB system, with the following additional parameters: $r_l = 0.025\Omega, P_{d0} = 1$pu, $pf = 0.95$lead, where r_l is the line's resistance and pf is the load's power factor.

In this system, V_l, $\theta_l - \delta$ are the algebraic variables, and δ, $\dot{\delta}$ are the differential variables. The algebraic equations (2.48) and (2.49) define V_l and $\theta_l - \delta$, which then drive δ through (2.44) and (2.45). By linearizing (2.45) and the power flow equations around the equilibrium, we simplified (2.44) to the following:

$$\Delta\ddot{\delta} + \frac{D}{M}\Delta\dot{\delta} = -\frac{C_5}{M}\eta \tag{2.50}$$

where C_5 is a function of the system state at the equilibrium point. The derivation of (2.50) and the expression for C_5 are presented in Appendix 2.9. Comparing (2.5) with (2.50) yields:

$$\gamma = \frac{D}{2M}, \omega_0 = 0, f = \frac{C_5}{M} \tag{2.51}$$

The expression for the autocorrelation of $\Delta\dot{\delta}$ is given in (2.16). Note that the normalized autocorrelation of $\Delta\dot{\delta}$ does not change with the bifurcation parameter (P_d), as it did for the SMIB system. In Appendix 2.9, it is shown that ΔV_l and $\Delta\delta - \Delta\theta_l$ are proportional to η (see (2.59) and (2.60)). As a result, they are memoryless; the variables have zero autocorrelation.

Fig. 2.8 shows the analytical and numerical solutions of the variances of ΔV_l and $\Delta\delta - \Delta\theta_l$. The results also show that the variance of $\Delta\dot{\delta}$ increases modestly with P_d as the system approaches the bifurcation. Unlike the SMIB system, the variance of ΔV_l is a good early warning sign of the bifurcation. It is also much more sensitive to the increase of P_d compared to $\Delta\delta - \Delta\theta_l$ and $\Delta\dot{\delta}$.

2.5.2 Discussion

As was the case with the SMIB system, when the power flowing on the transmission line in this system reaches its transfer limit, the algebraic equations become singular. However, unlike the previous system, the differential equations of this system do not become singular at the bifurcation point of the algebraic equations. Fig. 2.9 shows the sample trajectories of the two systems' rotor angles. Both signals are Gaussian stochastic processes.

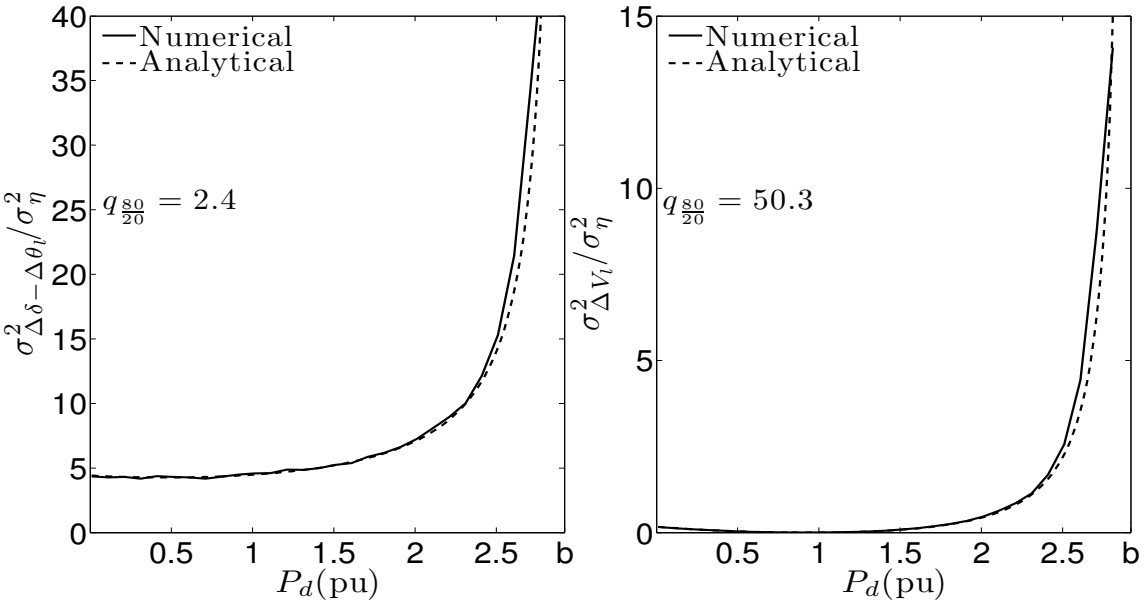

Figure 2.8: Variances of $\Delta\delta - \Delta\theta_l$ and ΔV_l for different load levels. Both variances increase with P_d as the system approaches the bifurcation.

The rotor angle in the SMIB system is an Ornstein–Uhlenbeck process while the rotor angle in the SMSL system varies like the position of the brownian particle (Horsthemke and Lefever 2006). The existence of the infinite bus in the former system causes this difference. One difference between the SMSL system and the SMIB system is the absence of the term comprising $\Delta\delta$ in (2.50) compared with (2.5). This causes the linearized state matrix to be independent of the bifurcation parameter. From (2.43), one can show that the normalized autocorrelation of $\Delta\dot{\delta}$ depends only on A and the time lag. Since A is state-independent in this system, the autocorrelation of $\Delta\dot{\delta}$ will be constant for a specific Δt.

The increase of the variances of both differential and algebraic variables is due to the non-linearity of the algebraic equations. Fig. 2.10 shows that as the load power increases, the perturbation of the load power causes a larger deviation in the load busbar voltage magnitude. Consequently, variance of this algebraic variable increases with P_d. Likewise, this nonlinearity causes the coefficient C_5 in (2.50) to increase as the load power is increased, increasing the variance of $\Delta\dot{\delta}$.

While voltage variance increases with load, this system does not technically show CSD before the bifurcation, since increases in both variance and autocorrelation are essential to conclude that CSD has occurred (Kuehn 2011). Also, the eigenvalues of the state

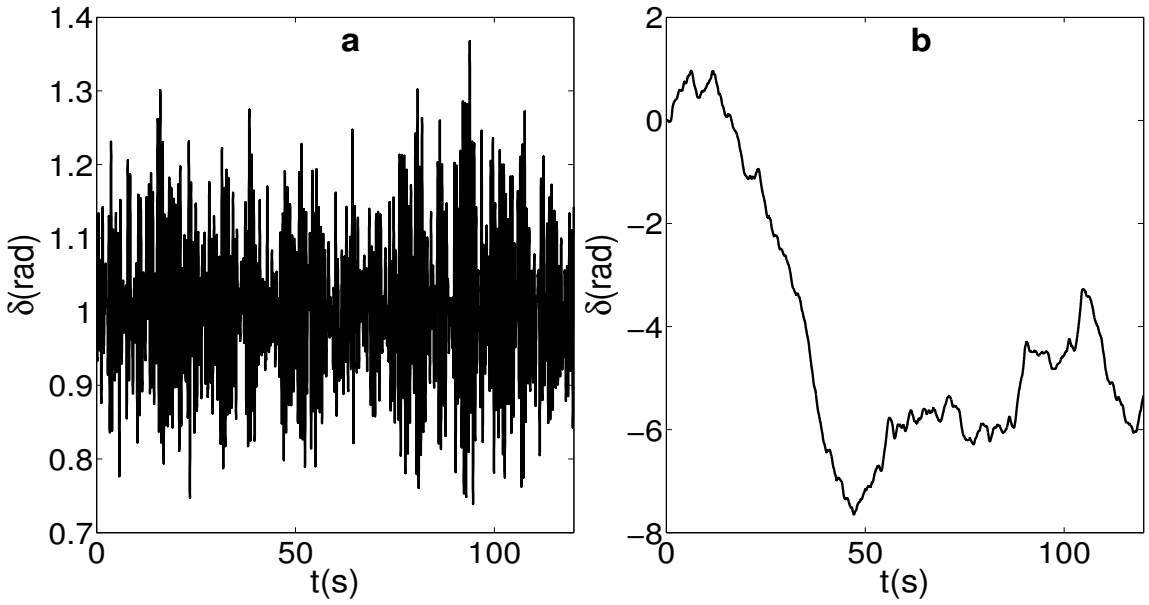

Figure 2.9: A sample trajectory of the rotor angle of (a) the SMIB system (b) the SMSL system.

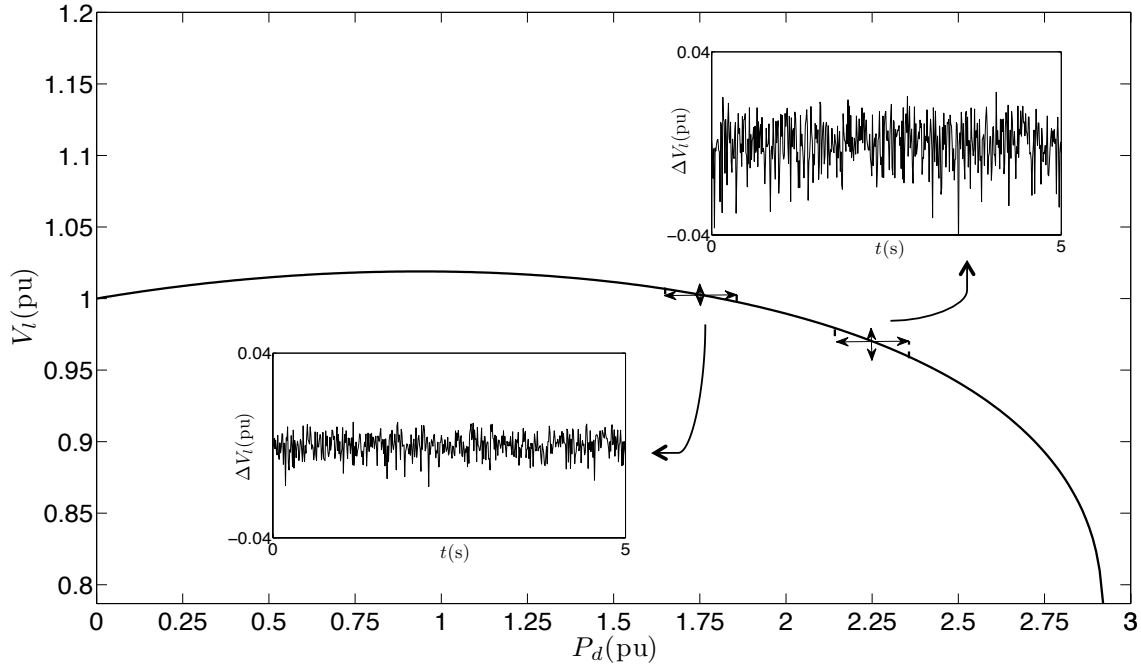

Figure 2.10: The load bus voltage as a function of load power. The load bus voltage magnitude becomes increasingly sensitive to power fluctuations as the system approaches the bifurcation. This increased sensitivity raises the voltage magnitude's variance.

matrix of this system do not vary with load. This confirms that CSD does not occur in this system, since the poles of the dynamical system do not move toward the right-half plane as the bifurcation parameter increases (Scheffer et al. 2009), (Kuehn 2011).

2.6 Three-Bus System

Real power systems have properties that are common to both the SMIB in Sec. 2.4 and the SMSL in Sec. 2.5. In order to explore CSD for a system that has both an infinite bus, and the potential for voltage collapse case, this section looks at the three-bus system in Fig. 2.11.

2.6.1 Model and Results

The three-bus system consists of a generator connected to a load bus through a transmission line, which is connected to an infinite bus through another transmission line. In the SMIB system, the bifurcation occurred in the differential equations. Increasing the load in the three-bus system causes a saddle-node bifurcation in the algebraic equations $F_1\left(\delta, \underline{y}, 0\right) = 0, \underline{F_2}\left(\delta, \underline{y}, 0\right) = 0$ (in terms of (2.1), (2.2)), as in the SMSL system. However, unlike in the SMSL system, the bifurcation in these algebraic equations also causes a bifurcation in the differential equation (2.5).

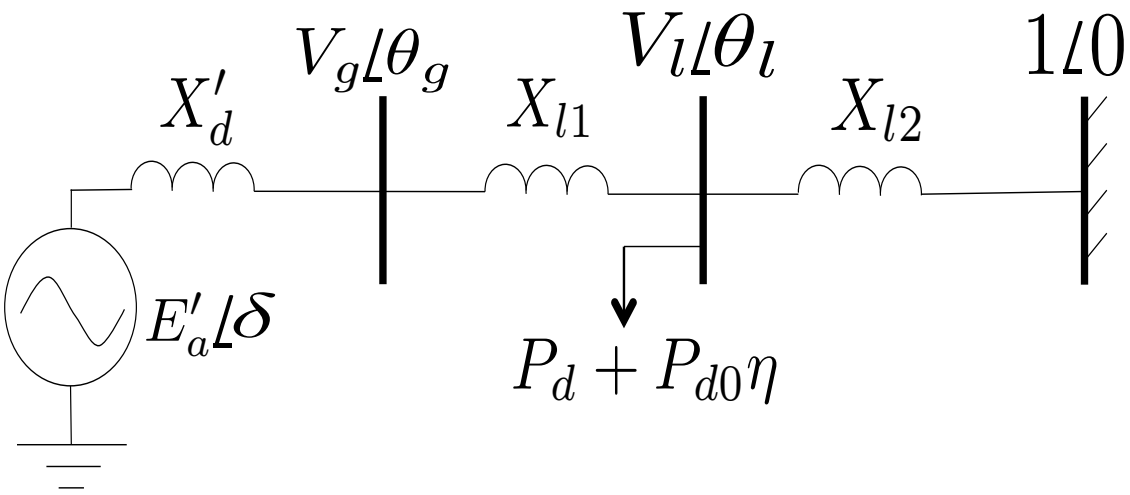

Figure 2.11: Three–bus system.

Table 2.1: Three-bus system parameters

Case no.	X_{l1}(pu)	X_{l2}(pu)	X'_d(pu)	$D\left(\frac{\text{pu}}{rad/s}\right)$
A	0.1	0.35	0.1	0.03
B	0.3	0.35	0.1	0.001

We studied this system for two different cases. Our goal in studying these two cases was to show that the CSD signs for some variables can vary differently with changing the system parameters. Table. 2.1 shows the system parameters for two cases. The rest of the parameters are similar to those in the SMIB system.

The algebraic equations of the three-bus system are as follows:

$$\left(\frac{E'_a V_l}{X}\sin\left(\delta-\theta_l\right)-\frac{2}{3}P_d\right)/M = 0 \tag{2.52}$$

$$\frac{E'_a V_l}{X}\sin\left(\delta-\theta_l\right)-\frac{V_l}{X_{l2}}\sin\left(\theta_l\right)-P_{d0}\eta = P_d \tag{2.53}$$

$$\frac{E'_a V_l}{X}\cos\left(\delta-\theta_l\right)+\frac{V_l}{X_{l2}}\cos\left(\theta_l\right) = V_l^2\cdot\left(\frac{1}{X}+\frac{1}{X_{l2}}\right) \tag{2.54}$$

where $X = X_d^{'} + X_{l1}$, V_l, θ_l are voltage magnitude and angle of the load busbar. Equation (2.52) is equivalent to $F_1\left(\delta, \underline{y}, 0\right)$ in (2.1), and (2.53), (2.54), which are the simplified active and reactive power flow equations at the load busbar, are equivalent to $F_2\left(\delta, \underline{y}, 0\right)$ in (2.2). We assumed that $P_{g0} = {}^{2P_d}/_3$, which is reflected in (2.52).

The following equalities relate this system to the general model in (2.5):

$$\gamma = \frac{D}{2M}; \omega_0^2 = \frac{-C_6}{M}; f = \frac{-C_7}{M} \tag{2.55}$$

where C_6 and C_7 are functions of the system state at the equilibrium point. The derivation and expressions for C_6, C_7 are presented in Appendix 2.10. Fig. 2.12 shows C_6, C_7 versus P_d. When the load increases, C_6 approaches 0, and a bifurcation in the differential equation (2.5) and (2.55) occurs.

Using (2.55), the expressions in Sec. 2.3.2, and (2.76), (2.77) in Appendix 2.10, we calculated the variances and autocorrelations of $\Delta\delta, \Delta\dot{\delta}, \Delta V_l$ and $\Delta\theta_l$. We chose the autocorrelation time lag Δt of the variables to be equal to 0.14s taking a similar approach

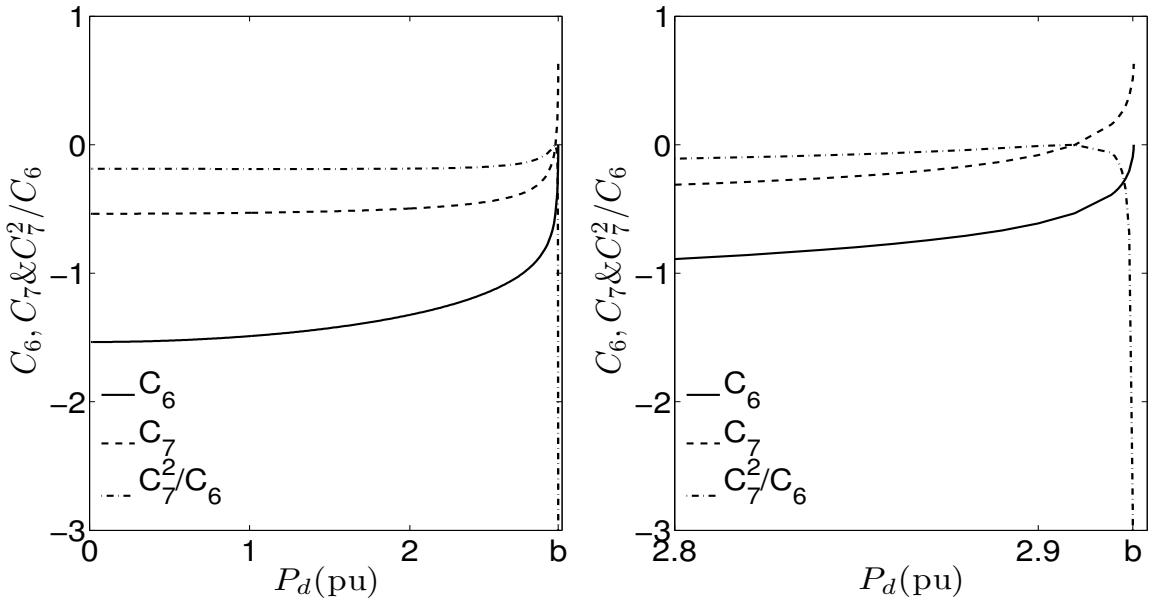

Figure 2.12: Three variables C_6, C_7 and C_7^2/C_6 derived by linearizing the Three-bus system model. The left panel shows the variables versus P_d for Case B. The right panel shows a close-up view of the variables near the bifurcation. Note that as $P_d \to P_{d,cr}$, $C_6 \to 0$ while C_7 approaches a finite value of ~ 0.6. $C_7^2/C_6 \to \infty$, as $P_d \to P_{d,cr}$.

as in Sec. 2.4.2. Although the chosen Δt may not be optimal for all of the variables, it represents a reasonable compromise between simplicity (choosing just one Δt) and usefulness as early warning signs. Figs. 2.13,2.14 compare the analytical solutions with the numerical solutions of the variances and autocorrelations of $\Delta\delta$, $\Delta\dot{\delta}$, ΔV_l and $\Delta\theta_l$.

Fig. 2.13 shows that although the growth rates of the autocorrelations of $\Delta\delta, \Delta\dot{\delta}$ are not large, the autocorrelations increase monotonically in both cases. As mentioned in Sec. 2.4.3, it is possible to have larger indicators (growth ratios) by subtracting a bias value from the autocorrelations. On the other hand, the variances of $\Delta\delta, \Delta\dot{\delta}$ in Fig. 2.13, do not monotonically increase for case B. We will explain this behavior in the next subsection. As a result, they are not reliable indicators of proximity to the bifurcation.

Fig. 2.14 shows that although both variances of ΔV_l and $\Delta\theta_l$ increase with P_d, increase of the variance of ΔV_l is more significant. Also, the variance of $\Delta\theta_l$ does not increase monotonically with P_d for case B. As a result, the variance of ΔV_l seems to be a better indicator of the system stability.

In Fig. 2.14, the autocorrelation of ΔV_l until very near the bifurcation is small compared to those in Fig. 2.13. This is caused by C_{26} being very small in (2.76), so ΔV_l is tied to the differential variables weakly. As a result, ΔV_l behaves in part like η—the white random variable, and hence its autocorrelation is not a good indicator of proximity to the bifurcation. In addition, nonmonotonicity of the autocorrelations of $\Delta V_l,\ \Delta\theta_l$ for case B in Fig. 2.14 shows that they are not good early warning signs of bifurcation.

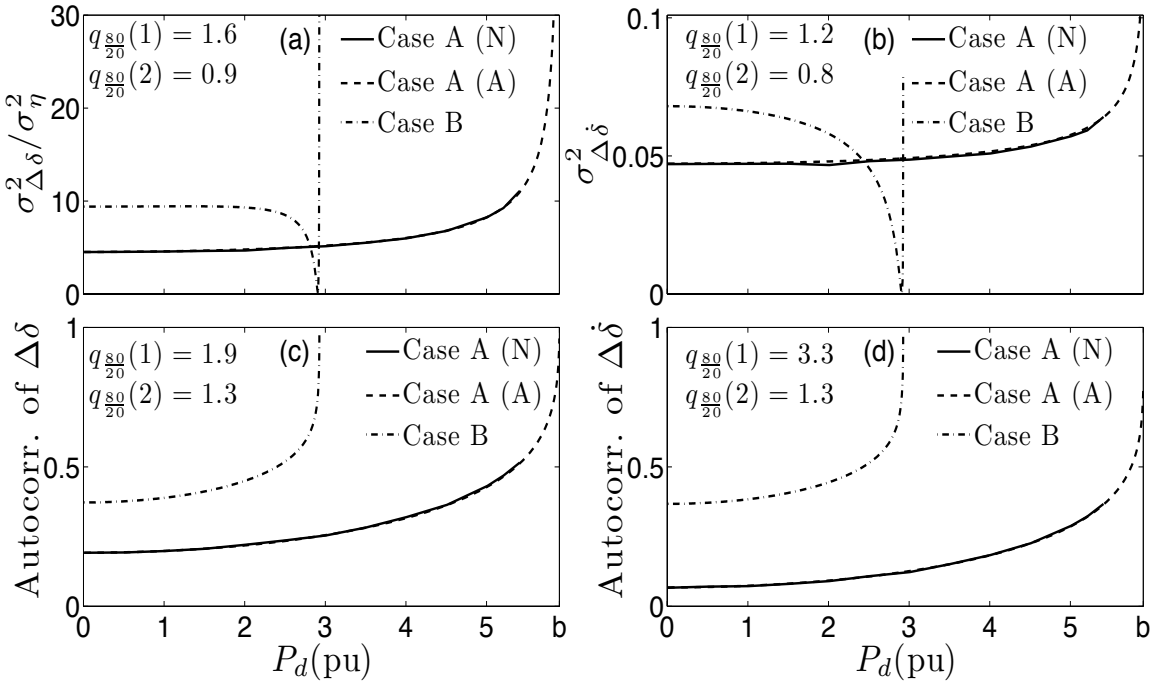

Figure 2.13: Panels a,b show the variances of $\Delta\delta, \Delta\dot{\delta}$ versus load power (P_d). Panels c,d show the autocorrelations of $\Delta\delta, \Delta\dot{\delta}$ versus P_d. The ratios $q_{\frac{80}{20}}(1), q_{\frac{80}{20}}(2)$ are for case A, case B respectively. CaseA(N), CaseA(A) denote numerical and analytical solutions for case A.

2.6.2 Discussion

After studying this system with a range of different parameters, we found that autocorrelations of the differential variables and variance of the voltage magnitude are consistently good indicators of proximity to the bifurcation.

On the other hand, as shown in Fig. 2.13, variance in the differential variables is not a reliable indicator. Namely, variances change non-monotonically (i.e., they do not always increase) and, importantly, may exhibit very abrupt changes. Fig. 2.12 provides

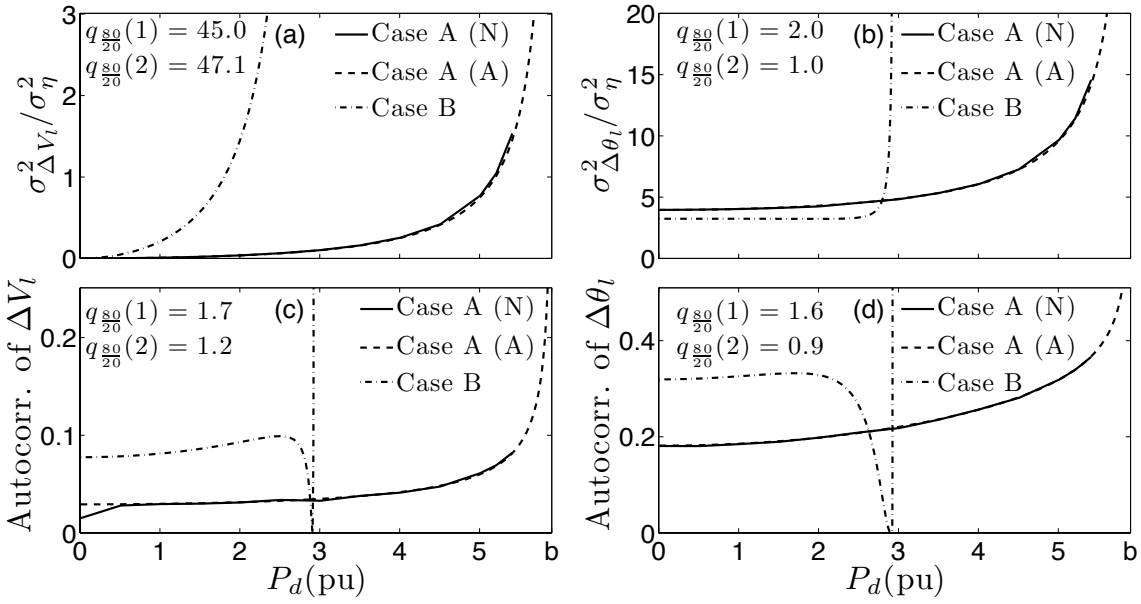

Figure 2.14: Panels a,b show the variances of $\Delta V_l, \Delta\theta_l$ versus P_d. Panels c,d show the autocorrelations of $\Delta V_l, \Delta\theta_l$ versus P_d.

some clues as to the reason for this latter phenomenon. In this figure, the absolute value of C_7 decreases with P_d and becomes zero very close to the bifurcation point, at $P_{d|C_7=0}$. Therefore, the variances of $\Delta\delta$ and $\Delta\dot{\delta}$, which are proportional to C_7^2, decrease and vanish at $P_{d|C_7=0}$. Past this point, $|C_7|$ increases, while C_6 continues to decrease and vanishes at b. Therefore, the variances of $\Delta\delta$ and $\Delta\dot{\delta}$, which are proportional to ${}^{C_7^2}/_{C_6}$, increase to infinity in the very narrow interval $\big(P_{d|C_7=0},\ b\big)$; see Fig. 2.12. This explains the sharp features in Figs. 2.13(a), 2.13(b); a similar explanation can be given to such a feature in Figs. 2.14(c), 2.14(d). Therefore, neither the variances of $\Delta\delta, \Delta\dot{\delta}$ or the autocorrelations of $\Delta V_l, \Delta\theta_l$ are good indicators of proximity to bifurcation.

The results for this system clearly show that not all of the variables in a power system will show CSD signs long before the bifurcation. Although autocorrelations and variances of all variables increase before the bifurcation, some of them increase only very near the bifurcation or the increase is not monotonic. Hence, these variables are not useful indicators of proximity to the bifurcation. In the three-bus system, autocorrelation in the differential equations was a better indicator of proximity than autocorrelation in ΔV_l or $\Delta\theta_l$, which are not directly associated with the differential equations. Also, ΔV_l was the

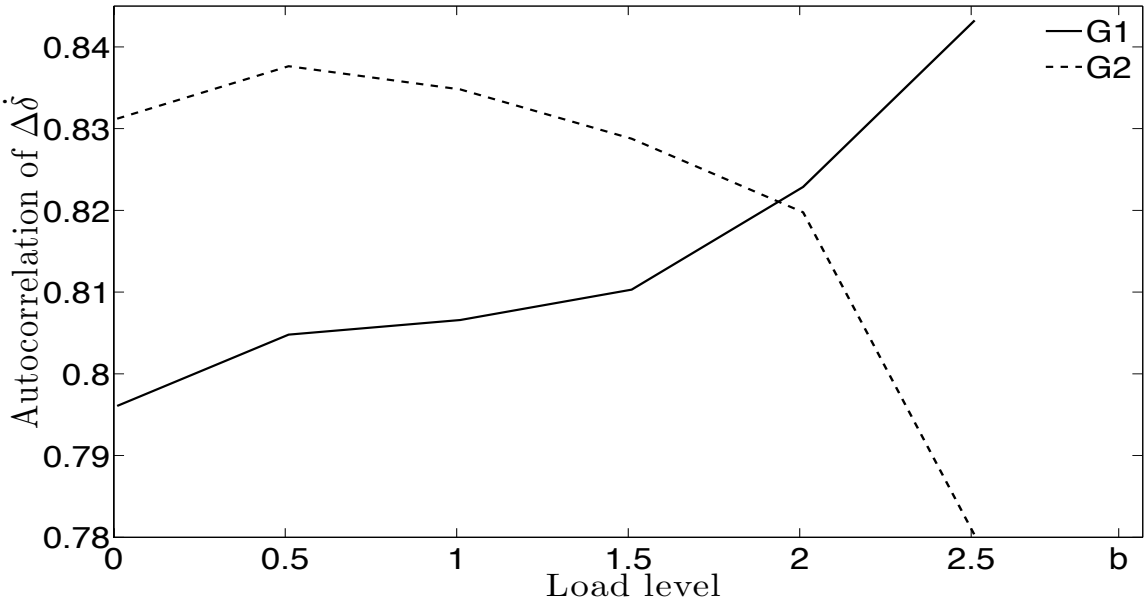

Figure 2.15: Autocorrelation of $\Delta\dot{\delta}$ for two machines in the Three-bus system with two generators. G_1 is the same generator as in the Three-bus system and G_2 is the new generator.

only variable whose variance shows a gradual and monotonic increase with the bifurcation parameter.

2.7 CSD in multi-machine systems

In order to compare these analytical results to results from more practical power system, this section presents numerical results for two multi-machine systems.

The first system was similar to the Three-bus system (case B in Sec. 2.6). The only difference was that instead of infinite bus, a generator similar to the other generator was used. The numerical simulation results were similar to the Three-bus system, except for the autocorrelation of $\Delta\dot{\delta}$. Fig. 2.15 shows that the autocorrelation of $\Delta\dot{\delta}$ increases for one of the machines, while it decreases for the other one. This shows that the autocorrelation of $\Delta\dot{\delta}$ is not a reliable indicator of the proximity to the bifurcation in this system.

The second system we studied was the New England 39-bus system, using the system data from (Pai 1989) We simulated this system for different load levels using the power system analysis toolbox (PSAT) (Milano 2005). In order to change the system loading, each load was multiplied by the same factor. At each load level, we added white noise to each

load. As one would expect, increasing the loads moves the system towards voltage collapse. For solving the stochastic DAEs, we used the fixed-step trapezoidal solver of PSAT with the step size of 0.01s. The noise intensity was kept constant for all load levels.

The simulation results show that the variances and autocorrelations of bus voltage magnitudes increase with load. However, similar to the Three-bus system, the autocorrelations of voltage magnitudes are very small, indicating that in practice, these variables would not be good indicators of proximity. The variances and autocorrelations of generator rotor angles and speeds and bus voltage angles did not consistently show an increasing pattern. Fig. 2.16 shows the variances and autocorrelations of the voltage magnitudes of five buses and the rotor angles of five generators of the system. The buses and generators were arbitrarily chosen. As in previous results, the autocorrelation time lag was chosen to be 0.1s.

Exciters, governors and frequency-dependent loads were not included in the results shown here. However, tests with exciters and governors indicated that that adding these elements to the simulations did not substantially change the conclusions. Considering the frequency-dependence of loads raised the rate at which the autocorrelation of voltage magnitudes increased. On the other hand, it decreased the rate of increase of the variance of voltage magnitudes. Nevertheless, the rate of increase of variance still remained significant. In this case, variance and autocorrelation of voltage magnitudes provide useful early warning of the bifurcation. In contrast, variances and autocorrelations of other variables do not provide a consistent early warning.

The results in this section suggest that autocorrelations of differential variables show nonmonotonic behavior in some cases, which limits their application as early waning signs of bifurcation.

Comparing the measure $q_{\frac{80}{20}}$ for variances and autocorrelations of voltage magnitudes shows that some variables at some buses have larger growth ratios than others. As suggested in (Podolsky and Turitsyn 2013a) and (Podolsky and Turitsyn 2013b), this may be associated with the contribution of the variables to the leading mode near the threshold

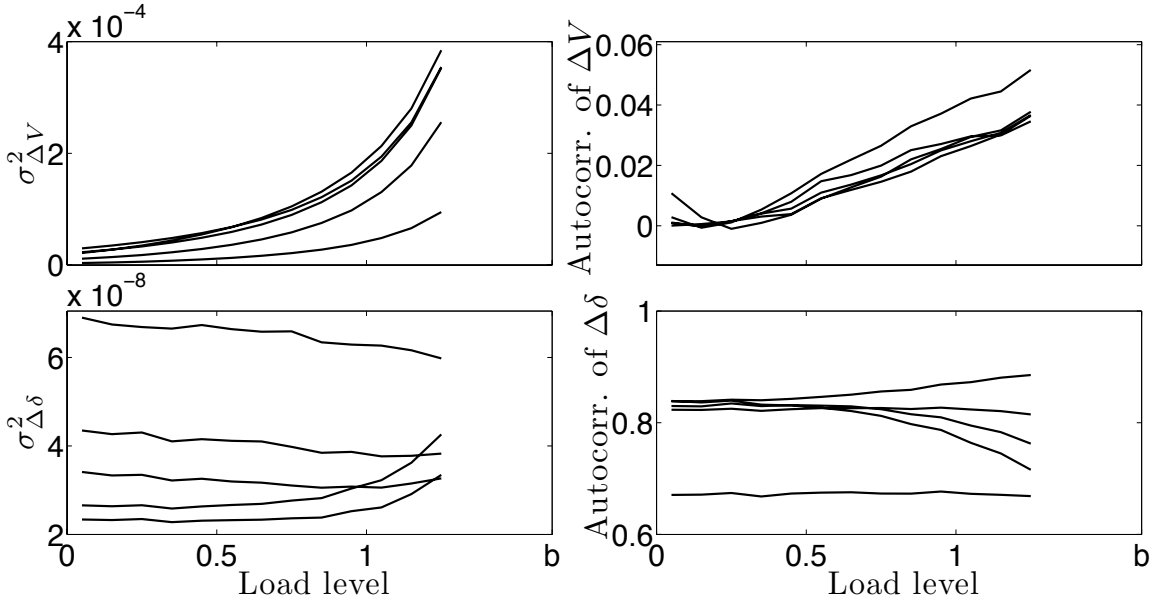

Figure 2.16: The variances and autocorrelations of five bus voltage magnitudes and five generator rotor angles of the 39-bus system. Load level is the ratio of the values of the system's loads to their nominal values.

of collapse. However, except for cases that are very close to (~1% away) the bifurcation, eigenvalue analysis shows that there are several simultaneously dominant modes. The results indicate that the mode whose damping decreases the fastest is most strongly connected to the variance of bus voltages. Table 2.2 shows that, in general, the buses with the largest increases in variances have larger activity in the dominant mode. On the other hand, autocorrelations do not show a similar pattern. While the exact reasons for this are not yet clear, Fig. 2.3 and the analytical results indicate that the autocorrelation functions of variables can take many different shapes, which affects the growth ratio of their autocorrelations.

Table 2.2 shows the buses with the highest $q_{\frac{80}{20}}$ indices for bus voltage variance, as well as the relative activity of these bus voltage magnitudes in the dominant mode. In order to calculate the relative activity of the bus voltages in the dominant mode, we first calculated the right modal matrix of the state matrix. Then, using a matrix which relates the differential and algebraic variables, we calculated the matrix that relates the algebraic variables and the system modes (For further details, see Sec. 3.4). The entries of each column of this matrix gives the relative activity of the algebraic variables in one of the modes. It should be noted that the entries shown in Table 2.2 are a small subset of the

Table 2.2: The largest indices $q_{\frac{80}{20}}$ (for variance) and the relative activity in the dominant mode for bus voltage magnitudes

Bus	$q_{\frac{80}{20}}$ (Variance)	relative activity
38	11.5944	0.0135
29	9.9317	0.0147
28	9.0663	0.0147
33	8.5141	0.0101
37	8.3509	0.007

entries of the column corresponding to the dominant mode, which is why their values are so small.

In many ways, this test case is a multi-machine version of the SMSL system. As with the SMSL and Three-bus systems, variances of bus voltage magnitudes are good early warning signs. However, unlike in the SMSL system, autocorrelation in voltage magnitudes increases, albeit only slightly in some cases, with system load. Unlike in the SMSL system, voltage magnitudes in the 39-bus case have non-zero autocorrelation for $\Delta t > 0$. This results from the fact that voltage magnitudes are coupled to the differential variables in this system.

Results from this system, as with the SMSL system, suggest that variance in voltage magnitudes is a useful early warning sign of voltage collapse. It is less clear from these results if changes in autocorrelation will be sufficiently large to provide a reliable early warning of criticality.

One important point about the numerical results presented in this chapter is that these results are averages over many simulations with randomly chosen sequences of η. This averaging is different from the quantities observed by power system operators. One should take this into account when using CSD signs for monitoring system stability. For example, Fig. 2.17 shows the variances of the voltage magnitudes of three buses in the 39-bus system. For each bus, mean variances (for 100 realizations) are shown for all load levels. For three load levels (low, medium and high load level), the actual measured variance from each of the 100 realizations (one minute windows) is also shown. The increases in voltage magnitude variance are significant in that there is no overlap between the variances at

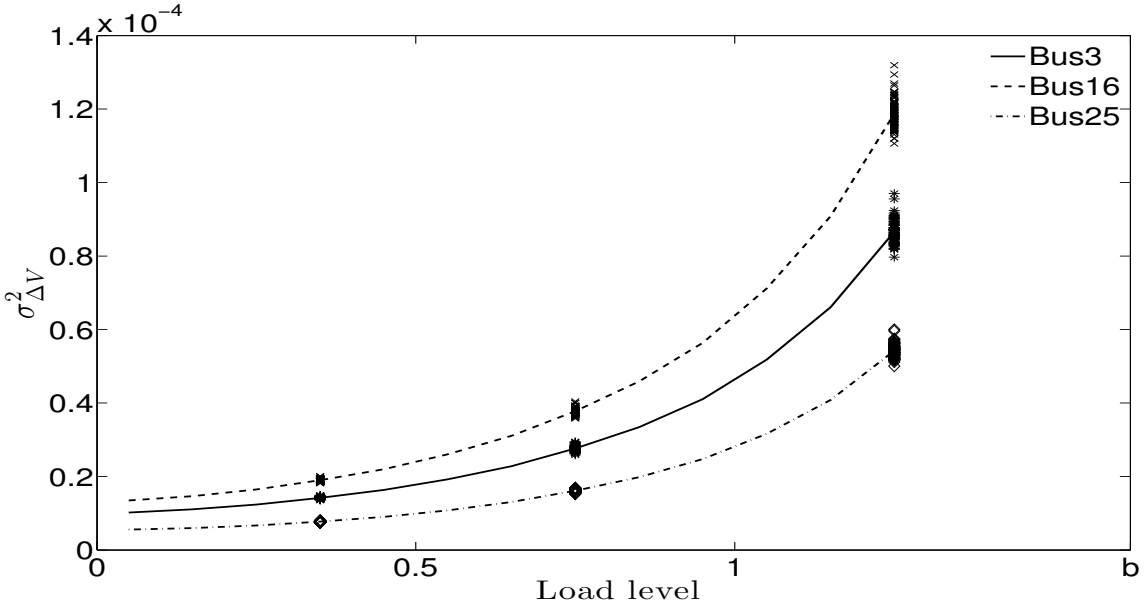

Figure 2.17: Variances of three bus voltages versus load level. For three load levels, variances for 100 realizations are shown. For other load levels, only mean of the variances are shown.

these three load levels even for a single realization. Therefore, we conclude that, at least given the assumptions underlying these simulations, it is possible to accurately estimate the distance to bifurcation based on the variance of a one-minute stream of voltage magnitude data.

2.8 Conclusion

In this chapter, we analytically and numerically solve the stochastic differential algebraic equations for three small power system models in order to understand critical slowing down in power systems. The results from the single machine infinite bus system and the Three-bus system models show that critical slowing down does occur in power systems, and illustrate that autocorrelation and variance in some cases can be good indicators of proximity to criticality in power systems. The results also show that the way in which the bifurcation parameter changes the system state matrix (A) importantly influences the observed changes in autocorrelation and variance. For example, the constant state matrix in the single machine single load system (see (2.7),(2.51)) caused the autocorrelation of the differential variable to be constant. On the other hand, in the SMIB and Three-bus systems, the state matrix changed with the the bifurcation parameter; that is, the coefficient

ω_0 in (2.7) changed with the bifurcation parameter P_m (for SMIB, see (2.28),(2.29)) or P_d (Three-bus, see (2.55)). As a result, the variance and autocorrelation of the differential variables changed with the bifurcation parameter, and in some cases indicate proximity to bifurcation.

Although the signs of critical slowing down do consistently appear as the systems approach bifurcation, only in a few of the variables did the increases in autocorrelation appear sufficiently early to give a useful early warning of potential collapse. On the other hand, variance in load bus voltages consistently showed substantial increases with load, indicating that variance in bus voltages can be a good indicator of voltage collapse in multi-machine power system models. This was verified for the New England 39-bus system. Determining intuitive analytical or physical explanations for why some variables show the signs of CSD better than others requires additional investigation, and is a subject for future research.

Together these results suggest that it is possible to obtain useful information about system stability from high-sample rate time-series data, such as that produced by synchronized phasor measurement units. Future research will focus on developing an effective power system stability indicator based on these results.

2.9 Appendix A

The derivation of (2.50) is presented in this section. By linearizing (2.45) around the equilibrium and replacing the obtained equation for P_g in (2.44), we obtained the following:

$$M\Delta\ddot{\delta} + D\Delta\dot{\delta} = -C_{12}\Delta V_l - C_{13}\left(\Delta\delta - \Delta\theta_l\right) \tag{2.56}$$

where C_{12} and C_{13} are:=

$$C_{12} = E_a^{'}\left|Y_{gl}\right|\sin\left(\theta_{l0} - \delta_0 - \pi/2 + \phi_{gl}\right) \tag{2.57}$$

$$C_{13} = V_{l0}E_a^{'}\left|Y_{gl}\right|\cos\left(\theta_{l0} - \delta_0 - \pi/2 + \phi_{gl}\right) \tag{2.58}$$

where $|Y_{gl}| = \sqrt{G_{gl}^2 + B_{gl}^2}$, $\phi_{gl} = \arctan\left({}^{B_{gl}}/_{G_{gl}}\right)$. By linearizing (2.48) and (2.49) around the equilibrium and solving for ΔV_l and $\Delta\delta - \Delta\theta_l$, we obtained the following:

$$\Delta V_l = C_{14}\eta \tag{2.59}$$

$$\Delta\delta - \Delta\theta_l = C_{15}\eta \tag{2.60}$$

where C_{14} and C_{15} are:

$$\begin{bmatrix} C_{14} \\ C_{15} \end{bmatrix} = \begin{bmatrix} C_{19}P_{d0} - C_{17}Q_{d0} \\ C_{18}P_{d0} - C_{16}Q_{d0} \end{bmatrix} / (C_{17}C_{18} - C_{16}C_{19}) \tag{2.61}$$

where $C_{16} - C_{19}$ are given below:

$$C_{16} = E_a^{'} |Y_{gl}| \sin\left(\theta_{l0} - \delta_0 + {}^{\pi}/_{2} - \phi_{gl}\right) \tag{2.62}$$

$$+2G_{ll}V_{l0}$$

$$C_{17} = V_{l0}E_a^{'} |Y_{gl}| \cos\left(\theta_{l0} - \delta_0 + {}^{\pi}/_{2} - \phi_{gl}\right) \tag{2.63}$$

$$C_{18} = -E_a^{'} |Y_{gl}| \cos\left(\theta_{l0} - \delta_0 + {}^{\pi}/_{2} - \phi_{gl}\right) \tag{2.64}$$

$$-2B_{ll}V_{l0}$$

$$C_{19} = V_{l0}E_a^{'} |Y_{gl}| \sin\left(\theta_{l0} - \delta_0 + {}^{\pi}/_{2} - \phi_{gl}\right) \tag{2.65}$$

Using (2.59) and (2.60), we rewrote (2.56) as (2.50) where C_5 is:

$$C_5 = \frac{\left(C_{13}C_{18} + C_{12}C_{19}\right) P_{d0} - \left(C_{13}C_{16} + C_{12}C_{17}\right) Q_{d0}}{C_{16}C_{19} - C_{17}C_{18}} \tag{2.66}$$

2.10 Appendix B

The derivation of C_6, C_7 is presented in this section. By using (2.1) and linearizing (2.52)-(2.54) around the equilibrium, we have the following:

$$\Delta\ddot{\delta} = -\left(D\Delta\dot{\delta} + C_{20}\Delta V_l + C_{21}\left(\Delta\delta - \Delta\theta_l\right)\right)/M \tag{2.67}$$

$$0 = -P_{d0}\eta + C_{22}\Delta V_l + C_{21}\Delta\delta + C_{23}\Delta\theta_l \tag{2.68}$$

$$0 = -\Delta V_l + C_{24}\Delta\delta + C_{25}\Delta\theta_l \tag{2.69}$$

where C_{20} through C_{25} are as follows:

$$C_{20} = \frac{E'_a}{X}\sin\left(\delta_0 - \theta_{l0}\right) \tag{2.70}$$

$$C_{21} = \frac{E'_a V_{l0}}{X}\cos\left(\delta_0 - \theta_{l0}\right) \tag{2.71}$$

$$C_{22} = C_{20} - {\sin(\theta_{l0})}/{X_{l2}} \tag{2.72}$$

$$C_{23} = -C_{21} - \frac{V_{l0}}{X_{l2}}\cos\left(\theta_{l0}\right) \tag{2.73}$$

$$C_{24} = -\beta E'_a \sin\left(\delta_0 - \theta_{l0}\right) \tag{2.74}$$

$$C_{25} = -C_{24} - (1-\beta)\cdot\sin\left(\theta_{l0}\right) \tag{2.75}$$

where $\beta = X_{l2}/(X + X_{l2})$. Using (2.68) and (2.69), we solved for ΔV_l and $\Delta\theta_l$:

$$\Delta V_l = C_{26}\Delta\delta + C_{27}\eta \tag{2.76}$$

$$\Delta\theta_l = C_{28}\Delta\delta + C_{29}\eta \tag{2.77}$$

where C_{26} through C_{29} are as follows:

$$\begin{bmatrix} C_{26} \\ C_{27} \\ C_{28} \\ C_{29} \end{bmatrix} = \begin{bmatrix} C_{23}C_{24} - C_{21}C_{25} \\ C_{25}P_{d0} \\ -C_{21} - C_{22}C_{24} \\ P_{d0} \end{bmatrix} /(C_{22}C_{25} + C_{23}) \tag{2.78}$$

Equations (2.67), (2.76) - (2.78) lead to the following expressions:

$$C_6 = C_{21}C_{28} - C_{20}C_{26} - C_{21} \tag{2.79}$$

$$C_7 = C_{21}C_{29} - C_{20}C_{27} \tag{2.80}$$

Bibliography

Abraham, S. and J. Efford (2004). Final report on the August 14, 2003 blackout in the United states and Canada: causes and recommendations. Technical report, US–Canada Power Syst. Outage Task Force.

Ajjarapu, V. and B. Lee (1992, Feb.). Bifurcation theory and its application to nonlinear dynamical phenomena in an electrical power system. *IEEE Trans. Power Syst. 7*(1), 424–431.

Anghel, M., K. A. Werley, and A. E. Motter (2007, Jan.). Stochastic model for power grid dynamics. In *40th Annual Hawaii Intl. Conf. Syst. Sci.* IEEE.

Avalos, R., C. Canizares, F. Milano, and A. Conejo (2009, Jan.). Equivalency of continuation and optimization methods to determine saddle-node and limit-induced bifurcations in power systems. *IEEE Trans. Circuits Syst. I, Reg. Papers 56*(1), 210 –223.

Ayasun, S., C. Nwankpa, and H. Kwatny (2004, Aug.). Computation of singular and singularity induced bifurcation points of differential-algebraic power system model. *IEEE Trans. Circuits Syst. I, Reg. Papers 51*(8), 1525 – 1538.

Begovic, M. M. and A. G. Phadke (1992). Control of voltage stability using sensitivity analysis. *IEEE Trans. Power Syst. 7*(1), 114–123.

Bergen, A. and V. Vittal (1999). *Power systems analysis* (2nd ed.). New Jersey: Prentice Hall.

Blanchard, P., R. L. Devaney, and G. R. Hall (2006). *Differential Equations*. Thomson Brooks/Cole.

Boerlijst, M. C., T. Oudman, and A. M. de Roos (2013). Catastrophic collapse can occur without early warning: examples of silent catastrophes in structured ecological models. *PLOS ONE 8*(4), e62033.

Canizares, C. A. (1995, February). On bifurcations, voltage collapse and load modeling. *IEEE Trans. Power Syst. 10*(1), 512–522.

Canizares, C. A. et al. (2002). Voltage stability assessment: concepts, practices and tools. *Power Syst. Stability Subcommittee Special Publication IEEE/PES*.

Cañizares, C. A., N. Mithulananthan, F. Milano, and J. Reeve (2004, May.). Linear performance indices to predict oscillatory stability problems in power systems. *IEEE Trans. Power Syst. 19*(2), 1104–1114.

Chertkov, M., S. Backhaus, K. Turtisyn, V. Chernyak, and V. Lebedev (2011). Voltage collapse and ODE approach to power flows: Analysis of a feeder line with static disorder in consumption/production. *arXiv preprint arXiv:1106.5003*.

Chiang, H. D., I. Dobson, R. J. Thomas, J. S. Thorp, and L. Fekih-Ahmed (1990). On voltage collapse in electric power systems. *IEEE Trans. Power Syst. 5*(2), 601–611.

Coffey, W., Y. Kalmykov, and J. Waldron (2004). *The Langevin Equation: With Applications in Physics, Chemistry, and Electrical Engineering* (2nd ed.). World Scientific series in contemporary physics. Singapore: World Scientific.

Cotilla-Sanchez, E., P. D. H. Hines, and C. Danforth (2012, Dec.). Predicting critical transitions from time series synchrophasor data. *IEEE Trans. Smart Grid 3*(4), 1832 –1840.

Dakos, V., S. Kéfi, M. Rietkerk, E. H. van Nes, and M. Scheffer (2011). Slowing down in spatially patterned ecosystems at the brink of collapse. *Amer. Natur. 177*(6), E153–E166.

Dakos, V., M. Scheffer, E. H. Van Nes, V. Brovkin, V. Petoukhov, and H. Held (2008, Sep.). Slowing down as an early warning signal for abrupt climate change. *Proc. Natl. Acad. Sci. 105*(38), 14308–14312.

De Marco, C. and A. Bergen (1987, Dec.). A security measure for random load disturbances in nonlinear power system models. *IEEE Trans. Circuits Syst. 34*(12), 1546–1557.

Demello, F. P. and C. Concordia (1969). Concepts of synchronous machine stability as affected by excitation control. *IEEE Trans. Power Apparatus Syst.* (4), 316–329.

Dhople, S., Y. Chen, L. DeVille, and A. Dominguez-Garcia (2013, Dec.). Analysis of power system dynamics subject to stochastic power injections. *IEEE Trans. Circuits Syst. I, Reg. Papers 60*(12), 3341–3353.

Dobson, I. (1992, Mar.). Observations on the geometry of saddle node bifurcation and voltage collapse in electrical power systems. *IEEE Trans. Circuits Syst. I, Fundam. Theory Appl. 39*(3), 240–243.

Dobson, I. (1994). The irrelevance of load dynamics for the loading margin to voltage collapse and its sensitivities. In *Bulk Power Syst. Voltage Phenom. III, Voltage stability, Security, Control, Proc. ECC/NSF workshop, Davos, Switzerland*.

Dobson, I. and H. D. Chiang (1989, Sep). Towards a theory of voltage collapse in electric power systems. *Syst. Control Lett. 13*(3), 253–262.

Dong, Z. Y., J. H. Zhao, and D. Hill (2012, Nov.). Numerical simulation for stochastic transient stability assessment. *IEEE Trans. Power Syst. 27*(4), 1741 –1749.

FERC and NERC (2012, Apr.). Arizona–Southern California outages on September 8, 2011: Causes and recommendations. Technical report.

Gardiner, C. W. (2010). *Stochastic Methods: A Handbook for the Natural and Social Sciences* (4th ed.). Berlin, Germany: Springer.

Ghanavati, G., P. D. H. Hines, T. I. Lakoba, and E. Cotilla-Sanchez (2013, Sep.). Calculation of the autocorrelation function of the stochastic single machine infinite bus system. In *North American Power Symposium*.

Glavic, M. and T. Van Cutsem (2009, Aug.). Wide-area detection of voltage instability from synchronized phasor measurements. Part I: Principle. *IEEE Trans. Power Syst. 24*(3), 1408 –1416.

Hastings, A. and D. B. Wysham (2010). Regime shifts in ecological systems can occur with no warning. *Ecology Lett. 13*(4), 464–472.

Hauer, A. J. F., D. J. Trudnowski, and J. G. DeSteese (2007, Jun.). A perspective on WAMS analysis tools for tracking of oscillatory dynamics. In *IEEE Power and Energy Soc. General Meeting (PES)*, pp. 1–10.

Hines, P. D. H., E. Cotilla-Sanchez, B. O'hara, and C. Danforth (2011). Estimating dynamic instability risk by measuring critical slowing down. In *Power Energy Soc. General Meeting*, pp. 1–5. IEEE.

Horsthemke, W. and R. Lefever (2006). *Noise-induced Transitions* (2nd. ed.). Berlin, Germany: Springer.

Hou, G. and V. Vittal (2012, Nov.). Trajectory sensitivity based preventive control of voltage instability considering load uncertainties. *IEEE Trans. Power Syst. 27*(4), 2280 – 2288.

Kuehn, C. (2011, Jun.). A mathematical framework for critical transitions: Bifurcations, fast-slow systems and stochastic dynamics. *Phys. D: Nonlinear Phen. 240*(12), 1020–1035.

Kundur, P., N. J. Balu, and M. G. Lauby (1994). *Power system stability and control* (1st ed.). New York: McGraw-hill.

Kundur, P., J. Paserba, V. Ajjarapu, G. Andersson, A. Bose, C. Canizares, N. Hatziargyriou, D. Hill, A. Stankovic, C. Taylor, T. Van Cutsem, and V. Vittal (2004, Aug.). Definition and classification of power system stability IEEE/CIGRE joint task force on stability terms and definitions. *IEEE Trans. Power Syst. 19*(3), 1387 – 1401.

Kwatny, H. G., R. F. Fischl, and C. O. Nwankpa (1995, Nov.). Local bifurcation in power systems: Theo. compu. appl. *Proc. IEEE 83*(11), 1456–1483.

Lenton, T., V. Livina, V. Dakos, E. Van Nes, and M. Scheffer (2012). Early warning of climate tipping points from critical slowing down: comparing methods to improve robustness. *Philos. Trans. Royal Soc. A: Math., Phys. Eng. Sci. 370*(1962), 1185–1204.

Litt, B., R. Esteller, J. Echauz, M. D'Alessandro, R. Shor, T. Henry, P. Pennell, C. Epstein, R. Bakay, M. Dichter, et al. (2001). Epileptic seizures may begin hours in advance of clinical onset: a report of five patients. *Neuron 30*(1), 51–64.

Mannella, R. and V. Peter (2012, Mar.). Itô versus Stratonovich: 30 years later. *Fluct. Noise Lett. 11*(01), 1240010.

Milano, F. (2005). An open source power system analysis toolbox. *IEEE Trans. Power Syst. 20*(3), 1199–1206.

Milano, F. and R. Zarate-Minano (2013, Nov.). A systematic method to model power systems as stochastic differential algebraic equations. *IEEE Trans. Power Syst. 28*(4), 4537–4544.

Nwankpa, C., S. Shahidehpour, and Z. Schuss (1992, Nov.). A stochastic approach to small disturbance stability analysis. *IEEE Trans. Power Syst. 7*(4), 1519–1528.

Pai, M. (1989). *Energy function analysis for power system stability* (1st ed.). MA, USA: Kluwer Academic Publishers.

Podolsky, D. and K. Turitsyn (2013a, Jul.). Critical slowing-down as indicator of approach to the loss of stability. *arXiv preprint arXiv:1307.4318*.

Podolsky, D. and K. Turitsyn (2013b). Random load fluctuations and collapse probability of a power system operating near codimension 1 saddle-node bifurcation. In *IEEE Power and Energy Soc. General Meeting (PES)*.

Revel, G., A. Leon, D. Alonso, and J. Moiola (2010, Apr.). Bifurcation analysis on a multimachine power system model. *IEEE Trans. Circuits Syst. I, Reg. Papers 57*(4), 937 –949.

Rümelin, W. (1982). Numerical treatment of stochastic differential equations. *SIAM J. Numer. Anal.*, 604–613.

Scheffer, M., J. Bascompte, W. A. Brock, V. Brovkin, S. R. Carpenter, V. Dakos, H. Held, E. H. Van Nes, M. Rietkerk, and G. Sugihara (2009, Sep.). Early–warning signals for critical transitions. *Nature 461*(7260), 53–59.

Stratonovich, R. L. (1963). *Introduction to the Theory of Random Noise*. Gordon and Breach.

Susuki, Y. and I. Mezic (2012). Nonlinear koopman modes and a precursor to power system swing instabilities. *IEEE Trans. Power Syst. 27*(3), 1182–1191.

Van Cutsem, T. (2000, Feb.). Voltage instability: phenomena, countermeasures, and analysis methods. *Proc. IEEE 88*(2), 208 –227.

Veraart, A. J., E. J. Faassen, V. Dakos, E. H. van Nes, M. Lürling, and M. Scheffer (2011). Recovery rates reflect distance to a tipping point in a living system. *Nature 481*(7381), 357–359.

Wang, K. and M. L. Crow (2013, Aug.). The Fokker–Planck equation for power system stability probability density function evolution. *IEEE Trans. Power Syst. 28*(3), 2994–3001.

Wang, Y., D. J. Hill, R. H. Middleton, and L. Gao (1993). Transient stability enhancement and voltage regulation of power systems. *IEEE Trans. Power Syst. 8*(2), 620–627.

Wei, D. and X. Luo (2009). Noise-induced chaos in single-machine infinite-bus power systems. *Europhys. Lett. 86*(5), 50008, 6 pp.

CHAPTER 3: INVESTIGATING EARLY WARNING SIGNS OF OSCILLATORY INSTABILITY IN SIMULATED PHASOR MEASUREMENTS

3.1 Abstract

Chapter 2 examined critical slowing down (CSD) in power system in the vicinity of a saddle-node bifurcation. This chapter investigates the occurrence of CSD as a power system approaches a Hopf bifurcation. The results for a small power system test case show that the variance of load bus voltage magnitude increases measurably as the system approaches a Hopf bifurcation, which is similar to the findings in the previous chapter for the saddle-node bifurcation. This property can potentially be used as a method for monitoring oscillatory stability in power grid using high-resolution phasor measurements. Also, this chapter examines why some variables show the signs of CSD better than others using the eigenvalue analysis of the system's state matrix.

3.2 Introduction

One of the most important grid conditions that operators need to monitor for is oscillatory stability. Oscillatory stability problems are typically associated with a pair of complex eigenvalues crossing the imaginary axis of the complex plane after a system undergoes a contingency (Kundur et al. 1994).

Numerous methods are proposed for monitoring inter-area oscillations such as (Browne et al. 2008), (Cañizares et al. 2004) and (Kakimoto et al. 2006) (For more information, see Sec. 1.5.2). In this chapter, we show that changes of statistics of some of system variables can be a potentially helpful complement to existing methods.

Prior research (Cotilla-Sanchez et al. 2012), (Podolsky and Turitsyn 2013a), (Ghanavati et al. 2013) and (Podolsky and Turitsyn 2013b) has shown that the signs of CSD occur in power systems, in the vicinity of saddle-node bifurcations. However, the results in chapter 2 showed that CSD signs do not appear in all variables in the vicinity of a saddle-node bifurcation, in several power system models.

In this chapter, we investigate changes in autocorrelation and variance of system variables as a power system model approaches a Hopf bifurcation. The results show that increasing variance of bus voltage magnitudes is a good early warning sign of Hopf bifurcation. Thus, monitoring for this value could potentially be used as an indicator of oscillatory stability problems in power system. Sec. 3.3 presents the simulation and results of study of changes in autocorrelation and variance of a Three-bus test case in the vicinity of Hopf bifurcation. Sec. 3.4 examines why some variables show the signs of CSD better than others by calculation of the activity of variables in the system's dominant mode. Sec. 3.5 highlights the results and contributions made in this chapter.

3.3 Simulation and results

This section presents the simulation of a small power system test case, with which we study the occurrence of CSD in the vicinity of a Hopf bifurcation. First, we present the test case and the simulation method used. Then, the changes of variances and autocorrelations of system variables in the vicinity of Hopf bifurcation are shown.

3.3.1 Test Case and Simulation

Fig. 3.1 shows the single-line diagram of a Three-bus test system model (Ghasemi 2006) under study. The two generators in this system are modeled with a standard sixth order generator model (Kundur et al. 1994), and are equipped with exciters. A governor is connected to the first generator. The system data are given in Appendix A. We simulated this system using the power system analysis toolbox (PSAT) (Milano 2005). Here, we assume that the load power varies stochastically, with normally distributed fluctuations. However, since the variance of white noise is infinite, we assumed that the load perturbations have finite correlation time. We also assumed that the correlation time of noise is negligible relative to the response-time of the system. Numerically, this correlation time is assumed to be equal to the integration time step of (3.1) below. Adding noise to the system load adds randomness to the system. Therefore, a set of stochastic differential-algebraic

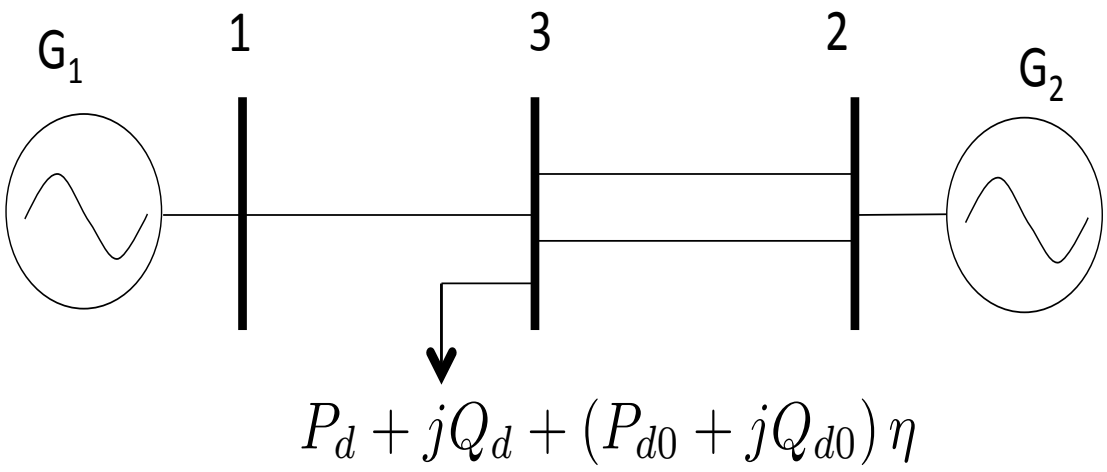

Figure 3.1: Three-bus test system

equations (SDAEs) describe this system:

$$\dot{\underline{x}} = f\left(\underline{x}, \underline{y}\right) \tag{3.1}$$

$$0 = g\left(\underline{x}, \underline{y}, \eta\right) \tag{3.2}$$

where $\underline{x}, \underline{y}$ represent the vector of differential and algebraic variables respectively, η is the gaussian random variable added to the load $\eta \sim \mathcal{N}(0, 0.01)$, f, g represent the set of differential and algebraic equations of the system, respectively. A subset of algebraic equations are power flow equations, into which the noise is added:

$$P_k - P_{k0}\eta = V_k \cdot \sum_{m=1}^{n} (G_{km} V_m \cos\theta_{km} + B_{km} V_m \sin\theta_{km}) \tag{3.3}$$

$$Q_k - Q_{k0}\eta = V_k \cdot \sum_{m=1}^{n} (G_{km} V_m \sin\theta_{km} - B_{km} V_m \cos\theta_{km}) \tag{3.4}$$

where $n = 3$; P_k and Q_k are injected active and reactive power at each bus; P_{k0}, Q_{k0} are constant values; G_{km} and B_{km} are the conductance and the susceptance of the line between bus k and bus m; V_m is the voltage magnitude of bus m; $\theta_{km} = \theta_k - \theta_m$, where θ_k, θ_m are voltage angles of buses k, m. The differential and algebraic equations that describe the generator, exciter and turbine governor are available in (Milano 2008).

We solved the resulting SDAEs using a fixed-step trapezoidal differential-algebraic equations solver for different load levels. For each load level, we simulated the system around the equilibrium. Each load's active and reactive powers fluctuate around their mean values. The time for each simulation was 120s and the integration step size was 0.01s. We assumed that the noise level is constant (i.e. P_{k0}, Q_{k0} are constant in (3.3), (3.4)) when the load is varied, so as to make sure that the increase of variables' variances is not due to the increase of the noise level. At the end of the simulation, we subtracted means of the time-series of the algebraic and differential variables before calculating their variances and autocorrelations. For each load level, we ran simulations 100 times, and calculated the average of variances and autocorrelations of variables. In this work, we vary P and Q proportionally, so that the power factor remains constant.

As the load increases, the system passes through a Hopf bifurcation. Fig. 3.2 shows the PV curve for this system. Hopf bifurcation occurs before the maximum power transfer limit (the nose point of the PV curve). Fig. 3.3 shows the trajectory of the eigenvalues of the system as the load increases. Only the three pairs of eigenvalues closest to the right-half plane are shown. In this and subsequent figures, the dotted line shows a point close to the bifurcation at which we did eigenvalue analysis (see Sec. 3.4) to find out why variances and autocorrelations of the variables show different patterns in the vicinity of the bifurcation.

3.3.2 Autocorrelations and variances of the system variables

Figs. 3.4–3.7 show variance and autocorrelation of several variables that can be measured in real time. Before calculating the variances and autocorrelations, the variables' means were subtracted from their values. Horizontal axis is the ratio of P_d to the nominal load (P_{dn}). These figures demonstrate that the bus voltage magnitudes are the only variables whose variances show a monotonic and, importantly, gradual increase over the entire range of load values. Among the angle variables, only the variance of θ_3 shows a monotonic and gradual increase starting with $P_d/P_{dn} \approx 0.6$, and its increase is less pronounced than that of $\sigma^2_{\Delta V}$. In contrast to the variances, the autocorrelations of the voltage magnitudes increase

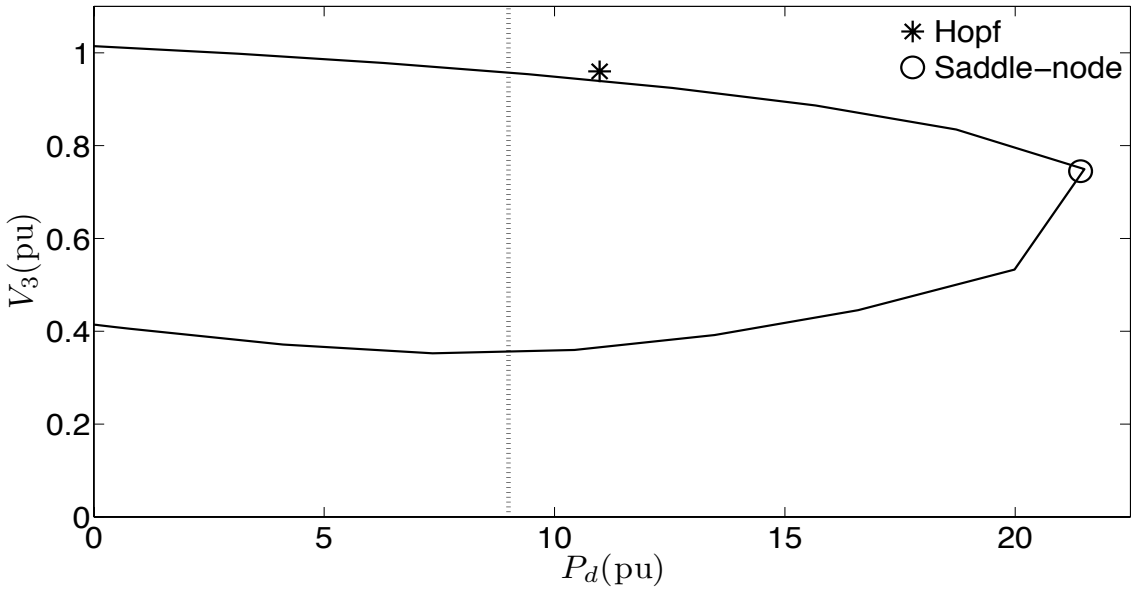

Figure 3.2: PV curve for the Three-bus system. The vertical dotted line shows the nominal load power $(9\mathrm{pu})$.

conspicuously only very near the bifurcation, while variances and autocorrelations of other variables (Figs. 3.5–3.7) are not even monotonic over most of the range of the load level. Therefore, among all the measurable quantities in the Three-bus system, only the load bus voltage variance is a reliable early sign of the bifurcation.

3.4 Discussion

From the description in Sec. 3.3.2, we conclude that a good early warning sign of a Hopf bifurcation in power systems is the same as for saddle-node bifurcation (see chapter 2). We emphasize the word "early". Indeed, it is well-known that variance and autocorrelation of most variables increases according to certain universal laws near a bifurcation (Kuehn 2011). However, our results demonstrate that only a small subset of such variables - namely, the bus voltage magnitudes' variance - exhibits a consistent increase sufficiently far from the bifurcation. Therefore, only these variables can serve as a useful warning sign, which can potentially be detected early enough to avert a system collapse.

Let us point out that this conclusion is supported by the eigenvalue analysis. It is well-known that right eigenvectors of the state matrix give the relative activity of state (i.e. differential) variables when the corresponding mode is excited (Kundur et al. 1994).

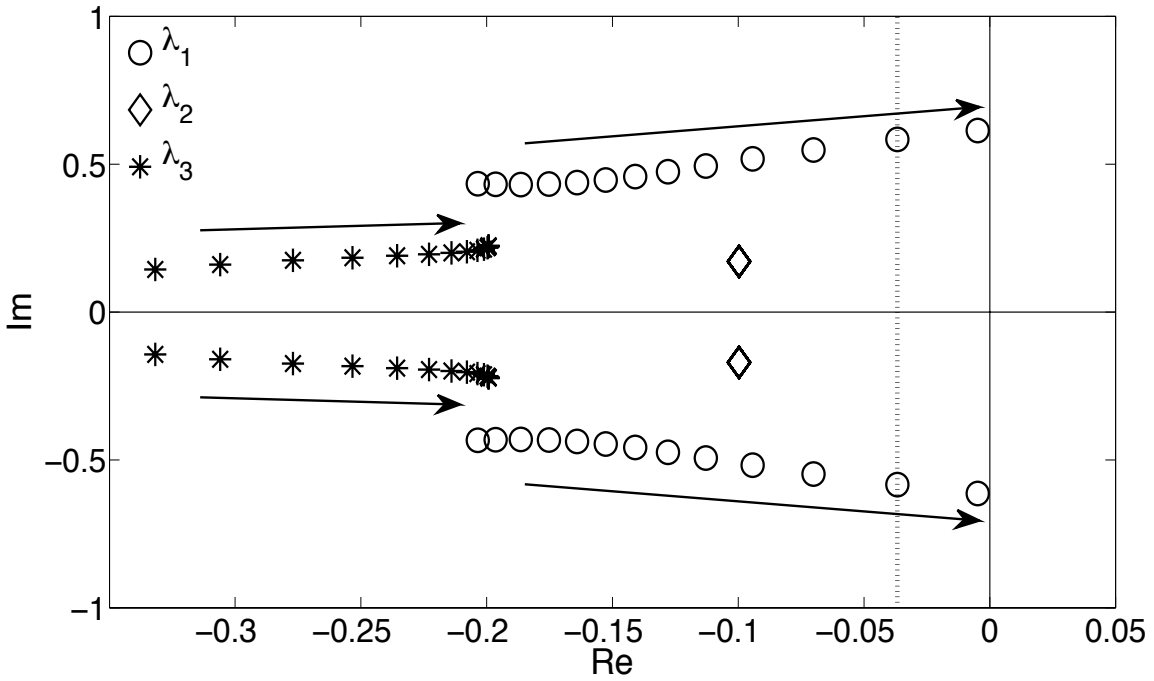

Figure 3.3: Trajectory of the three pairs of dominant eigenvalues of the Three-bus system as the load is increased. The arrows show the direction of the eigenvalues' movement in the complex plane as the load is increased. The increment of bifurcation parameter P_d is 0.9pu. Near the bifurcation, the next (fourth) smallest real part of eigenvalues is approximately -0.7.

Eigenvectors are obtained from linearization of (3.1), (3.2), whereby these equations reduce to:

$$\Delta \underline{\dot{x}} = A \Delta \underline{x} \tag{3.5}$$

where A is:

$$A = f_x - f_y g_y^{-1} g_x \tag{3.6}$$

where f_x, f_y, g_x, g_y are matrices of partial derivatives of (3.1) and (3.2) with respect to the differential and algebraic variables. Note that g_y is nonsingular before the saddle-node point. The solution of (3.5) is represented as:

$$\Delta \underline{x} = \phi \underline{z} \tag{3.7}$$

where ϕ is a matrix whose columns are right eigenvectors of the state matrix, $\underline{z}$ is the time-dependent vector of transformed state variables such that each variable is associated with only one mode (Kundur et al. 1994). In order to determine the relative activity of algebraic

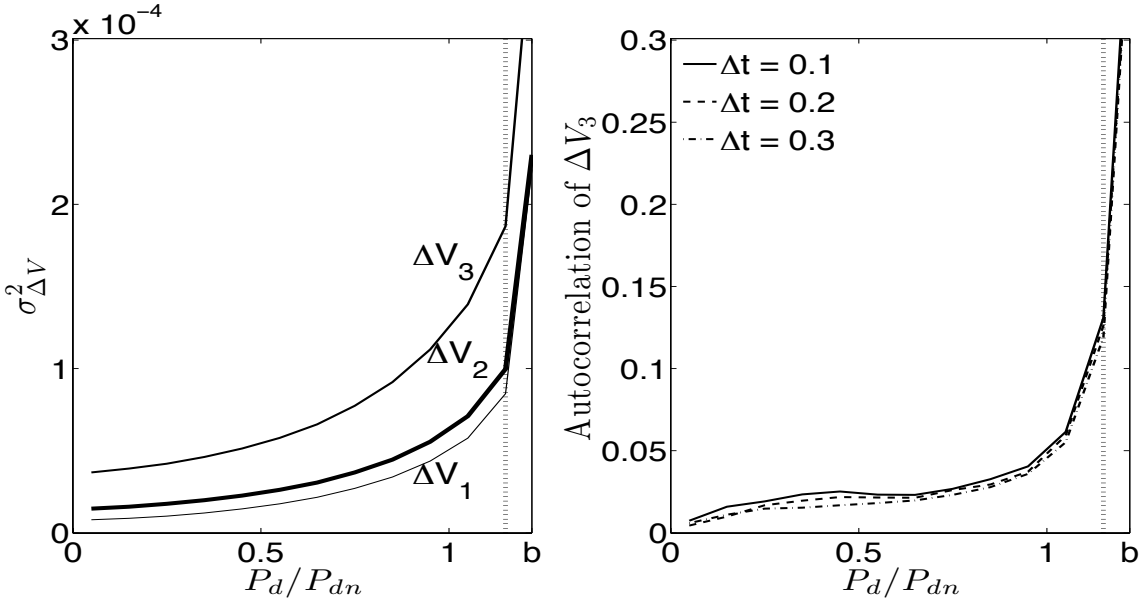

Figure 3.4: Variance and autocorrelation of the voltage magnitude of the load bus versus load level. Note that the autocorrelation $\langle \Delta V(t) \Delta V(t + \Delta t) \rangle$ is shown only for ΔV_3; it is similar for the other two voltages.

variables, we linearized (3.2) (with no noise in the load):

$$\Delta \underline{y} = -g_y^{-1} g_x \Delta \underline{x} \tag{3.8}$$

Then (3.7) and (3.8) yield:

$$\Delta \underline{y} = C \underline{z} \tag{3.9}$$

where $C = -g_y^{-1} g_x \phi$. The columns of C give the relative activity of algebraic variables in corresponding modes.

To identify the most "active" variables, one looks for a group of the entries of the eigenvectors (columns of ϕ) for the state variables, or the columns of matrix C for the algebraic variables. Strictly speaking, one should do so for all the dominant modes, whose eigenvalues have the smallest real part, because their response to an external disturbance (e.g. noise in the load) would decay most slowly. However, out of the three dominant modes shown in Fig. 3.3 we have focused only on the one with the smallest real part for the specific value of load $P_d = 10.4$pu (see the vertical dotted line in Fig. 3.3), and demonstrate that even such restricted analysis agrees with the results provided by Figs. 3.4–3.7. In Table 3.1 we show the magnitudes of only those entries of the corresponding column of ϕ and of C

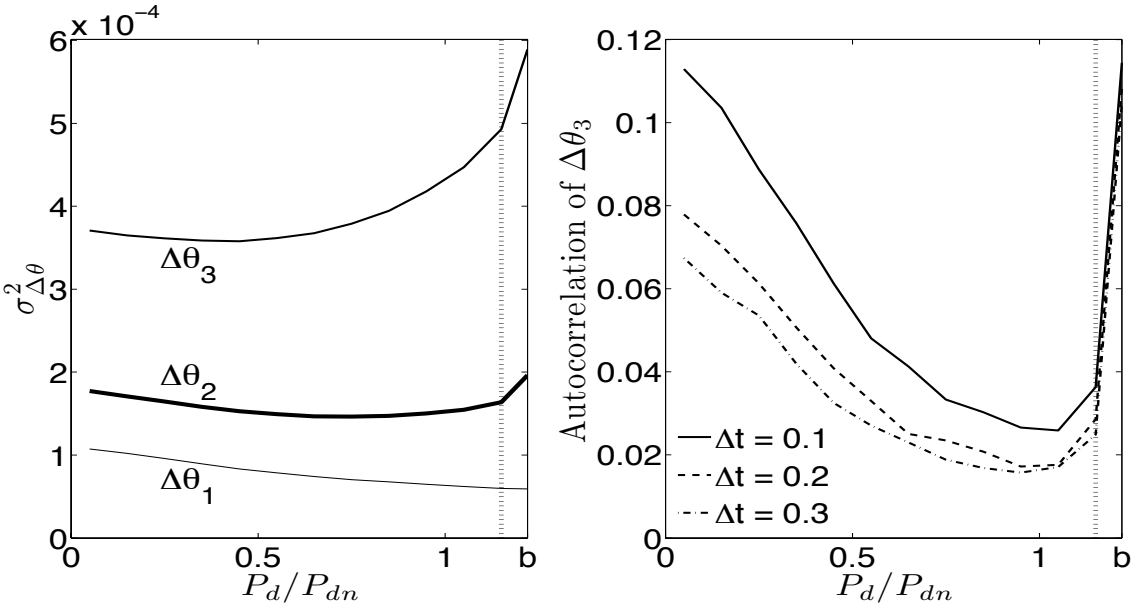

Figure 3.5: Variance and autocorrelation of the voltage angle of the load bus versus load level. Note that the autocorelation $\langle \Delta\theta(t)\Delta\theta(t+\Delta t)\rangle$ is shown only for $\Delta\theta_3$; it is similar for the other two angles.

which can be directly measured. There are other entries as well, which explains why the displayed entries do not satisfy the conventional normalization:

$$|u_1|^2 + |u_2|^2 + ... = 1 \tag{3.10}$$

where u_i is the i-th entry of a column of ϕ or C. We see that the "activity" of the state variables $\delta_{1,2}, \dot{\delta_{1,2}}$ is too small compared to that of other state variables. This is reflected in Figs. 3.6 and 3.7 by the fact that these variables do not show any substantial increase in variance except perhaps very near the bifurcation point. The "activity" of voltage magnitudes $V_{1,2,3}$ and angles $\theta_{1,2,3}$ is also not very high (in light of the normalization (3.10)). Yet, the "activity" of $V_{1,2,3}$ relative to other variables is, apparently, high enough for the variance of $V_{1,2,3}$ to exhibit conspicuous increase near the bifurcation. Note that of the three angles, θ_3 has the largest "activity", and its variance's increase is comparable to that of $V_{1,2,3}$. The other two angles have too small "activities", and their variances do not show monotonic growth as P_d approaches the Hopf bifurcation value.

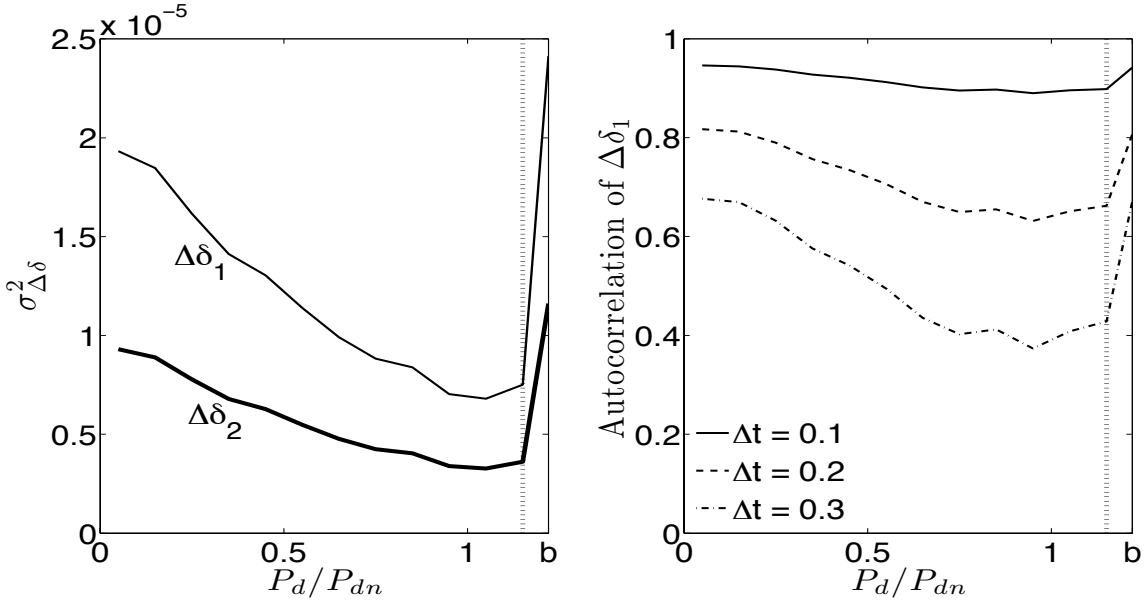

Figure 3.6: Variances and autocorrelations of the generators rotor angles versus load level. Note that the autocorelation $\langle \Delta\delta(t)\Delta\delta(t+\Delta t)\rangle$ is shown only for $\Delta\delta_1$; it is similar for the other generator angle.

Table 3.1: Relative activity of differential and algebraic variables in dominant mode

θ_1	θ_2	θ_3	V_1	V_2	V_3
0.0081	0.0631	0.0946	0.1525	0.1476	0.1664
δ_1	δ_2	$\dot{\delta_1}$	$\dot{\delta_2}$		
0.0661	0.0254	$1e-4$	$4e-5$		

3.5 Conclusion

In this chapter, we showed that critical slowing down occurs in power system for Hopf bifurcation. As shown in chapter 2 for the saddle-node bifurcation, the results show that CSD signs for the Hopf bifurcation are better observable in some variables than others as well. We showed that this occurs because fluctuations of some variables are more aligned with the direction of dominant mode. Specifically, we found that variance of load bus voltage magnitude is a good early warning sign of Hopf bifurcation. This property along with the availability of fast PMU measurements can potentially help in developing a method for monitoring of oscillatory stability in power grid using phasor measurements.

3.6 System data

System base power is 100 MVA.

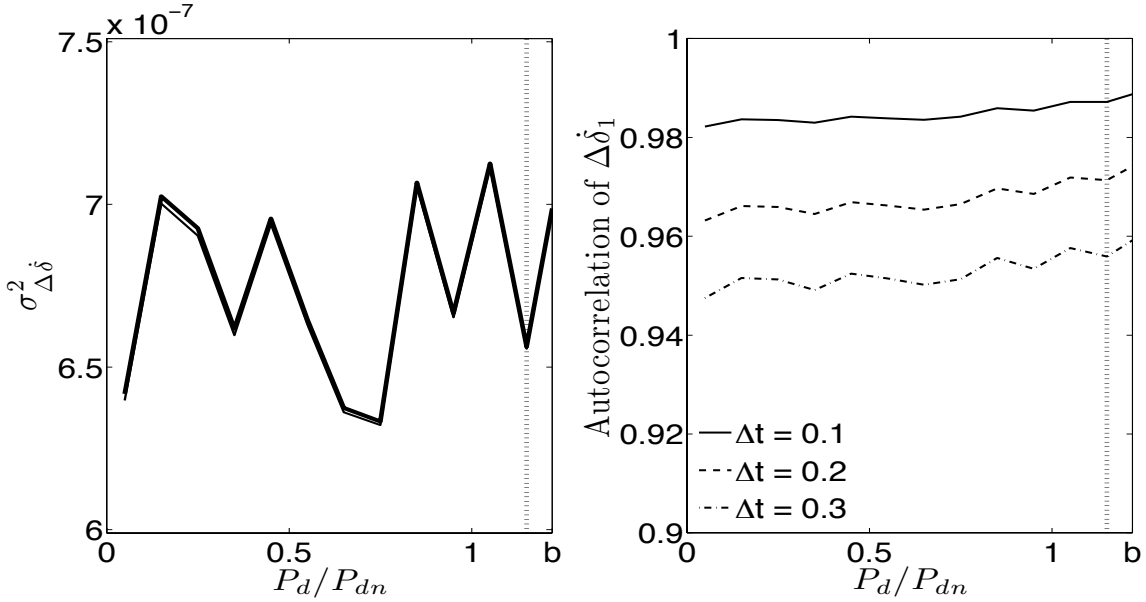

Figure 3.7: Variances and autocorrelations of the generators speed deviations versus load level. Variances of $\Delta\dot{\delta}_1$ and $\Delta\dot{\delta}_2$ are very close, so their difference is not observable in the left-hand side panel. Note that the autocorelation $\langle\Delta\dot{\delta}(t)\Delta\dot{\delta}(t+\Delta t)\rangle$ is shown only for $\Delta\dot{\delta}_1$; it is similar for the other generator speed.

Nominal load and generation:

$P_d = 900\text{MW}, Q_d = 300\text{MVAR}, P_{g2} = 400\text{MW}$

Synchronous generator:

Bus no.	Base MVA	r(pu)	X_d(pu)	X'_d(pu)
1	555.5	0	1.81	0.3
2	700	0	1.81	0.3
	$X"_d$(pu)	T'_{do}(s)	$T"_{do}$(s)	X_q(pu)
1	0.217	7.8	0.022	1.76
2	0.217	7.8	0.022	1.76
	X'_q(pu)	$X"_q$(pu)	T'_{qo}(s)	$T"_{qo}$(s)
1	0.61	0.217	0.9	0.074
2	0.61	0.217	0.9	0.074
	M(s)	D(pu)		
1	9.06	0		
2	13.06	0		

Exciter:

Exciter model is PSAT's Type III model (Milano 2008).

Gen. no.	v^f_{max}	v^f_{min}	K_0	T_2	T_1
1	40	-40	20	12	1
2	40	-40	20	12	1
	v^f_0	S_0	T_e	T_r	
1	0	0	0.04	0.05	
2	0	0	0.04	0.05	

Turbine Governor:

Turbine Governor model is PSAT's Type II model (Milano 2008).

Gen. no.	R	P_{max}	P_{min}	T_2	T_1
1	0.2	10	0.3	5	0

Bibliography

Abraham, S. and J. Efford (2004). Final report on the August 14, 2003 blackout in the United states and Canada: causes and recommendations. Technical report, US–Canada Power Syst. Outage Task Force.

Ajjarapu, V. and B. Lee (1992, Feb.). Bifurcation theory and its application to nonlinear dynamical phenomena in an electrical power system. *IEEE Trans. Power Syst. 7*(1), 424–431.

Bacher, R., U. Naf, M. Renggli, W. Buhlmann, and H. Glavitsch (2003, Nov.). Report on the blackout in Italy on 28 september 2003. Technical report, Swiss Federal Office of Energy.

Boerlijst, M. C., T. Oudman, and A. M. de Roos (2013). Catastrophic collapse can occur without early warning: examples of silent catastrophes in structured ecological models. *PloS one 8*(4), e62033.

Browne, T. J., V. Vittal, G. T. Heydt, and A. R. Messina (2008). A comparative assessment of two techniques for modal identification from power system measurements. *IEEE Trans. Power Syst. 23*(3), 1408–1415.

Cañizares, C. A., N. Mithulananthan, F. Milano, and J. Reeve (2004). Linear performance indices to predict oscillatory stability problems in power systems. *IEEE Trans. Power Syst. 19*(2), 1104–1114.

Cotilla-Sanchez, E., P. D. H Hines, and C. M. Danforth (2012). Predicting critical transitions from time series synchrophasor data. *IEEE Trans. Smart Grid 3*(4), 1832–1840.

FERC and NERC (2012, Apr.). Arizona–Southern California outages on September 8, 2011: causes and recommendations. Technical report.

Ghanavati, G., P. D. Hines, T. Lakoba, and E. Cotilla-Sanchez (2013a). Calculation of the autocorrelation function of the stochastic single machine infinite bus system. In *Proc. North Amer. Power Symp.*, 1–6.

Ghanavati, G., P. D. Hines, T. I. Lakoba, and E. Cotilla-Sanchez (2013b). Understanding early indicators of critical transitions in power systems from autocorrelation functions. *IEEE Trans. Circuits Syst. I. 61*(9), 2747–2760.

Ghasemi, H. (2006). *On-line monitoring and oscillatory stability margin prediction in power systems based on system identification*. Ph. D. thesis, University of Waterloo.

Hastings, A. and D. B. Wysham (2010). Regime shifts in ecological systems can occur with no warning. *Ecology Lett. 13*(4), 464–472.

Kakimoto, N., M. Sugumi, T. Makino, and K. Tomiyama (2006). Monitoring of interarea oscillation mode by synchronized phasor measurement. *IEEE Trans. Power Syst. 21*(1), 260–268.

Klein, M., G. Rogers, and P. Kundur (1991, Aug.). A fundamental study of inter-area oscillations in power systems. *IEEE Trans. Power Syst. 6*(3), 914–921.

Kosterev, D., S. Yirga, and V. Venkatasubramanian (1997, Mar.). Validation report of the august 10, 1996 WSCC disturbance. Technical report, Western Systems Coordinating Council.

Kuehn, C. (2011, Jun.). A mathematical framework for critical transitions: Bifurcations, fast-slow systems and stochastic dynamics. *Phys. D: Nonlinear Phen. 240*(12), 1020–1035.

Kundur, P. (1994). *Power system stability and control*. Tata McGraw-Hill Education.

Kundur, P., J. Paserba, V. Ajjarapu, G. Andersson, A. Bose, C. Canizares, N. Hatziargyriou, D. Hill, A. Stankovic, C. Taylor, et al. (2004). Definition and classification of power system stability IEEE/CIGRE joint task force on stability terms and definitions. *IEEE Trans. Power Syst. 19*(3), 1387–1401.

Mantzaris, J. C., A. Metsiou, and C. D. Vournas (2013, Nov.). Analysis of interarea oscillations including governor effects and stabilizer design in south-eastern europe. *IEEE Trans. Power Syst. 28*(4), 4948–4956.

Milano, F. (2005). An open source power system analysis toolbox. *IEEE Trans. Power Syst. 20*(3), 1199–1206.

Milano, F. (2008, June). *Power System Analysis Toolbox Quick Reference Manual for PSAT version 2.1. 2*.

Podolsky, D. and K. Turitsyn (2013). Random load fluctuations and collapse probability of a power system operating near codimension 1 saddle-node bifurcation. *Power Energy Soc. Gen. Meeting*, 1–5.

Podolsky, D. and K. Turitsyn (2013). Critical slowing-down as indicator of approach to the loss of stability. *arXiv preprint arXiv:1307.4318*.

Scheffer, M., J. Bascompte, W. A. Brock, V. Brovkin, S. R. Carpenter, V. Dakos, H. Held, E. H. Van Nes, M. Rietkerk, and G. Sugihara (2009). Early-warning signals for critical transitions. *Nature 461*(7260), 53–59.

CHAPTER 4: IDENTIFYING USEFUL STATISTICAL INDICATORS OF PROXIMITY TO INSTABILITY IN STOCHASTIC POWER SYSTEMS

4.1 Abstract

The results in chapters 2 and 3 show that autocorrelation and variance in voltage measurements tend to increase as power systems approach instability. To determine the practical implications of such results, this chapter seeks to identify the conditions under which these statistical indicators provide reliable early warning of instability in power systems. First, the chapter derives and validates a semi-analytical method for quickly calculating the expected variance and autocorrelation of all voltages and currents in an arbitrary power system model. Building on this approach, the chapter describes the conditions under which filtering can be used to detect these signs in the presence of measurement noise. Finally, several experiments show which types of measurements are good indicators of proximity to instability for particular types of state changes. For example, increased variance in voltages can reliably indicate the location of increased stress, while growth of autocorrelation in certain line currents is a reliable indicator of system-wide instability.

4.2 Introduction

The goal of this chapter is to present a general method for estimating the autocorrelation and variance of state variables from a power system model and to use the results to determine which variables in a power system provide useful early warning of critical transitions in the presence of measurement noise. To this end, Sec. 4.3 presents a semi-analytical method for calculating the variance and autocorrelation of algebraic and differential variables. This method enables the fast calculation of voltage and current statistics for many potential operating scenarios in large power systems, and unlike the method in (Podolsky and Turitsyn 2013b), is not limited to the immediate vicinity of a bifurcation. Sec. 4.4 illustrates the method using the 39-bus test case and shows that some variables are better indicators of proximity to instability than others. Sec. 4.5 extends the analysis to systems

with measurement noise and presents a method for detecting CSD in the presence of measurement noise. Sec. 4.6 uses this approach to identify stressed areas in a power network. Finally, the conclusions of the chapter are presented in Sec. 4.7.

4.3 Calculation of Autocorrelation and Variance in Multimachine Power Systems

This section presents a semi-analytical method for the fast calculation of variance (σ^2) and autocorrelation $(R(\Delta t))$ of bus voltage magnitudes and line currents in power system. Fluctuations of load and generation are well known sources of stochasticity in power systems. While this section models only randomness in load, the method can be readily extended to the case of stochasticity in power injections.

4.3.1 System Model

Adding stochastic load to the set of general differential-algebraic equations (DAE) that model a power system gives (similar to 3.1 and 3.2):

$$\dot{\underline{x}} = f\left(\underline{x}, \underline{y}\right) \tag{4.1}$$

$$0 = g\left(\underline{x}, \underline{y}, \underline{u}\right) \tag{4.2}$$

where f, g represent differential and algebraic equations, $\underline{x}, \underline{y}$ are vectors of differential and algebraic variables (generator rotor angles, bus voltage magnitudes, etc.), and $\underline{u}$ is the vector of load fluctuations. The algebraic equations consist of nodal power flow equations and static equations for components such as generator, exciter, and turbine governor. The differential equations describe the dynamic behavior of the equipment. In this chapter, for modeling load fluctuations, we take an approach similar to (Perninge et al. 2010), (Hauer et al. 2007) and assume that load fluctuations $\underline{u}$ follow the Ornstein–Uhlenbeck process:

$$\dot{\underline{u}} = -E\underline{u} + \underline{\xi} \tag{4.3}$$

where E is a diagonal matrix whose diagonal entries equal t_{corr}^{-1}, where t_{corr} is the correlation time of the load fluctuations, and $\underline{\xi}$ is a vector of independent Gaussian random variables:

$$\begin{aligned} \mathrm{E}\left[\underline{\xi}\,(t)\right] &= 0 && (4.4) \\ \mathrm{E}\left[\xi_i\,(t)\,\xi_j\,(s)\right] &= \delta_{ij}\sigma_{\xi}^2\delta_I(t-s) && (4.5) \end{aligned}$$

where t, s are two arbitrary times, δ_{ij} is the Kronecker delta function, σ_{ξ}^2 is the intensity of noise and δ_I represents the unit impulse (delta) function. Equations (4.1)–(4.3) form the set of SDAEs that models a power system with stochastic load.

We also consider the frequency-dependence of loads, which can measurably impact the statistics of voltage magnitudes as shown in chapter 2. Loads are thus modeled as follows (Berg 1973), (Milano 2010):

$$\begin{aligned} \Delta\omega &= \frac{1}{2\pi f_n}\frac{d\,(\theta-\theta^0)}{dt} && (4.6) \\ P &= P^0\,(1+\Delta\omega)^{\beta_P} && (4.7) \\ Q &= Q^0\,(1+\Delta\omega)^{\beta_Q} && (4.8) \end{aligned}$$

where $\Delta\omega$ is the frequency deviation at the load bus, θ^0, P^0, Q^0 are the baseline voltage angle, active and reactive power of each load, β_P, β_Q are exponents that determine the level of frequency dependence, f_n is the nominal frequency and θ is the bus voltage angle.

Using this model, we studied the New England 39-bus test case (Pai 1989). As load increases, a Hopf bifurcation occurs just before the nose of the PV curve (see (Lerm et al. 2003) and (Rosehart and Cañizares 1999)).

4.3.2 Solution Method

Linearizing (4.2) gives the following:

$$\Delta\underline{y} = \begin{bmatrix} -g_y^{-1}g_x & -g_y^{-1}g_u \end{bmatrix} \begin{bmatrix} \Delta\underline{x} \\ \Delta\underline{u} \end{bmatrix} \qquad (4.9)$$

where g_x, g_y, g_u are the Jacobian matrices of g with respect to $\underline{x}, \underline{y}, \underline{u}$. Linearizing (4.1) and (4.3) and eliminating $\Delta\underline{y}$ via (4.9) gives the following:

$$\begin{bmatrix} \Delta\dot{\underline{x}} \\ \Delta\dot{\underline{u}} \end{bmatrix} = \begin{bmatrix} A_s & -f_y g_y^{-1} g_u \\ 0 & -E \end{bmatrix} \begin{bmatrix} \Delta\underline{x} \\ \Delta\underline{u} \end{bmatrix} + \begin{bmatrix} 0 \\ I_n \end{bmatrix} \underline{\xi} \tag{4.10}$$

where f_x, f_y are the Jacobian matrices of f with respect to $\underline{x}, \underline{y}$ and $A_s = f_x - f_y g_y^{-1} g_x$; I_n is an identity matrix, with n being the length of $\underline{u}$. If we let $\underline{z} = \begin{bmatrix} \Delta\underline{x} & \Delta\underline{u} \end{bmatrix}^T$, (4.10) can be re-written in the standard form:

$$\dot{\underline{z}} = A\underline{z} + B\underline{\xi} \tag{4.11}$$

The covariance matrix of $\underline{z}$ ($\sigma_{\underline{z}}$) satisfies the Lyapunov equation (Gardiner 2010):

$$A\sigma_{\underline{z}} + \sigma_{\underline{z}} A^T = -BB^T \tag{4.12}$$

which can be solved efficiently in $O(n^3)$ operations using MATLAB's `lyap` function. To stress the difference between the solution from (4.12) and the results of direct numerical simulation of (4.1)–(4.3), we will refer to the former solution as semi-analytical. The reason why we refer to it as semi-analytical is that we solve the Lyapunov equation using a numerical algorithm to calculate the covariance matrix rather than deriving explicit expressions for covariance and correlations matrices as in chapter 2. Therefore, our method is not entirely analytical. It is not completely numerical either since it is not based on solving SDAEs numerically.

The stationary autocorrelation matrix can be computed given $\sigma_{\underline{z}}$ and an equation from (Gardiner 2010):

$$\mathrm{E}\left[\underline{z}(t)\,\underline{z}^T(s)\right] = \exp\left[-A\,|\Delta t|\right]\sigma_{\underline{z}} \tag{4.13}$$

where $\Delta t = t - s$. From (4.12) and (4.13) the normalized autocorrelation function of z_i can be calculated:

$$R_{z_i}(\Delta t) = \mathrm{E}\left[z_i(t)\, z_i^T(s)\right] / \sigma_{z_i}^2 \tag{4.14}$$

The covariance matrix of the algebraic variables, $\sigma_{\underline{\Delta y}}$, is found from (4.9) and (4.12):

$$\sigma_{\Delta \underline{y}} = K \sigma_{\underline{z}} K^T \tag{4.15}$$

where K is the matrix from (4.9). Similarly, the autocorrelation function of $\Delta \underline{y}(t)$ is:

$$\mathrm{E}\left[\Delta \underline{y}(t)\, \Delta \underline{y}^T(s)\right] = K \cdot \mathrm{E}\left[\underline{z}(t)\, \underline{z}^T(s)\right] K^T \tag{4.16}$$

Finally, the covariance and autocorrelation matrices for voltage magnitudes are a subset of the matrices from (4.15) and (4.16).

Fluctuation-induced deviations of the current magnitudes, ΔI_{ik}, in a line between buses i and k can be found by linearizing the following:

$$I_{ik} = Y_{ii} V_i e^{j(\phi_{ik} - \phi_{ik} + \theta_i - \theta_k)} + Y_{ik} V_k \tag{4.17}$$

where I_{ik} is the magnitude of the current of the line between buses i, k; V_i, θ_i are the voltage magnitude and angle of bus i; Y_{ii}, ϕ_{ii} and Y_{ik}, ϕ_{ik} are magnitudes and angles of the diagonal and off-diagonal elements of the Y_{BUS} matrix. By linearizing (4.17) one can find $\Delta \underline{I}$ from Δy and then compute the covariance and autocorrelation matrices of $\Delta \underline{I}$ from equations similar to (4.15) and (4.16).

Comparing the semi-analytical method with the numerical solution shows that the former is significantly more time-efficient. For the numerical simulations in this chapter, we solved (4.1)–(4.3) using the trapezoidal DAE solver in the Power System Analysis Toolbox (PSAT) (Milano 2005). To find numerical values for σ^2 and $R(\Delta t)$ we ran 100 240s simulations, with an integration step size of 0.01s, and then computed the statistics. For the 39-bus case with 140 variables, solving for σ_z^2 using the semi-analytical method

took approximately 0.08s, whereas calculating the variances using numerical simulations took about 24 hours.

4.4 Useful early warning signs: voltage magnitudes and line currents

This section applies the method in Sec. 4.3 to calculate the autocorrelation and variance of voltages and currents in the 39-bus test case. These results are subsequently used to identify particular locations and variables in which the statistical early-warning signs are most clearly observable.

4.4.1 Autocorrelation and Variance of Voltages

Using the methods described in Sec. 4.3, we calculated $\sigma^2,\ R\left(\Delta t\right)$ of bus voltage magnitudes in the 39-bus test case both semi-analytically and numerically using PSAT. In order to see how these statistics change as the system state moves toward the bifurcation, we increased all loads uniformly, multiplying each load by the same factor. For the correlation time and intensity of noise we used: $t_{corr} = 1$s and $\sigma_u^2 = 10^{-4}$ pu. The values of β_P, β_Q in (A.2), (A.3) were chosen randomly from within $[2, 3]$ and $[1, 2]$, respectively (Berg 1973). For all results in this chapter, we chose the autocorrelation time lag $\Delta t = 0.2$s, based on the criteria for choosing an optimal Δt described in chapter 2.

Fig. 4.1 shows several typical, illustrative examples of how $\sigma^2,\ R\left(\Delta t\right)$ of bus voltage magnitudes depend on load level in the 39-bus case. These results show that, as anticipated from CSD theory, both σ^2 and $R\left(\Delta t\right)$ of voltage magnitudes increase as the system approaches the bifurcation. However, not all of these signs appear sufficiently early to detect the bifurcation and take mitigating actions. For example, $\sigma^2_{\Delta V}$ in buses 7, 14, and 26 exhibits a conspicuous increase when the load level is 10–15$\%$ below the bifurcation. These variables are good early warning signs (EWS) of the impending bifurcation. In contrast, $\sigma^2_{\Delta V}$ in buses 20 and 36 is not a useful warning sign as its increase occurs too close to the bifurcation. The situation with autocorrelation is reversed, as shown in the second panel of Fig. 4.1.

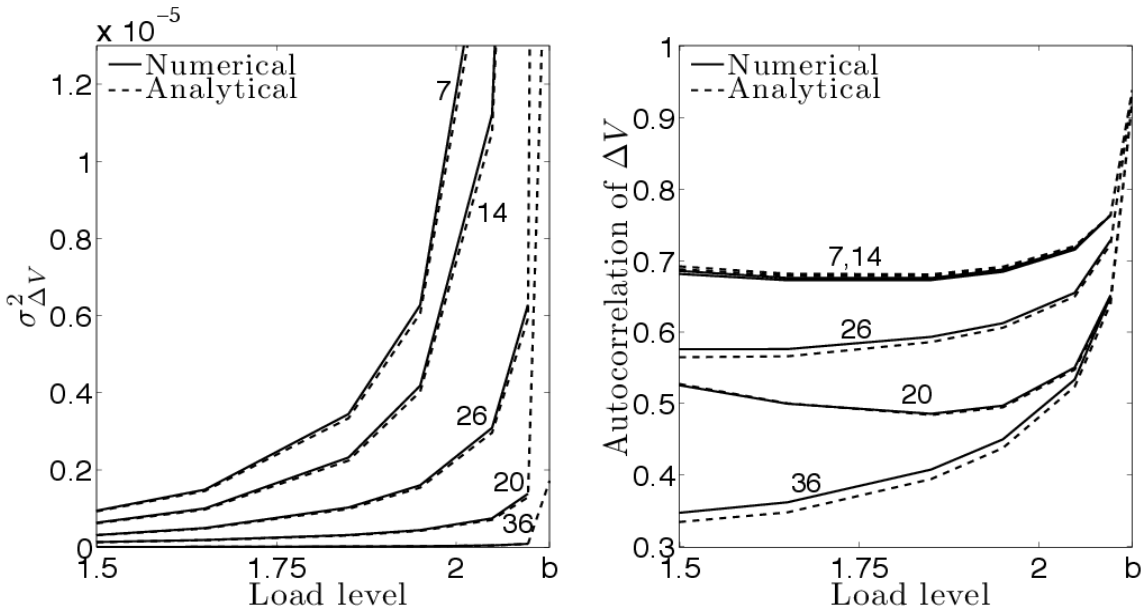

Figure 4.1: Variance and autocorrelation of voltage magnitudes for five buses in the 39-bus test case versus load level. Load level is the ratio of the system loads to their nominal values. b denotes the bifurcation point. The bus number associated with each curve is shown next to it. Here and everywhere below the autocorrelation time lag $t - s = 0.2$s.

By examining σ^2 and $R(\Delta t)$ for all buses in our test system, we have concluded that, as Fig. 4.1 illustrates, good EWS occur in two different types of buses. We found that σ^2 is a good EWS for load buses, whereas $R(\Delta t)$ is a good EWS at buses that are close to generators with low inertia. In addition, we found that $\sigma^2_{\Delta V}$ at generator buses is much smaller than at load buses, largely due to generator voltage control systems. As explained in Sec. 4.5, this limits the use of $R_{\Delta V}(\Delta t)$ at generator buses as an EWS.

4.4.2 Autocorrelation and Variance of Line Currents

The fact that autocorrelation of voltages is not uniformly useful as an EWS prompted us to look at other variables, particularly currents, that might be more useful indicators. Results for σ^2 and $R(\Delta t)$ of currents, shown in Fig. 4.2, suggest that while $\sigma^2_{\Delta I}$ of almost all lines increase measurably with the increase of the load level, increased $R_{\Delta I}(\Delta t)$ is clearly observable only in some of the lines, such as line $[6\ 31]$. As was the case with voltages, the common characteristic of lines that show clear increases in $R_{\Delta I}(\Delta t)$ is that they are connected to a generator with low or moderate inertia. The explanation for

this appears to be that increased $R_{\Delta I}\,(\Delta t)$ is closely tied to the way that generators respond to perturbations as the system approaches bifurcation. Increases in $R_{\Delta I}(\Delta t)$ are not clearly observable in lines that are close to load centers, such as line $[4\ 14]$ in Fig. 4.2.

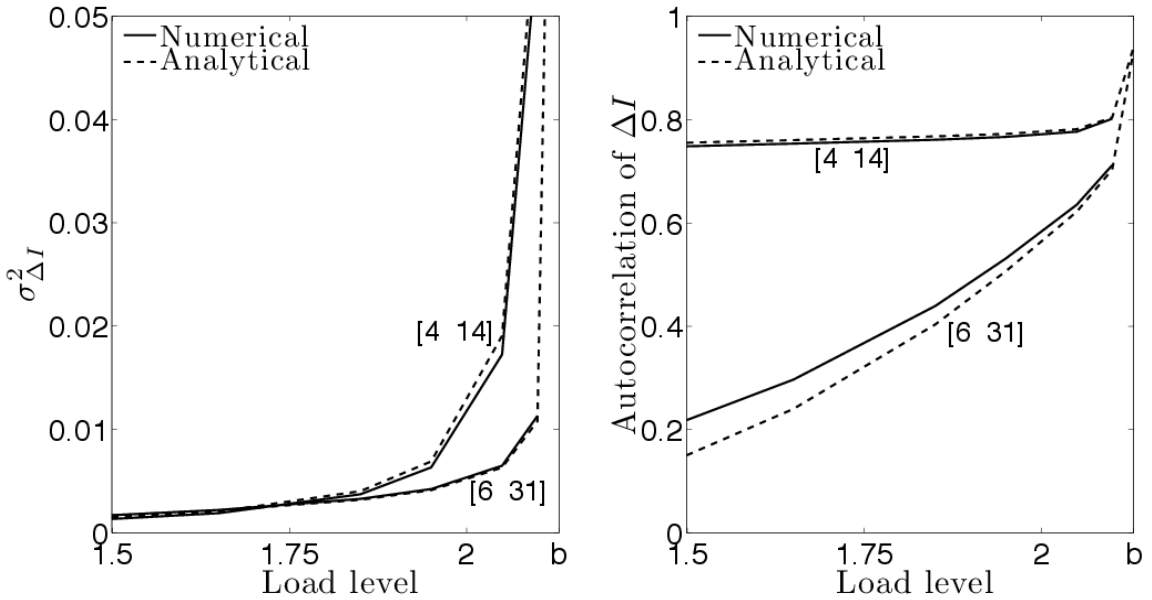

Figure 4.2: Variance and autocorrelation of current of two lines. The numbers in brackets are bus numbers at two ends of the lines.

Examining changes in $\sigma^2,\ R\,(\Delta t)$ of several state variables showed that only magnitudes of voltages and line currents signal the proximity to the bifurcation well under certain conditions mentioned above. Other variables such as voltage angle, current angle, generator rotor angle and generator speed did not show measurable or clear monotonically increasing patterns in $\sigma^2,\ R\,(\Delta t)$ that can indicate proximity to a bifurcation.

4.5 Detectability after measurement noise

This section examines the detectability of increases in σ^2 and $R\,(\Delta t)$ of voltages and currents given the presence of measurement noise. In addition, we present a method for reducing the impact of measurement noise using a band-pass filter.

4.5.1 Impact of Measurement Noise on Variance and Autocorrelation

Clearly, measurement noise will adversely impact the observability of increases in $\sigma^2,\ R\,(\Delta t)$ of voltages and currents. In order to model this impact, we assumed that

measurement noise at each bus is normally distributed with a standard deviation that is proportional to the steady-state mean voltage for this load level: $\sigma_\eta = 0.01 \langle V \rangle$. As a result the measured variance, $\sigma^2_{\Delta V_m}$, of a bus voltage increases to:

$$\sigma^2_{\Delta V_m} = \sigma^2_{\Delta V} + \sigma^2_\eta \tag{4.18}$$

where $\sigma^2_{\Delta V}$ is the variance before adding measurement noise.

Applying this method, Fig. 4.3 shows σ^2 and $R(\Delta t)$ for the voltage magnitudes of the same five buses used in Sec. 4.4.1, but after adding measurement noise. The results show that measurement noise causes the increases in $\sigma^2_{\Delta V_m}$ to occur only close to the bifurcation, except for bus 36. In fact, $\sigma^2_{\Delta V_m}$ decreases for most buses, until close to the bifurcation. The reason for this decrease is that, based on (4.18), σ^2_η decreases with $\langle V \rangle$, and $\langle V \rangle$ decreases as the system moves toward the nose of the PV curve. Also, because of the 1% measurement noise, $\sigma^2_\eta > \sigma^2_{\Delta V}$ until close to the bifurcation for most buses. For bus 36, which is a generator bus, σ^2 is almost constant since $\langle V \rangle$ (and as a result of σ^2_η) is held constant by the exciter; $\sigma^2_\eta \gg \sigma^2_{\Delta V}$ for generator buses.

Fig. 4.3 also shows that $R_{\Delta V_m}(\Delta t)$ increases significantly near the bifurcation for buses 7, 14 and, to a lesser extent, for bus 26. Appendix 4.8 demonstrates that the increase in $R_{\Delta V_m}(\Delta t)$ of these buses is largely an artifact of adding measurement noise: it is primarily due to increases in σ^2 rather than that of $R(\Delta t)$. Autocorrelation of ΔV_m is almost zero for buses 20, 36 since the uncorrelated measurement noise dominates the voltage of buses near generators.

Thus, measurement noise essentially washes out the useful EWS that we reported in Sec. 4.4.1. In addition, there is another issue impacting the detectability of EWS, which we discuss in the next subsection.

4.5.2 Spread of Statistics

One important point regarding the detection of increased σ^2 and $R(\Delta t)$ is that the measured statistics of a *sample* of a variable's measurement data (which an operator can

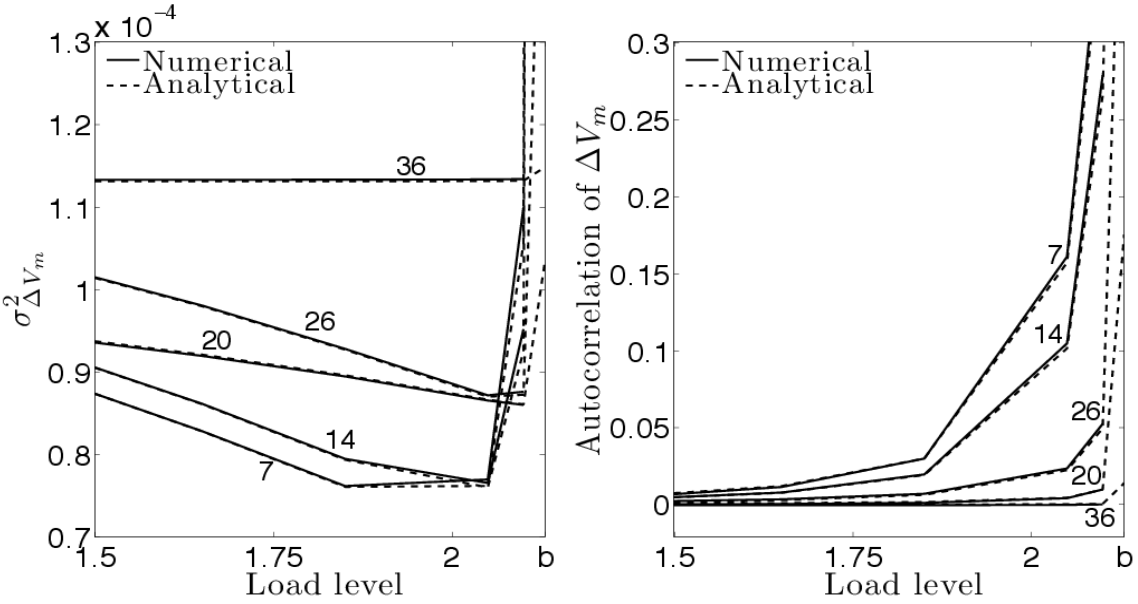

Figure 4.3: Variances and autocorrelations of voltage magnitudes of five buses in the 39-bus test case versus load level, accounting for measurement noise.

observe in finite time) are different from the mean statistical properties of that variable over infinitely many measurements. Although the mean of these statistics typically grows as the system approaches a bifurcation, the variance (spread) of these statistics that results from finite sample sizes can cause difficulty in estimating the distance to the bifurcation.

In order to quantify the detectability of an increase in σ^2 or $R\left(\Delta t\right)$, we introduce an index $q_{95/80}$ (see Fig. 4.4):

$$q_{95/80} = \int_{a}^{\infty} f_{X(80\%)} dx + \int_{-\infty}^{a} f_{X(95\%)} dx \tag{4.19}$$

where X is the statistic of interest (σ^2 or $R\left(\Delta t\right)$), $f_{X(80\%)}$ and $f_{X(95\%)}$ are the probability density functions (pdfs) of X for load levels of 80% and 95% of the bifurcation, and a is the point where the two distributions intersect. This measure ranges from 0 to 1, where 0 suggests that there is no overlap between the two distributions, such that detectability is unimpeded by the statistic's spread, while $q_{95/80} = 1$ means that the two distributions completely overlap—i.e. the statistic does not increase. When the statistic has a decreasing

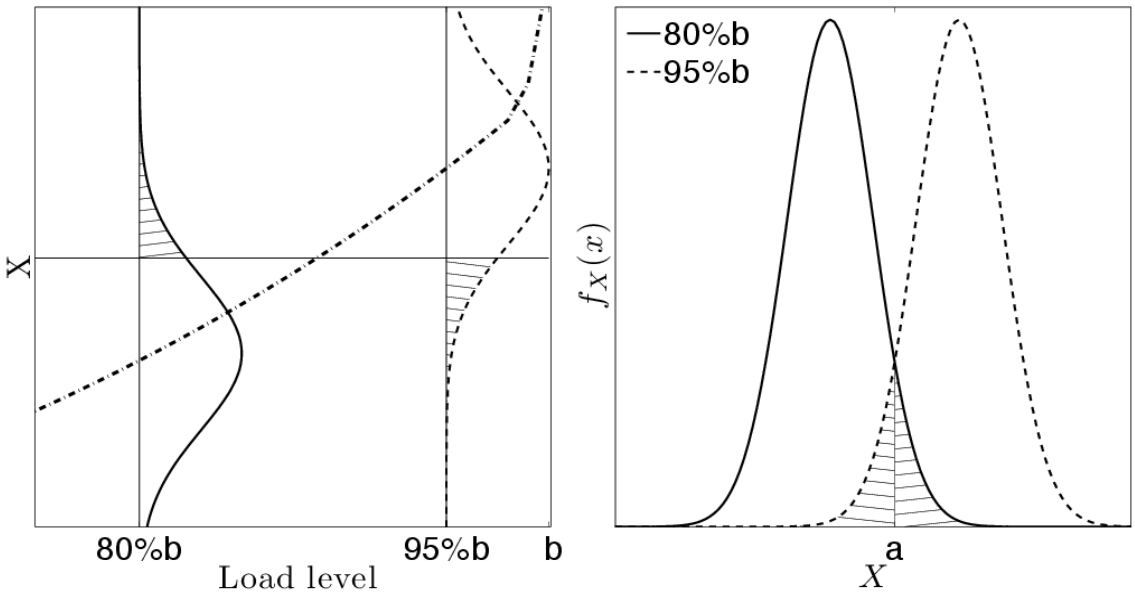

Figure 4.4: The left panel shows the empirical pdfs of X, which can be σ^2 or $R(\Delta t)$ of measurements for two load levels. Measure $q_{95/80}$ is equal to the sum of the hatched areas. The dash-dot line shows the mean of X versus load level. The right panel shows an alternative view of the pdfs.

trend, we declare $q_{95/80} = NA$. $q_{95/80}$ roughly corresponds to the probability of being able to correctly distinguish between the measured statistics at 80% and 95% load levels.

4.5.3 Filtering Measurement Noise

In this section, we explore the use of a band-pass filter to reduce the impact of measurement noise on the statistics of voltage and current measurements. The reason for filtering out the high frequency content of measurements is that the power spectral density (PSD) of voltages and currents (see Fig. 4.5) shows that the power of the system noise (i.e., voltage or current magnitude variations in response to load fluctuations) is concentrated mostly in its low frequencies. This appears to be typical for Hopf and saddle-node bifurcations in power systems. On the other hand, in order to detect CSD, it is necessary to remove slow trends that result not from CSD but from other factors, such as gradual changes in the system's operating point (Dakos et al. 2008). By experimentation, we found that a band-pass filter with a pass-band of [0.1, 2] Hz reduces the impact of measurement noise in this system optimally. The rationale for these bounds can be seen from Fig. 4.5,

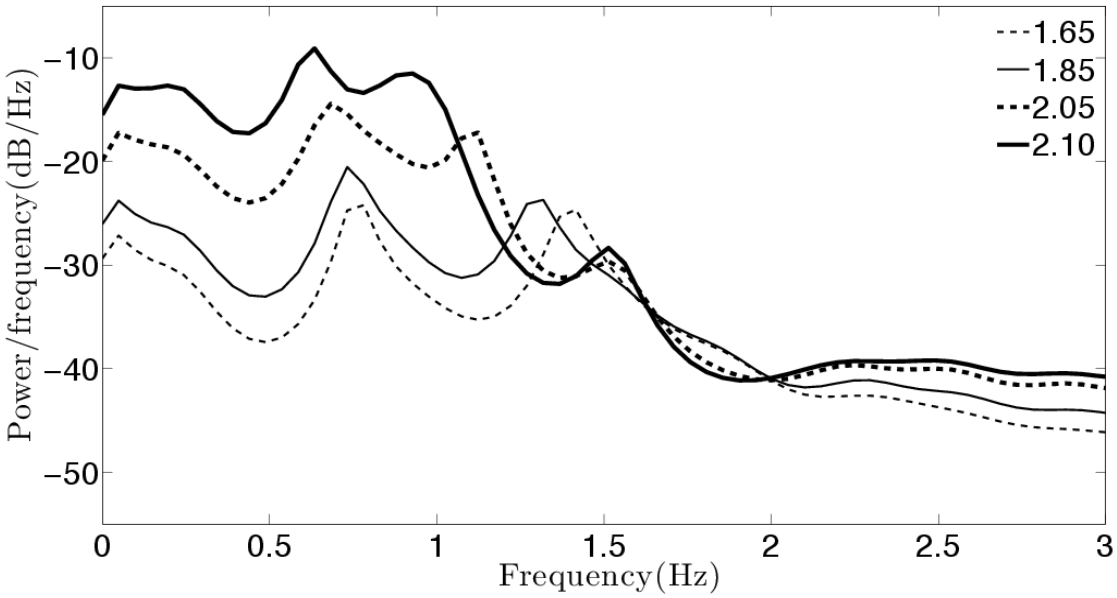

Figure 4.5: Power spectral density of the current of line [6 31] for several load levels listed in the legend. Bifurcation is at load level=2.12.

which shows the PSD of a typical current magnitude in our system. We use this filter for all "filtered" results reported subsequently.

Fig. 4.6 shows $\sigma^2_{\Delta V}$, $R_{\Delta V}(\Delta t)$ of buses 7, 36 after filtering measurement noise. Comparing Fig. 4.6 with Fig. 4.3 shows that using the band-pass filter significantly improves the detectability of increases in $\sigma^2_{\Delta V_7}$, which is close to load centers, but is not effective for bus 36, which is connected to a generator. The reason is that, even with filtering, it is still necessary that σ^2 without measurement noise be sufficiently large so that measurement noise does not dominate it. σ^2 of measurement noise after filtering will approximately be:

$$\sigma^2_{\eta f} = \sigma^2_{\eta} \cdot \frac{f_H - f_L}{(f_s/2)} \tag{4.20}$$

where $\sigma^2_{\eta f}$ is the variance of measurement noise after filtering; f_H, f_L are upper and lower cut-off frequencies of the filter; and f_s is the sampling frequency of measurements. Assuming $\sigma^2_{\eta} = 1e-4$ and $f_s = 60$Hz, we get $\sigma^2_{\eta f} = 6.3 \times 10^{-6}$. From Fig. 4.1, one can see that only $\sigma^2_{\Delta V}$ of the load buses exceeds this value near the bifurcation.

Fig. 4.6 also shows that after filtering out measurement noise, the increase in $R_{\Delta V_7}(\Delta t)$ is detectable near the bifurcation. However, as mentioned in Sec. 4.5.1, in-

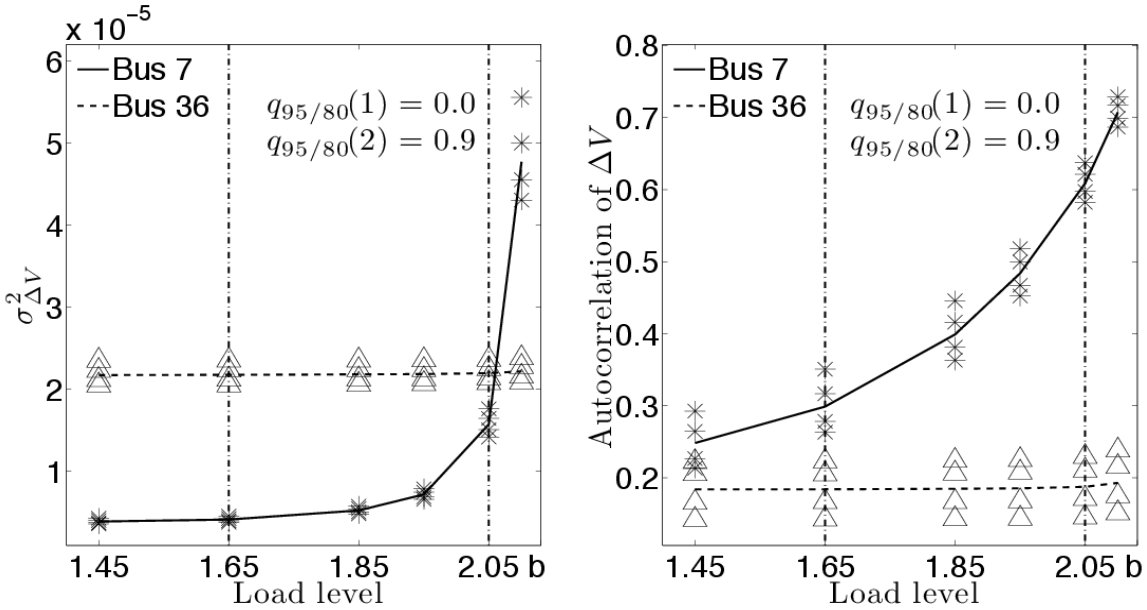

Figure 4.6: Variance and autocorrelation of voltage magnitude of buses 7,36 versus the load level after filtering the measurement noise. In this and subsequent figures, the lines show the mean and the discrete symbols $(*, \triangle)$ represent 5th, 25th, 75th, 95th percentiles of values of σ^2, $R\,(\Delta t)$ for 100 realizations at each load level. The vertical dash-dot lines show $Load\,level = 80\%b,\ 95\%b$.

creases in $R(\Delta t)$ primarily result from increases in $\sigma^2_{\Delta V}$, and thus do not provide additional information regarding the proximity of the system to the bifurcation. Since $\sigma^2_\eta \gg \sigma^2_{\Delta V}$ for generator buses, $R_{\Delta V_{36}}\,(\Delta t)$ also does not increase measurably as the system approaches the bifurcation, even after filtering.

Similar to the case without measurement noise, $R\,(\Delta t)$ of line currents close to generators increase more clearly than that of lines near load centers. Fig. 4.7 shows $\sigma^2,\ R\,(\Delta t)$ of currents of lines $[6\ 31]$ and $[4\ 14]$ after filtering the noise.

In general, filtering noise from line currents is easier than from voltages since the ratio of σ^2 of the system noise (defined above) to σ^2 of measurement noise is larger for currents.

Fig. 4.8 shows the index $q_{95/80}$ for $\sigma^2_{\Delta V}$ across the 39-bus test case after filtering measurement noise. The results in Fig. 4.8 illustrate our earlier statement that $\sigma^2_{\Delta V}$ of buses near load centers are good EWS of the bifurcation while $\sigma^2_{\Delta V}$ of generator buses are not.

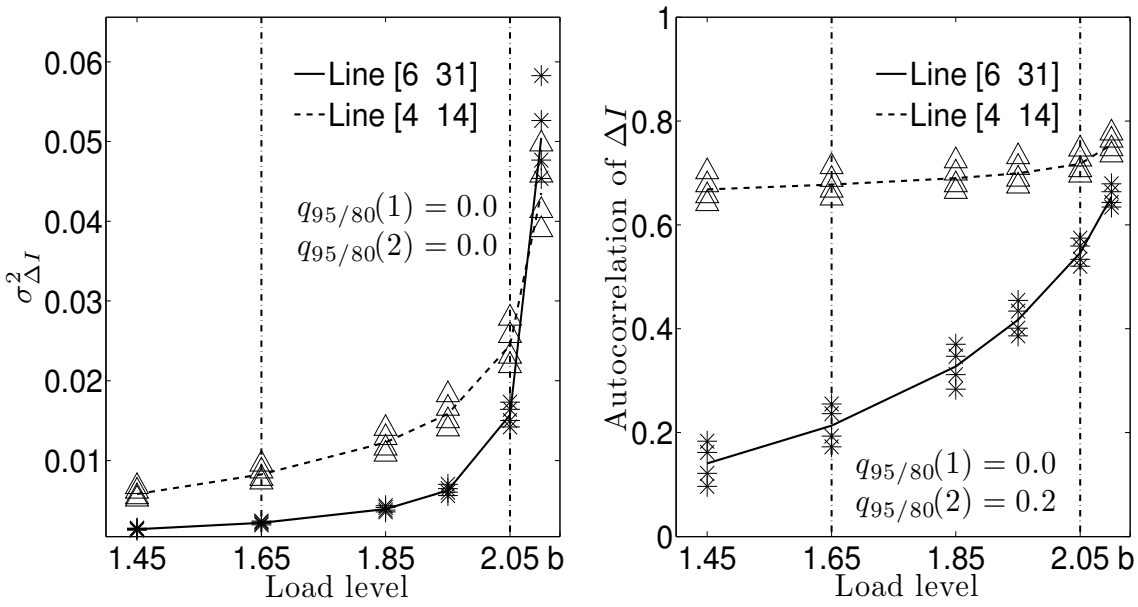

Figure 4.7: Variance and autocorrelation of currents of lines [6 31], [4 14] after filtering the measurement noise.

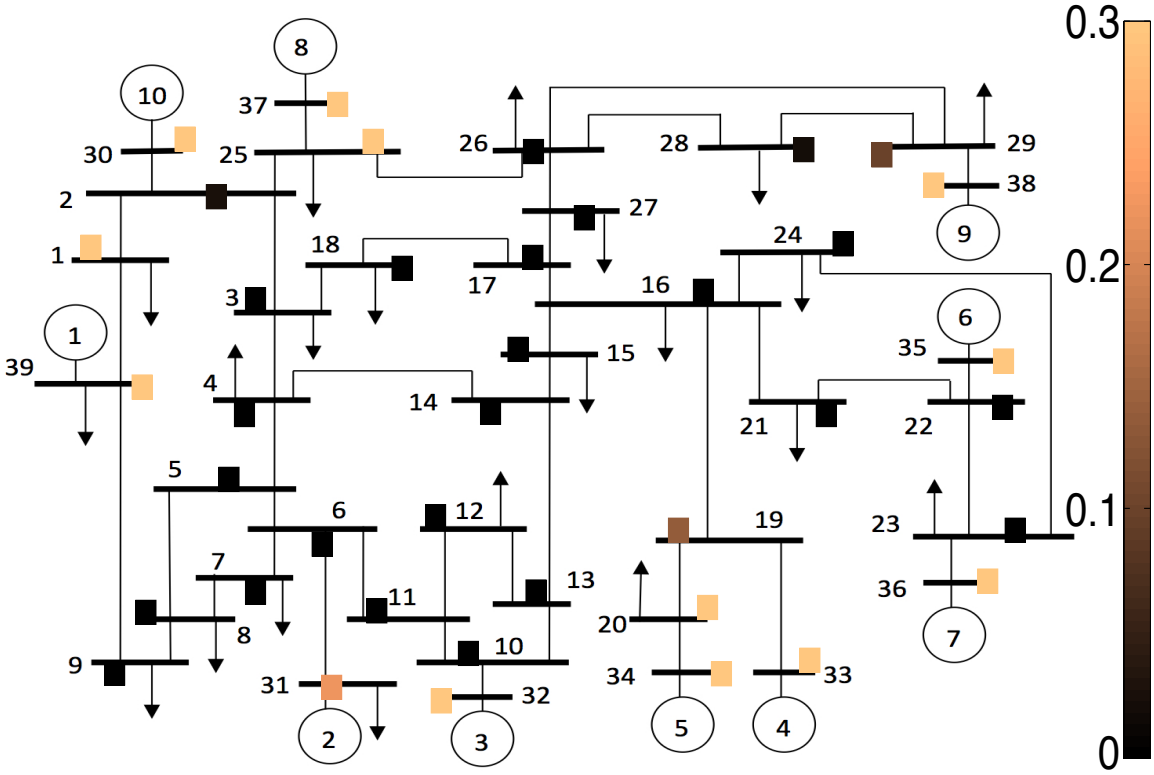

Figure 4.8: Index $q_{95/80}$ for $\sigma^2_{\Delta V}$ of bus voltages across the 39-bus test case. Here, and in Fig. 4.9, each rectangle represents the index $q_{95/80}$ for $\sigma^2_{\Delta V}$ of the bus next to it. In order to illustrate the results more clearly, we show $q_{95/80} = 0.3$ for measurements with $q_{95/80} > 0.3$, because quantities with this spread become indistinguishable.

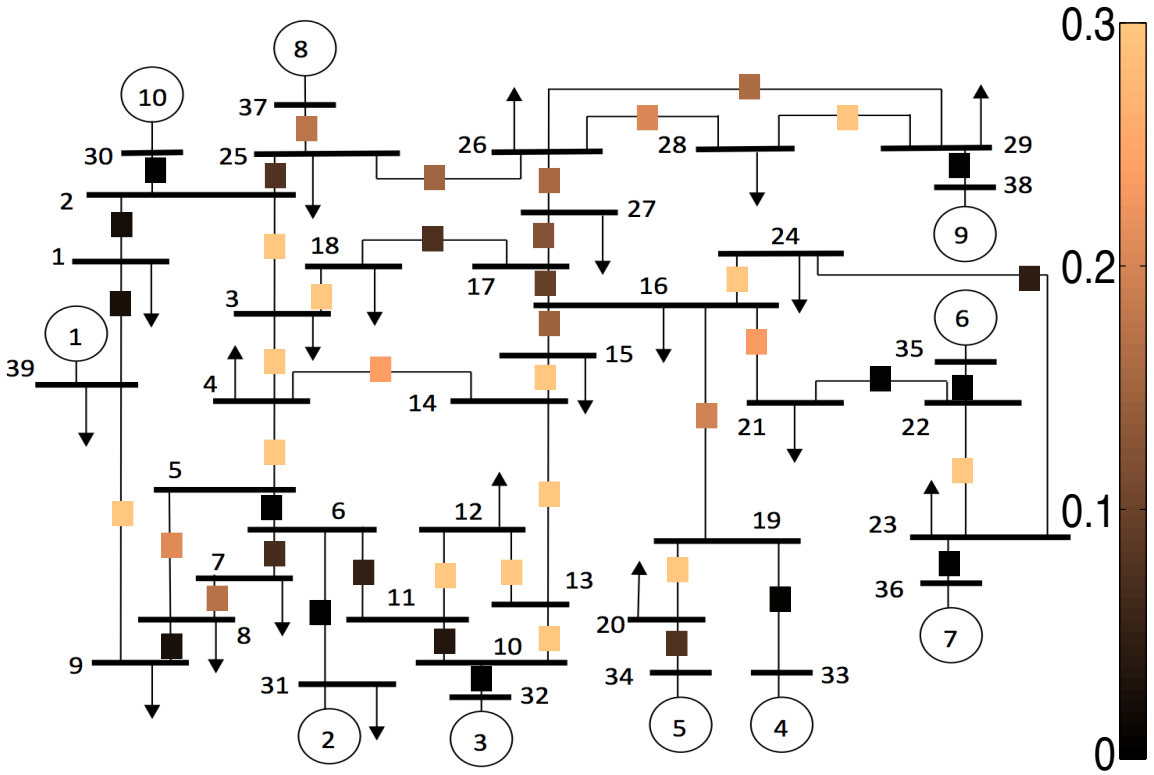

Figure 4.9: Index $q_{95/80}$ for $R_{\Delta I}(\Delta t)$ of lines across the 39-bus test case. Each rectangle represents index $q_{95/80}$ for $R_{\Delta I}(\Delta t)$ of the line next to it.

Fig. 4.9 shows the index $q_{95/80}$ for $R_{\Delta I}(\Delta t)$ of lines across the 39-bus test case after filtering the measurement noise. The results in Fig. 4.9 show that $R_{\Delta I}(\Delta t)$ of the lines near generators provide good EWS of the bifurcation while $R_{\Delta I}(\Delta t)$ of the rest of the lines do not provide useful EWS.

Note that while filtering of measurement noise can be helpful in detecting the increase in $\sigma^2_{\Delta V}$ of buses near load centers, it is not helpful in detecting an increase in $R_{\Delta V}(\Delta t)$ of these buses. This is because the $R_{\Delta V}(\Delta t)$ of such buses are not inherently good indicators of the proximity to the bifurcation; See Sec. 4.4.1. Also, filtering measurement noise will not be helpful in retrieving the statistics of the bus voltages close to generators since their variances are small compared to that of measurement noise. On the contrary, $R_{\Delta I}(\Delta t)$ of lines near generators provide good EWS for the bifurcation, while $\sigma^2_{\Delta I}$ of almost all lines provide good EWS.

4.6 Detecting Locations of Increased Stress

This section examines the potential to use statistical properties of measurements to detect the locations of increased stress in a power system. By studying two scenarios, we investigated whether patterns of change in σ^2 and $R(\Delta t)$ in a stressed area are different from the rest of the grid, so they can be helpful in identifying the location of the stressed area.

4.6.1 Transmission line tripping

In the first scenario, we disconnected lines between buses 4, 14 and buses 4, 5 in order to increase stress in the area close to bus 4. For this experiment, the load level was held constant at 1.45 times the nominal (Note that the system stress due to this load level does not cause the disconnection of the two lines). We calculated the ratio of $\sigma^2_{\Delta V}$ and $\sigma^2_{\Delta I}$ for the stressed case to the variances at the normal operating condition $(\text{Ratio}(\sigma^2))$. We also calculated the difference between $R_{\Delta V}(\Delta t)$ and $R_{\Delta I}(\Delta t)$ for the two cases $(\text{Diff}(R(\Delta t)))$. Values of $\text{Ratio}(\sigma^2)$, $\text{Diff}(R(\Delta t))$ that are sufficiently larger than 1 or 0 indicate significant increase in σ^2 or $R(\Delta t)$, respectively. Fig. 4.10(a) shows $\text{Ratio}(\sigma^2_{\Delta V})$ after adding measurement noise and filtering. The five bus voltages shown have the highest mean of $\text{Ratio}(\sigma^2)$ among all buses. The figure shows that the voltage of the buses near bus 4 have the largest $\text{Ratio}(\sigma^2_{\Delta V})$ among the system buses. As with voltages, $\sigma^2_{\Delta I}$ close to bus 4 showed more growth than $\sigma^2_{\Delta I}$ in the rest of the system. These results suggest that larger increases in $\sigma^2_{\Delta V}$ and $\sigma^2_{\Delta I}$ in one area of the system, relative to the rest of the system, can indicate that this area is stressed.

Our results from Sec. 4.5 identified certain lines whose autocorrelation of currents can be good EWS of bifurcation. We now comment on what behavior these autocorrelations exhibit in this experiment. It turns out that not all of these autocorrelations show a measurable increase; the five lines whose currents' autocorrelations show the largest increases are shown in Fig. 4.10(b). While it is not possible to pinpoint the location of the disturbance based only on these statistical characteristics, it is possible to tell, based on the

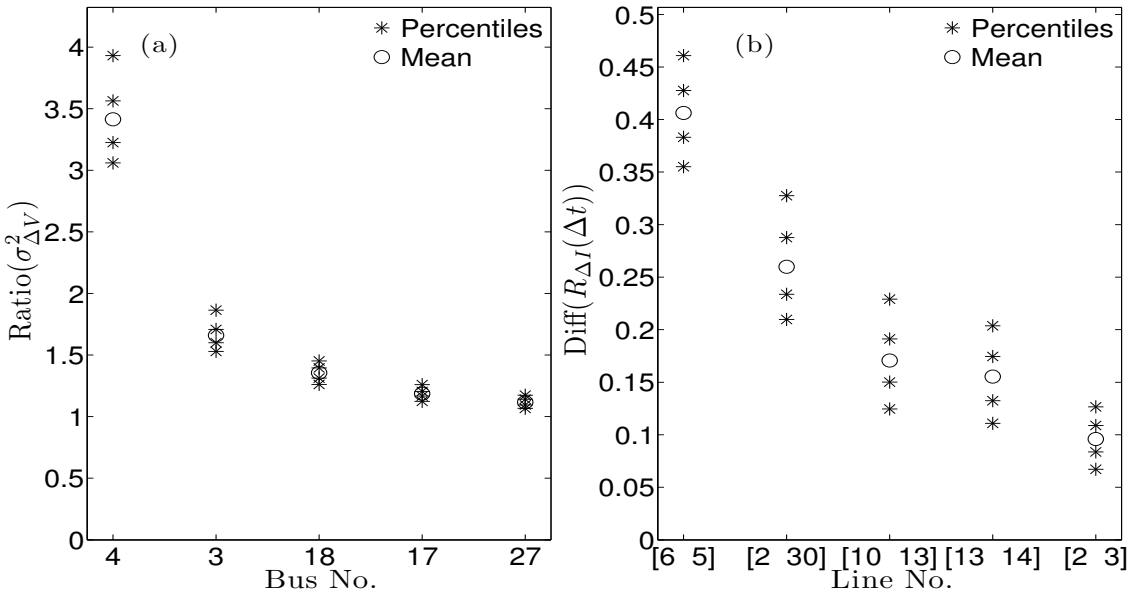

Figure 4.10: Panel (a) shows Ratio $\left(\sigma^2_{\Delta V}\right)$ after disconnecting the two lines connected to bus 4. The mean of the Ratio $\left(\sigma^2_{\Delta V}\right)$ for the 5 buses that show the highest increases in variance, as well as the 5th, 25th, 75th, 95th percentiles of their values, are shown. Panel (b) shows Diff $\left(R_{\Delta I}\left(\Delta t\right)\right)$ for 5 lines that exhibit the largest increases in $R_{\Delta I}\left(\Delta t\right)$. The results are shown after filtering of measurement noise.

statistics, that the disturbance has occurred in a certain area of the network. This knowledge would reinforce the information obtained from monitoring variances of voltages and currents. As explained in Sec. 4.5.1, $R_{\Delta V}\left(\Delta t\right)$ does not provide useful information regarding which areas in the grid are most stressed.

4.6.2 Capacitor tripping

This section provides an example in which the statistical measures, σ^2 and $R\left(\Delta t\right)$, (at least partially) indicate the location of stress in the network, but the mean voltages $\langle V \rangle$ do not change enough to be good indicators. This example was designed to test the hypothesis that σ^2 and $R\left(\Delta t\right)$ can provide information that is not readily available from the mean values.

For this example, we added a new bus (bus 40) and an under-load tap changing (ULTC) transformer that connects bus 40 with bus 15. We also transferred the load of bus 15 to bus 40. Fig. 4.11 shows the P-V curve of bus 40 for three cases. In Case A, the system is in normal operating condition. In Case B, a 3-MVAR capacitor at bus 40

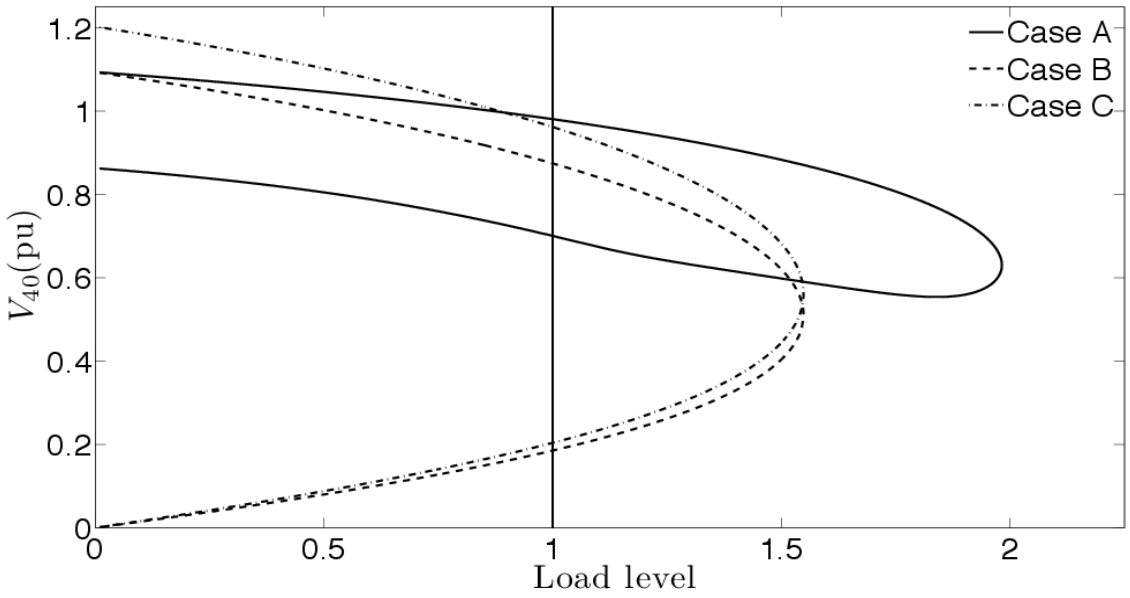

Figure 4.11: PV curve for the three cases described in Sec. 4.6.2. The vertical line corresponds to the base load level.

is disconnected and in Case C, the tap changer changes the tap from 1 to 1.1 in order to return the voltage to the normal operating range ($[0.95\ 1.05]$ pu). Fig. 4.11 shows that the disconnection of the capacitor reduces the stability margin significantly, which manifests itself in lower voltage at bus 40. However, the increase in the ULTC's tap ratio to 1.1 returns the voltage to a value close to its normal level.

Fig. 4.12(a) shows Ratio $(\sigma^2_{\Delta I}) = {}^{\sigma^2_{\Delta I,case\,C}}/_{\sigma^2_{\Delta I,case\,A}}$ for five lines, after filtering the measurement noise. These five line currents show the largest increase in $\sigma^2_{\Delta I}$ among all lines. The first three highest Ratio $(\sigma^2_{\Delta I})$ occur in lines that are close to the stressed area. However, some of the lines that are close to that area do not show significant or any increase in $\sigma^2_{\Delta I}$. For example, $\sigma^2_{\Delta I}$ of line $\begin{bmatrix} 14 & 15 \end{bmatrix}$ decreases. Nevertheless, considering lines with the highest growth in $\sigma^2_{\Delta I}$ can clearly be helpful in identifying the location of the area of the system under excessive stress. As was the case for line currents, the results show that buses that exhibit the largest increases in $\sigma^2_{\Delta V}$ are close to the stressed area. Fig. 4.12(b) shows Diff $(R_{\Delta I}(\Delta t)) = R_{\Delta I,,case\,C}(\Delta t) - R_{\Delta I,,case\,A}(\Delta t)$ for 5 lines. The positive values indicate the increase in $R_{\Delta I}(\Delta t)$. The results in Fig. 4.12(b) show that lines that exhibit the largest increase in $R_{\Delta I}(\Delta t)$ are close to the stressed area.

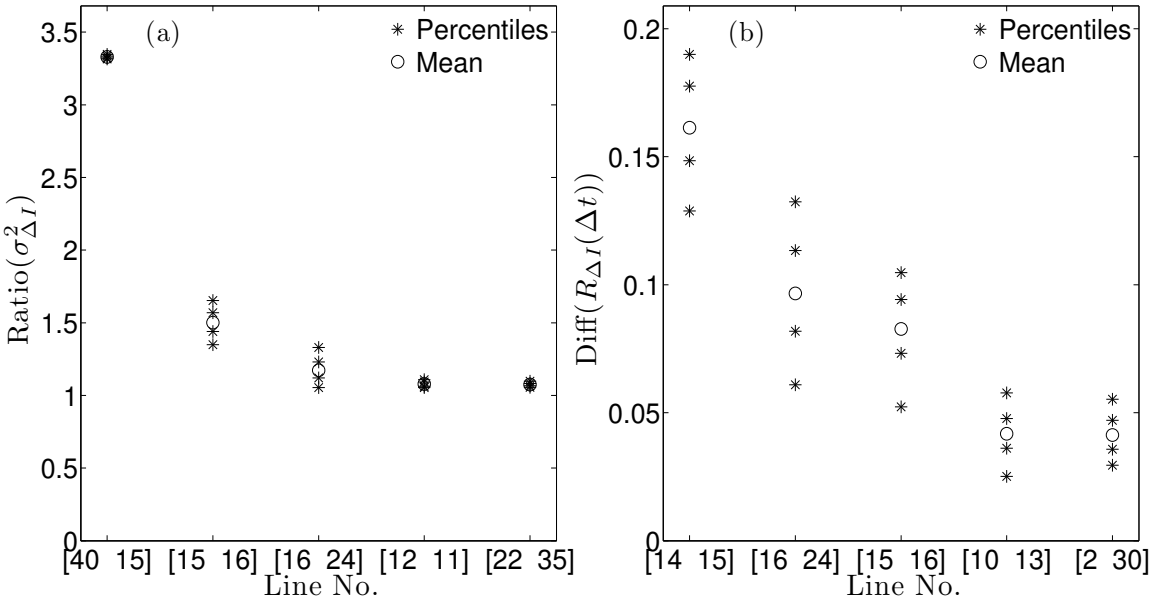

Figure 4.12: Panel (a) shows $\sigma^2_{\Delta I,case\,C}/\sigma^2_{\Delta I,case\,A}$ for 5 lines that exhibit the largest increase in $\sigma^2_{\Delta I}$ among all lines. Panel (b) shows $R_{\Delta I,,case\,C}\,(\Delta t) - R_{\Delta I,,case\,A}\,(\Delta t)$ for 5 lines that exhibit the largest increase in $R_{\Delta I}\,(\Delta t)$.

4.6.3 Discussion

The results presented in this section show that comparing $\sigma^2_{\Delta V}$ and $\sigma^2_{\Delta I}$ for a stressed operating condition with their variances for the normal operating condition can be useful in detecting stressed areas of a power system. The reason for this is that the variances of voltage and current magnitudes show larger increases near the stressed area of a power system, compared to variances in the rest of the system. The results also show that $R_{\Delta I}\,(\Delta t)$ can be helpful in detecting the stressed area's approximate location, although it may not be helpful in pinpointing the exact location of the stress. Autocorrelation of bus voltages were not found to be useful for pinpointing the stressed location for the reason explained in Appendix 4.8.

4.7 Conclusions

Building upon theoretical aspects of the CSD phenomenon in power system discussed in chapters 2 and 3, this chapter investigates the application of CSD for monitoring power system stability.

In this chapter, we first derived a semi-analytical method for quickly computing the expected autocorrelation and variance for any voltage or current in a dynamic power system model. Computing the statistics in this way was shown to be orders of magnitude faster than obtaining the same result by simulation, and allows one to quickly identify locations and variables that are reliable indicators of proximity to instability. Using this method, we showed that the variance of voltage magnitudes near load centers, the autocorrelation of line currents near generators, and the variance of almost all line currents increased measurably as the 39-bus test case approached bifurcation. We found that these trends persist, even in the presence of measurement noise, provided that the data are band-pass filtered. Finally, the chapter provides results suggesting that the statistics of voltage and current data can be helpful in identifying not only whether a system is seeing increased stress, but also the location of the stress.

Together, these results suggest that, under certain conditions, these easily measured statistical quantities in synchrophasor data can be useful indicators of stability. However, it is necessary to take further steps to use these results for stability monitoring of a power system. First, it is essential to take into account the impact of filtering measurement noise in the semi-analytical method. Also, it is crucial to have a realistic estimate of measurement noise characteristics.

4.8 Appendix A

The equation for $R_{\Delta V_m}(\Delta t)$ before band-pass filtering is:

$$\mathrm{E}[\Delta V_m(t)\Delta V_m(s)]/\sigma^2_{\Delta V_m} = \mathrm{E}[\Delta V(t)\Delta V(s)]/\left(\sigma^2_{\Delta V}+\sigma^2_{\eta}\right) \tag{4.21}$$

If $\sigma^2_{\Delta V} \ll \sigma^2_{\eta}$, $R_{\Delta V_m}(\Delta t)$ will be almost zero. This is the case for generator buses or buses close to generators such as buses $20, 36$. However, if $\sigma^2_{\Delta V}$ increases such that $\sigma^2_{\Delta V} \sim \sigma^2_{\eta}$ and $R_{\Delta V}(\Delta t)$ is sufficiently larger than 0 (> 0.2), then $R_{\Delta V_m}(\Delta t)$ will rise significantly with load level, in part because of increase in $R_{\Delta V}(\Delta t)$ and in part because of increase in $\sigma^2_{\Delta V}$. This happens for buses close to load centers such as $7, 14$. Comparing $R(\Delta t)$ of

voltage of buses $7, 14$ in Fig. 4.1 with those in Fig. 4.3 shows that these quantities increase significantly after adding measurement noise while their increase without measurement noise is much smaller. This shows that the increase in $R_{\Delta V_m}(\Delta t)$ for load buses is more due to the increase in $\sigma^2_{\Delta V}$ than due to the increase in $R_{\Delta V}(\Delta t)$.

Bibliography

Alvarado, F., I. Dobson, and Y. Hu (1994, May). Computation of closest bifurcations in power systems. *IEEE Trans. Power Syst. 9*(2), 918–928.

Anderson, P. M. and A. Bose (1983, Aug.). A probabilistic approach to power system stability analysis. *IEEE Trans. Power Apparatus Syst. 102*(8), 2430–2439.

Anghel, M., K. A. Werley, and A. E. Motter (2007, Jan.). Stochastic model for power grid dynamics. In *40th Annual Hawaii Intl. Conf. Syst. Sci.*

Avalos, R. J., C. A. Cañizares, F. Milano, and A. J. Conejo (2009, Jan.). Equivalency of continuation and optimization methods to determine saddle-node and limit-induced bifurcations in power systems. *IEEE Trans. Circuits Syst. I 56*(1), 210–223.

Berg, G. (1973, Mar.). Power system load representation. In *Proc. IEE*, Volume 120, pp. 344–348.

Boerlijst, M. C., T. Oudman, and A. M. de Roos (2013). Catastrophic collapse can occur without early warning: examples of silent catastrophes in structured ecological models. *PLOS ONE 8*(4), e62033, 6 pp.

Browne, T. J., V. Vittal, G. T. Heydt, and A. R. Messina (2008, Aug.). A comparative assessment of two techniques for modal identification from power system measurements. *IEEE Trans. Power Syst. 23*(3), 1408–1415.

Bu, S., W. Du, H. Wang, Z. Chen, L. Xiao, and H. Li (2012, May). Probabilistic analysis of small-signal stability of large-scale power systems as affected by penetration of wind generation. *IEEE Trans. Power Syst. 27*(2), 762–770.

Chertkov, M., S. Backhaus, K. Turtisyn, V. Chernyak, and V. Lebedev (2011, Jun.). Voltage collapse and ODE approach to power flows: Analysis of a feeder line with static disorder in consumption/production. *arXiv preprint arXiv:1106.5003*.

Cotilla-Sanchez, E., P. D. H. Hines, and C. Danforth (2012, Dec.). Predicting critical transitions from time series synchrophasor data. *IEEE Trans. Smart Grid 3*(4), 1832 –1840.

Dakos, V., M. Scheffer, E. H. van Nes, V. Brovkin, V. Petoukhov, and H. Held (2008, Sep.). Slowing down as an early warning signal for abrupt climate change. *Proc. Natl. Acad. Sci. 105*(38), 14308–14312.

De Marco, C. and A. Bergen (1987, Dec.). A security measure for random load disturbances in nonlinear power system models. *IEEE Trans. Circuits Syst. 34*(12), 1546–1557.

Dhople, S., Y. Chen, L. DeVille, and A. Dominguez-Garcia (2013, Dec.). Analysis of power system dynamics subject to stochastic power injections. *IEEE Trans. Circ. Syst. I 60*(12), 3341–3353.

Dong, Z. Y., J. H. Zhao, and D. Hill (2012, Nov.). Numerical simulation for stochastic transient stability assessment. *IEEE Trans. Power Syst. 27*(4), 1741–1749.

Gardiner, C. W. (2010). *Stochastic Methods: A Handbook for the Natural and Social Sciences* (4th ed.). Berlin, Germany: Springer.

Ghanavati, G., P. D. H. Hines, T. I. Lakoba, and E. Cotilla-Sanchez (2014, Sep.). Understanding early indicators of critical transitions in power systems from autocorrelation functions. *IEEE Trans. Circuits Syst. I 61*(9), 2747–2760.

Ghasemi, H. and C. A. Cañizares (2008). Confidence intervals estimation in the identification of electromechanical modes from ambient noise. *IEEE Trans. Power Syst. 23*(2), 641–648.

Grijalva, S. (2012, Feb.). Individual branch and path necessary conditions for saddle-node bifurcation voltage collapse. *IEEE Trans. Power Syst. 27*(1), 12–19.

Haesen, E., C. Bastiaensen, J. Driesen, and R. Belmans (2009, May). A probabilistic formulation of load margins in power systems with stochastic generation. *IEEE Trans. Power Syst. 24*(2), 951–958.

Haque, M. (2003, Jan.). On-line monitoring of maximum permissible loading of a power system within voltage stability limits. *IEE Proc. Gen. Trans. Dist. 150*(1), 107–112.

Hauer, A. J. F., D. J. Trudnowski, and J. G. DeSteese (2007, Jun.). A perspective on WAMS analysis tools for tracking of oscillatory dynamics. In *IEEE Power and Energy Soc. General Meeting*, pp. 1–10.

Hou, G. and V. Vittal (2012, Nov.). Trajectory sensitivity based preventive control of voltage instability considering load uncertainties. *IEEE Trans. Power Syst. 27*(4), 2280–2288.

Huang, H. and C. Chung (2012, Nov.). Coordinated damping control design for DFIG-based wind generation considering power output variation. *IEEE Trans. Power Syst. 27*(4), 1916–1925.

Huang, H., C. Chung, K. W. Chan, and H. Chen (2013, Aug.). Quasi-Monte Carlo based probabilistic small signal stability analysis for power systems with plug-in electric vehicle and wind power integration. *IEEE Trans. Power Syst. 28*(3), 3335–3343.

Kakimoto, N., M. Sugumi, T. Makino, and K. Tomiyama (2006, Feb.). Monitoring of interarea oscillation mode by synchronized phasor measurement. *IEEE Trans. Power Syst. 21*(1), 260–268.

Kamwa, I., A. K. Pradhan, and G. Joós (2011, Feb.). Robust detection and analysis of power system oscillations using the Teager-Kaiser energy operator. *IEEE Trans. Power Syst. 26*(1), 323–333.

Kataoka, Y. (2003, Nov.). A probabilistic nodal loading model and worst case solutions for electric power system voltage stability assessment. *IEEE Trans. Power Syst. 18*(4), 1507–1514.

Kundur, P., J. Paserba, V. Ajjarapu, G. Andersson, A. Bose, C. Canizares, N. Hatziargyriou, D. Hill, A. Stankovic, C. Taylor, T. Van Cutsem, and V. Vittal (2004, Aug.). Definition and classification of power system stability IEEE/CIGRE joint task force on stability terms and definitions. *IEEE Trans. Power Syst. 19*(3), 1387 – 1401.

Lerm, A. A. P., C. A. Cañizares, and A. S. Silva (2003, May). Multiparameter bifurcation analysis of the South Brazilian power system. *IEEE Trans. Power Syst. 18*(2), 737–746.

Lim, J. M. and C. L. DeMarco (2013, Aug.). Model-free voltage stability assessments via singular value analysis of PMU data. In *Bulk Pow. Syst. Dyn. Cont.-IX Optim. Secu. Cont. Emer. Pow. Grid Symp.*, pp. 1–10.

Milano, F. (2005). An open source power system analysis toolbox. *IEEE Trans. Power Syst. 20*(3), 1199–1206.

Milano, F. (2010, May). *Power System Analysis Toolbox Quick Reference Manual for PSAT version 2.1. 6*.

Milano, F. and R. Zarate-Minano (2013, Nov.). A systematic method to model power systems as stochastic differential algebraic equations. *IEEE Trans. Power Syst. 28*(4), 4537–4544.

Mori, H. (1963). On the relaxation processes near the second order phase transition point. *Prog. Theor. Phys. 30*(4), 576–578.

Munoz, J., C. Canizares, K. Bhattacharya, and A. Vaccaro (2013, Nov.). An affine arithmetic-based method for voltage stability assessment of power systems with intermittent generation sources. *IEEE Trans. Power Syst. 28*(4), 4475–4487.

Nwankpa, C., S. Shahidehpour, and Z. Schuss (1992, Nov.). A stochastic approach to small disturbance stability analysis. *IEEE Trans. Power Syst. 7*(4), 1519–1528.

Odun-Ayo, T. and M. L. Crow (2012). Structure-preserved power system transient stability using stochastic energy functions. *IEEE Trans. Power Syst. 27*(3), 1450–1458.

Pai, M. (1989). *Energy function analysis for power system stability* (1st ed.). MA, USA: Kluwer Academic Publishers.

Perninge, M., V. Knazkins, M. Amelin, and L. Soder (2010, Aug.). Risk estimation of critical time to voltage instability induced by saddle-node bifurcation. *IEEE Trans. Power Syst. 25*(3), 1600–1610.

Podolsky, D. and K. Turitsyn (2013a, Jul.). Critical slowing-down as indicator of approach to the loss of stability. *arXiv preprint:1307.4318*.

Podolsky, D. and K. Turitsyn (2013b, Jul.). Random load fluctuations and collapse probability of a power system operating near codimension 1 saddle-node bifurcation. In *IEEE Power and Energy Soc. Gen. Meeting*, pp. 1–5.

Rosehart, W. D. and C. A. Cañizares (1999, Mar.). Bifurcation analysis of various power system models. *Intl. J. Elec. Pow. Energy Syst. 21*(3), 171–182.

Scheffer, M., J. Bascompte, W. A. Brock, V. Brovkin, S. R. Carpenter, V. Dakos, H. Held, E. H. Van Nes, M. Rietkerk, and G. Sugihara (2009). Early–warning signals for critical transitions. *Nature 461*(7260), 53–59.

Scheffer, M., S. R. Carpenter, T. M. Lenton, J. Bascompte, W. Brock, V. Dakos, J. van de Koppel, I. A. van de Leemput, S. A. Levin, E. H. van Nes, M. Pascual, and J. Vandermeer (2012, Oct.). Anticipating critical transitions. *Science 338*(6105), 344–348.

Schellenberg, A., W. Rosehart, and J. A. Aguado (2006, May). Cumulant-based stochastic nonlinear programming for variance constrained voltage stability analysis of power systems. *IEEE Trans. Power Syst. 21*(2), 579–585.

Verdejo, H., L. Vargas, and W. Kliemann (2012, Jul.). Stability of linear stochastic systems via Lyapunov exponents and applications to power systems. *Appl. Math. Comput. 218*(22), 11021–11032.

Wang, K., C. Chung, C. Tse, and K. Tsang (2000, Jan.). Improved probabilistic method for power system dynamic stability studies. In *IEE Proc. Gen. Trans. Dist.*, Volume 147, pp. 37–43.

Wang, K. and M. L. Crow (2013, Aug.). The Fokker–Planck equation for power system stability probability density function evolution. *IEEE Trans. Power Syst. 28*(3), 2994–3001.

Wei, D. and X. Luo (2009). Noise-induced chaos in single-machine infinite-bus power systems. *Europhys. Lett. 86*(5), 50008, 6 pp.

Yuan, B., M. Zhou, G. Li, and X.-P. Zhang (to be published). Stochastic small-signal stability of power systems with wind power generation. *IEEE Trans. Power Syst.*.

CHAPTER 5: CONCLUSIONS AND FUTURE DIRECTIONS

5.1 Conclusions

This dissertation aims to improve our understanding of early warning signs (EWS) of critical bifurcations such as saddle-node and Hopf in power systems, which can lead to catastrophic failures (i.e. a blackout) if they are not detected sufficiently early. The EWS under study are increases in variance and autocorrelation of state variables, which are due to a phenomenon in dynamical systems known as critical slowing down (CSD). The results of this research provide new methods for extracting information regarding the proximity of a power system to critical bifurcations as well as for identifying stressed locations of the system.

Starting with analytical studies, the results (see chapter 2) from calculation of autocorrelation function of state variables in three small power systems demonstrate that the CSD phenomenon does indeed occur in power systems. Numerical simulation of stochastic differential equations that model these systems confirms the findings from the analytical results. Together, numerical and analytical results show that this phenomenon occurs for both saddle-node and Hopf bifurcations.

The results also show that although CSD signs do consistently appear as the systems approach bifurcation, only in a few of the variables such as voltage magnitudes do the increases in autocorrelation and variance appear sufficiently early to give a useful early warning of potential collapse. Eigenvalue analysis presented in chapter 3 provides some explanation as to why CSD signs are better observable in some variables than others. Investigation of a system for which a Hopf bifurcation occurs as a result of increase in system loading, shows that fluctuations of the variables that show well observable increase in the statistics, are more aligned with the direction of the system's dominant mode.

The dissertation also presents (see chapter 4) a semi-analytical method for quickly computing the expected autocorrelation and variance for state variables in a dynamic power

system model. The results show that computing the statistics using this method is much faster than obtaining them by simulation, and allows one to quickly identify locations and variables that are reliable indicators of proximity to instability.

The results obtained using the semi-analytical method, show that not only is increase in autocorrelation and variance more clearly measurable in some variables than in others, but also CSD signs are better observable in some areas of a power system. After considering measurement noise, the results for a test system suggest that the variance of voltage magnitudes near load centers, the autocorrelation of line currents near generators, and the variance of almost all line currents show measurable increase as the system approaches a Hopf bifurcation, provided that the data are band-pass filtered.

Finally, the results from a couple of experiments show that it is possible to extract information about the location of the stress in the system from the statistics of voltages and currents. Comparing variances of voltages and currents for stressed operating conditions with their variances for the normal operating condition shows that variances of voltage and current magnitudes exhibit larger increases near the stressed area of a power system, which can be useful in detecting such an area. The results also show that autocorrelation of currents can be helpful in detecting the stressed area's approximate location, although it may not be helpful in pinpointing the exact location of the stress.

5.2 Future directions

A natural expansion upon the current work is to develop a power system stability indicator using statistics of measurements. Considering factors such as inaccuracy in power system parameters and models, calculating distance to a critical bifurcation using only deterministic models and mean values of measurements may not provide true risk or likelihood of failures. It might be possible to get a more accurate estimate about distance to a bifurcation by combining information from mean values with variance and autocorrelation of measurements. To this end, it would be helpful to expand the semi-analytical method so that it takes into account the impact of filtering measurement noise. There will also be other challenges for achieving a reliable statistics-based stability indicator, e.g.,

changes in load variations intensity and inaccurate modeling of measurement noise, which can impact measurements' statistics.

Considering the above, it might be worthwhile to investigate the impacts of more detailed models of measurement noise on the results presented in this work. Measurement noise can come from various elements of a measurement system such as current or voltage transformers, cables, and sensors or A/D converters (Zhu et al. 2006). Modeling each source in sufficient detail could help with better understanding of implications of measurement noise on measurements' statistics.

Also, studying patterns of change in statistics of power system variables that are not included in this work, might uncover helpful EWS. In this work, we studied statistical patterns of magnitude and angle of node voltages and line currents, and rotor angle and speed of generators. The results showed that statistics of voltage and current magnitudes in some cases provide helpful EWS for saddle-node and Hopf bifurcations. There are, however, other variables whose statistical properties might worth exploring in the future; one example here is the frequency of load nodes.

An additional research direction stems from stochastic methods used to analyze power system dynamics in this dissertation. In the current literature, there is little information regarding modeling renewable energy sources using stochastic calculus (Yuan et al. 2014). Building upon this work, one could develop a comprehensive stochastic framework for modeling and analysis of a power system with renewable sources, such as wind turbines and solar panels. Developing such a framework would enable the study of the impact of renewable sources on power system stability. Moreover, stochastic modeling of renewable sources could also be helpful for stability analysis of low voltage distribution systems, which might be of importance in the future due to increase in penetration of distributed generation in these systems (Cardell and Ilic 2004), (Nguyen and Turitsyn 2014). The following subsection briefly discusses some aspects of stochastic modeling of renewable energy sources.

5.2.1 Modeling renewable energy sources

Recently, some research has focused on development of stochastic models of wind and solar generation and examining their impact on power system dynamics. (Ajala and Sauer 2014) propose a stochastic model for a grid-connected three-phase photovoltaic system. (Bu et al. 2012) present an analytical method for calculation of the probability density function (PDF) of critical eigenvalues of a large-scale power system from the PDF of multiple grid-connected sources of wind power generation. (Yuan et al. 2014) present a method for calculation of steady-state expectation and variance of state variables of a power system model with stochastic wind excitation after a small disturbance. However, the current modeling approaches seem to be in an early stage and the results obtained using these models are sometimes significantly different. For example, (Bu et al. 2012) conclude that "stochastic variation of grid-connected wind generation can cause the system to lose stability even though the system is stable deterministically". On the contrary, (Yuan et al. 2014) state that stochastic excitation due to wind generation only leads to bounded fluctuations of the power system.

Various methods have been used for modeling stochastic excitation of renewable generation by wind and solar energy. (Ajala and Sauer 2014) model solar irradiance and temperature using the Wiener process. (Bu et al. 2012) use the Weibull distribution for modeling wind speed. (Yuan et al. 2014) model the input mechanical power of wind using the Wiener process. Further investigation is necessary to verify these methods.

APPENDIX A: SIMULATION SCRIPTS

The MATLAB scripts in this appendix can be used for running a dynamic simulation with stochastic changes in load using power system analysis toolbox (PSAT). In the simulations, loads vary randomly at each time-step and their values at any point of time are correlated to their values at previous times. Loads fluctuations follow the Ornstein–Uhlenbeck process (Perninge et al. 2010), (Hauer et al. 2007), which is a mean-reverting Gaussian process. Also, loads are assumed to be frequency-dependent:

$$\Delta\omega = \frac{1}{2\pi f_n}\frac{d\left(\theta-\theta^0\right)}{dt} \tag{A.1}$$

$$P = P^0\left(1+\Delta\omega\right)^{\beta_P} \tag{A.2}$$

$$Q = Q^0\left(1+\Delta\omega\right)^{\beta_Q} \tag{A.3}$$

A.1 Dynamic simulation driver

The script below (run_sim.m) is the driver for running dynamic simulations. It employs PSAT through a set of commands. First it loads data and perturbation files. Then it runs power flow. After initialization, time-domain simulation is performed. At the end output variables are saved in "output.mat". The script d039.m includes 39-bus test case data (Pai 1989).

run_sim.m

```
clear all;close all;clc;
tstart=tic;
global intstep VP_nos VQ_nos tcorr PQ Varout Varname P0 Q0;
RandStream.setDefaultStream(RandStream('mt19937ar','seed',...
```

```
sum(100*clock)));

intstep = 0.01;       % Integration Step Size
tbegin = 0;           % Initial Simulation time
tfinal = 120;         % Final Simulation time
tcorr = 1;            % Correlation time of noise

d039;
npq = size(PQ.con,1);
P0 = PQ.con(:,4);     % Initial value of loads' active power
Q0 = PQ.con(:,5);     % Initial value of loads' reactive
power

initpsat;             % Initialize PSAT global variables
datafile = 'd039';    % Test case data file
runpsat(datafile,'data');
runpsat('perturb','pert');   % "Perturb":  Perturbation file
Settings.freq = 60;
clpsat.readfile = 1;  % Read data file before running power
flow
runpsat('pf');        % Run power flow

%% SETTINGS FOR TIME DOMAIN SIMULATION
Settings.coi = 1;     % Use center of inertia for synchronous
machines
Settings.t0 = tbegin;
Settings.tf = tfinal;
Settings.pq2z = 0;    % Do not convert PQ loads to constant
```

```
% impedance loads after power flow
Settings.fixt = 1;   % Enable fixed time-step solver
Settings.tstep = intstep;
%%

VP_nos = zeros(npq,1);     % Vector of noise for load active
powers, see "perturb.m"
VQ_nos = zeros(npq,1);
nL = Line.n + Ltc.n + Phs.n + Hvdc.n + Lines.n;
Varname.idx = 1:DAE.n + DAE.m + 2*Bus.n + 5*nL;

runpsat('td');             % Running time domain (dynamic)
simulation
%% OUTPUT VARIABLES
%Index of output variables
ix_Va = DAE.n+1:DAE.n+Bus.n;   % Index of voltage angles
ix_Vm = DAE.n+Bus.n + ...      % Index of voltage magnitudes
1:DAE.n+2*Bus.n;
ix_I = DAE.n + DAE.m +...      % Index of line currents
2*Bus.n + 4*nL + 1:DAE.n + DAE.m + 2*Bus.n + 5*nL;
ix_P = DAE.n + DAE.m + ...     % Index of line active powers
2*Bus.n + 1:DAE.n + DAE.m + 2*Bus.n+nL;
ix_Q = DAE.n + DAE.m + ...     % Index of line reactive
powers
2*Bus.n +2*nL + 1:DAE.n + DAE.m + 2*Bus.n+3*nL;
ix_de = Syn.delta;             % Index of generator rotor
angles
ix_om = Syn.omega;             % Index of generator speed
```

```
%Output variable values
Va = Varout.vars(:,ix_Va);    % Va:  Bus voltage angles
Vm = Varout.vars(:,ix_Vm);    % Vm:  Bus voltage magnitudes
time = Varout.t;
deltas = Varout.vars(:,ix_de);
omegas = Varout.vars(:,ix_om);
Il = Varout.vars(:,ix_I);
Pl = Varout.vars(:,ix_P);
Ql = Varout.vars(:,ix_Q);
%%
save('output','Va','Vm','deltas','omegas','time','Pl','Ql','Il');
close all;
stime = toc(tstart)
```

A.2 Perturbation function

The following is the perturbation function (Perturb.m) for introducing disturbances such as opening a line, load changes, fault, etc. In this file, values of P^0 and Q^0 in A.2, A.3 are modified at each time step according to the Ornstein–Uhlenbeck process.

perturb.m

```
function perturb(t)
% Adding correlated noise (Ornstein-Uhlenbeck process) to
% load active and reactive powers
global intstep VP_nos VQ_nos tcorr Fl P0 Q0;


gamma = 1/tcorr;
nos_std = 0.01*sqrt(2*gamma);
rnd_vec = randn(size(Fl.con,1),1);
```

```
VP_nos = VP_nos*(1 - gamma * intstep) + nos_std * ...
sqrt(intstep) * rnd_vec;
VQ_nos = VQ_nos*(1 - gamma * intstep) + nos_std *...
sqrt(intstep) * rnd_vec;
Fl.con(:,2) = P0 .*(1+VP_nos); % Fl.con(:,2) will be
% multiplied later by (1+Delta omega)^beta_p to give load
% active power values at each time step
Fl.con(:,5) = Q0 .*(1+VQ_nos);   % Fl.con(:,5) will be
% multiplied by (1+Delta omega)^beta_q
```

Bibliography

Abraham, S. and J. Efford (2004). Final report on the August 14, 2003 blackout in the United states and Canada: causes and recommendations. Technical report, US–Canada Power Syst. Outage Task Force.

Ajala, O. and P. Sauer (2014). Stochastic processes in a grid-connected three-phase photovoltaic system. In *Power Energy Conf. Illinois*, pp. 1–8. IEEE.

Anghel, M., K. A. Werley, and A. E. Motter (2007, Jan.). Stochastic model for power grid dynamics. In *40th Annual Hawaii Intl. Conf. Syst. Sci.*

Avalos, R. J., C. A. Cañizares, F. Milano, and A. J. Conejo (2009, Jan.). Equivalency of continuation and optimization methods to determine saddle-node and limit-induced bifurcations in power systems. *IEEE Trans. Circuits Syst. I 56*(1), 210–223.

Bao, L., Z. Huang, and W. Xu (2003). Online voltage stability monitoring using var reserves. *IEEE Trans. Power Syst. 18*(4), 1461–1469.

Begovic, M. M. and A. G. Phadke (1992). Control of voltage stability using sensitivity analysis. *IEEE Trans. Power Syst. 7*(1), 114–123.

Berg, G. (1973, Mar.). Power system load representation. In *Proc. IEE*, Volume 120, pp. 344–348.

Blanchard, P., R. L. Devaney, and G. R. Hall (2006). *Differential Equations*. Thomson Brooks/Cole.

Boerlijst, M. C., T. Oudman, and A. M. de Roos (2013). Catastrophic collapse can occur without early warning: examples of silent catastrophes in structured ecological models. *PLOS ONE 8*(4), e62033, 6 pp.

Boettiger, C., N. Ross, and A. Hastings (2013). Early warning signals: the charted and uncharted territories. *Theoretical Ecology*, 1–10.

Browne, T. J., V. Vittal, G. T. Heydt, and A. R. Messina (2008, Aug.). A comparative assessment of two techniques for modal identification from power system measurements. *IEEE Trans. Power Syst. 23*(3), 1408–1415.

Bu, S., W. Du, H. Wang, Z. Chen, L. Xiao, and H. Li (2012, May). Probabilistic analysis of small-signal stability of large-scale power systems as affected by penetration of wind generation. *IEEE Trans. Power Syst. 27*(2), 762–770.

Cai, D., P. Regulski, M. Osborne, and V. Terzija (2013, Sep.). Wide area inter-area oscillation monitoring using fast nonlinear estimation algorithm. *IEEE Trans. Smart Grid 4*(3), 1721–1731.

Cañizares, C. A., N. Mithulananthan, F. Milano, and J. Reeve (2004, May). Linear performance indices to predict oscillatory stability problems in power systems. *IEEE Trans. Power Syst. 19*(2), 1104–1114.

Cardell, J. and M. Ilic (2004, Jun.). Maintaining stability with distributed generation in a restructured industry. In *Power Engineering Society General Meeting*, pp. 2142–2149. IEEE.

Centeno, V., J. De La Ree, A. Phadke, G. Michel, R. Murphy, and R. Burnett Jr (1993, Oct.). Adaptive out-of-step relaying using phasor measurement techniques. *IEEE Comput. Appl. Pow. 6*(4), 12–17.

Chertkov, M., S. Backhaus, K. Turtisyn, V. Chernyak, and V. Lebedev (2011, Jun.). Voltage collapse and ODE approach to power flows: Analysis of a feeder line with static disorder in consumption/production. *arXiv preprint arXiv:1106.5003*.

Chiang, H., I. Dobson, R. J. Thomas, J. S. Thorp, and L. Fekih-Ahmed (1990). On voltage collapse in electric power systems. *IEEE Trans. Power Syst. 5*(2), 601–611.

Cotilla-Sanchez, E., P. D. H. Hines, and C. Danforth (2012, Dec.). Predicting critical transitions from time series synchrophasor data. *IEEE Trans. Smart Grid 3*(4), 1832 –1840.

Dakos, V., S. Kéfi, M. Rietkerk, E. H. van Nes, and M. Scheffer (2011). Slowing down in spatially patterned ecosystems at the brink of collapse. *The American Naturalist 177*(6), E153–E166.

Dakos, V., M. Scheffer, E. H. van Nes, V. Brovkin, V. Petoukhov, and H. Held (2008, Sep.). Slowing down as an early warning signal for abrupt climate change. *Proc. Natl. Acad. Sci. 105*(38), 14308–14312.

De La Ree, J., V. Centeno, J. S. Thorp, and A. G. Phadke (2010). Synchronized phasor measurement applications in power systems. *IEEE Trans. Smart Grid 1*(1), 20–27.

De Marco, C. and A. Bergen (1987, Dec.). A security measure for random load disturbances in nonlinear power system models. *IEEE Trans. Circuits Syst. 34*(12), 1546–1557.

Demello, F. P. and C. Concordia (1969, Apr.). Concepts of synchronous machine stability as affected by excitation control. *IEEE Trans. Power Apparatus Syst. 88*(4), 316–329.

Dhople, S., Y. Chen, L. DeVille, and A. Dominguez-Garcia (2013, Dec.). Analysis of power system dynamics subject to stochastic power injections. *IEEE Trans. Circ. Syst. I 60*(12), 3341–3353.

Dobson, I. (1992, Mar.). Observations on the geometry of saddle node bifurcation and voltage collapse in electrical power systems. *IEEE Trans. Circ. Syst. I: Fund. Theo. App. 39*(3), 240 –243.

Dobson, I., T. Van Cutsem, C. D. Vournas, C. L. DeMarco, M. Venkatasubramanian, T. Overbye, and C. A. Canizares (2002). Voltage stability assessment: concepts, practices and tools. *Power System Stability Subcommittee Special Publication IEEE/PES*.

Dong, Z. Y., J. H. Zhao, and D. Hill (2012, Nov.). Numerical simulation for stochastic transient stability assessment. *IEEE Trans. Power Syst. 27*(4), 1741–1749.

FERC and NERC (2012, Apr.). Arizona–Southern California outages on September 8, 2011: causes and recommendations. Technical report.

Gardiner, C. W. (2010). *Stochastic Methods: A Handbook for the Natural and Social Sciences* (4th ed.). Berlin, Germany: Springer.

Ghanavati, G., P. D. H. Hines, T. Lakoba, and E. Cotilla-Sanchez (2013, Sep.). Calculation of the autocorrelation function of the stochastic single machine infinite bus system. In *Proc. North Amer. Power Symp.*, pp. 1–6.

Ghasemi, H. (2006). *On-line monitoring and oscillatory stability margin prediction in power systems based on system identification*. Ph. D. thesis, University of Waterloo.

Ghasemi, H. and C. A. Cañizares (2008, May). Confidence intervals estimation in the identification of electromechanical modes from ambient noise. *IEEE Trans. Power Syst. 23*(2), 641–648.

Glavic, M. and T. Van Cutsem (2009, Aug.). Wide-area detection of voltage instability from synchronized phasor measurements. part I: Principle. *IEEE Trans. Power Syst. 24*(3), 1408 –1416.

Gómez-Expósito, A., A. Abur, P. Rousseaux, A. de la Villa Jaén, and C. Gómez-Quiles (2011). On the use of PMUs in power system state estimation. In *Proc. 17th Power Syst. Compu. Conf.*, pp. 22–26.

Gou, B. and A. Abur (2001, Nov.). An improved measurement placement algorithm for network observability. *IEEE Trans. Power Syst. 16*(4), 819–824.

Hastings, A. and D. B. Wysham (2010). Regime shifts in ecological systems can occur with no warning. *Ecol. Lett. 13*(4), 464–472.

Hauer, A. J. F., D. J. Trudnowski, and J. G. DeSteese (2007, Jun.). A perspective on WAMS analysis tools for tracking of oscillatory dynamics. In *IEEE Power Energy Soc. Gen. Meeting*, pp. 1–10.

Horsthemke, W. and R. Lefever (2006). *Noise-induced Transitions* (2nd. ed.). Berlin: Springer.

Huang, Z., N. Zhou, F. Tuffner, and D. Trudnowski (2011). Use of modal sensitivity to operating conditions for damping control in power systems. In *44th Hawaii Intl. Conf. Syst. Sci.*, pp. 1–9.

Kakimoto, N., M. Sugumi, T. Makino, and K. Tomiyama (2006, Feb.). Monitoring of interarea oscillation mode by synchronized phasor measurement. *IEEE Trans. Power Syst. 21*(1), 260–268.

Klein, M., G. Rogers, and P. Kundur (1991, Aug.). A fundamental study of inter-area oscillations in power systems. *IEEE Trans. Power Syst. 6*(3), 914–921.

Kosterev, D., S. Yirga, and V. Venkatasubramanian (1997, Mar.). Validation report of the August 10, 1996 WSCC disturbance. Technical report, Western Systems Coordinating Council.

Kundur, P., N. J. Balu, and M. G. Lauby (1994). *Power system stability and control*, Volume 4. New York: McGraw-hill.

Kundur, P., G. Berube, L. Hajagos, and R. Beaulieu (2003, Jul.). Practical utility experience with and effective use of power system stabilizers. In *IEEE Power Energy Soc. Gen. Meeting*, Volume 3, pp. 1777–1785. IEEE.

Kundur, P., J. Paserba, V. Ajjarapu, G. Andersson, A. Bose, C. Canizares, N. Hatziargyriou, D. Hill, A. Stankovic, C. Taylor, T. Van Cutsem, and V. Vittal (2004, Aug.). Definition and classification of power system stability IEEE/CIGRE joint task force on stability terms and definitions. *IEEE Trans. Power Syst. 19*(3), 1387 – 1401.

Lenton, T., V. Livina, V. Dakos, E. Van Nes, and M. Scheffer (2012). Early warning of climate tipping points from critical slowing down: comparing methods to improve robustness. *Philos. Trans. Royal Soc. A: Math., Phys. Eng. Sci. 370*(1962), 1185–1204.

Lerm, A. A. P., C. A. Cañizares, and A. S. Silva (2003, May). Multiparameter bifurcation analysis of the South Brazilian power system. *IEEE Trans. Power Syst. 18*(2), 737–746.

Litt, B., R. Esteller, J. Echauz, M. D'Alessandro, R. Shor, T. Henry, P. Pennell, C. Epstein, R. Bakay, M. Dichter, et al. (2001). Epileptic seizures may begin hours in advance of clinical onset: a report of five patients. *Neuron 30*(1), 51–64.

Milano, F. (2005). An open source power system analysis toolbox. *IEEE Trans. Power Syst. 20*(3), 1199–1206.

Milano, F. (2010, May). *Power System Analysis Toolbox Quick Reference Manual for PSAT version 2.1. 6*.

Milano, F. and R. Zarate–Minano (2013, Nov.). A systematic method to model power systems as stochastic differential algebraic equations. *IEEE Trans. Power Syst. 28*(4), 4537–4544.

Milosevic, B. and M. Begovic (2003). Voltage-stability protection and control using a wide-area network of phasor measurements. *IEEE Trans. Power Syst. 18*(1), 121–127.

Nguyen, H. D. and K. Turitsyn (2014, Jul.). Voltage multistability and pulse emergency control for distribution system with power flow reversal. *arXiv:1407.1355*.

Nwankpa, C., S. Shahidehpour, and Z. Schuss (1992, Nov.). A stochastic approach to small disturbance stability analysis. *IEEE Trans. Power Syst. 7*(4), 1519–1528.

Odun-Ayo, T. and M. L. Crow (2012, Aug.). Structure-preserved power system transient stability using stochastic energy functions. *IEEE Trans. Power Syst. 27*(3), 1450–1458.

Pai, M. (1989). *Energy function analysis for power system stability* (1st ed.). MA, USA: Kluwer Academic Publishers.

Peng, J. H. and N. K. Nair (2012). Enhancing Kalman filter for tracking ringdown electromechanical oscillations. *IEEE Trans. Power Syst. 27*(2), 1042–1050.

Perninge, M., V. Knazkins, M. Amelin, and L. Soder (2010, Aug.). Risk estimation of critical time to voltage instability induced by saddle-node bifurcation. *IEEE Trans. Power Syst. 25*(3), 1600–1610.

Phadke, A. (1993, Apr.). Synchronized phasor measurements in power systems. *IEEE Comput. Appl. Pow. 6*(2), 10–15.

Podolsky, D. and K. Turitsyn (2013a, Jul.). Critical slowing-down as indicator of approach to the loss of stability. *arXiv preprint:1307.4318*.

Podolsky, D. and K. Turitsyn (2013b, Jul.). Random load fluctuations and collapse probability of a power system operating near codimension 1 saddle-node bifurcation. In *IEEE Power Energy Soc. Gen. Meeting*, pp. 1–5.

Popović, D., D. Kukolj, and F. Kulić (1998, Jul.). Monitoring and assessment of voltage stability margins using artificial neural networks with a reduced input set. *IEE Proc. Gen. Trans. Dist. 145*(4), 355–362.

Revel, G., A. Leon, D. Alonso, and J. Moiola (2010, Apr.). Bifurcation analysis on a multimachine power system model. *IEEE Trans. Circ. Syst. I 57*(4), 937 –949.

Romero, J. J. (2012, Oct.). Blackouts illuminate India's power problems. *IEEE Spectrum 49*(10), 11–12.

Rosehart, W. D. and C. A. Cañizares (1999, Mar.). Bifurcation analysis of various power system models. *Intl. J. Elec. Pow. Energy Syst. 21*(3), 171–182.

Scheffer, M., J. Bascompte, W. A. Brock, V. Brovkin, S. R. Carpenter, V. Dakos, H. Held, E. H. Van Nes, M. Rietkerk, and G. Sugihara (2009, Sep.). Early-warning signals for critical transitions. *Nature 461*(7260), 53–59.

Scheffer, M., S. Carpenter, J. A. Foley, C. Folke, and B. Walker (2001). Catastrophic shifts in ecosystems. *Nature 413*(6856), 591–596.

Smon, I., G. Verbic, and F. Gubina (2006, Aug.). Local voltage-stability index using Tellegen's theorem. *IEEE Trans. Power Syst. 21*(3), 1267–1275.

Stratonovich, R. L. (1963). *Introduction to the Theory of Random Noise*. Gordon and Breach.

Wang, K. and M. L. Crow (2013, Aug.). The Fokker–Planck equation for power system stability probability density function evolution. *IEEE Trans. Power Syst. 28*(3), 2994–3001.

Wang, Y., D. J. Hill, R. H. Middleton, and L. Gao (1993, May). Transient stability enhancement and voltage regulation of power systems. *IEEE Trans. Power Syst. 8*(2), 620–627.

Wei, D. and X. Luo (2009). Noise-induced chaos in single-machine infinite-bus power systems. *Europhys. Lett. 86*(5), 50008, 6 pp.

Yang, N., Q. Liu, and J. D. McCalley (1998, Nov.). TCSC controller design for damping interarea oscillations. *IEEE Trans. Power Syst. 13*(4), 1304–1310.

Yuan, B., M. Zhou, G. Li, and X. Zhang (2014). Stochastic small-signal stability of power systems with wind power generation. *IEEE Trans. Power Syst. (to be published.)*.

Zhong, Z., C. Xu, B. J. Billian, L. Zhang, S. Tsai, R. W. Conners, V. A. Centeno, A. G. Phadke, and Y. Liu (2005, Nov.). Power system frequency monitoring network (FNET) implementation. *IEEE Trans. Power Syst. 20*(4), 1914–1921.

Zhou, D. Q., U. Annakkage, and A. D. Rajapakse (2010). Online monitoring of voltage stability margin using an artificial neural network. *IEEE Trans. Power Syst. 25*(3), 1566–1574.

Zhou, N., J. W. Pierre, and D. Trudnowski (2012). A stepwise regression method for estimating dominant electromechanical modes. *IEEE Trans. Power Syst. 27*(2), 1051–1059.

Zhu, J., A. Abur, M. Rice, G. Heydt, and S. Meliopoulos (2006, Nov.). Enhanced state estimators. Technical report, PSERC.